

Neuromodulation of Thalamic Sensory Processing of Tactile Stimuli

Charles Rodenkirch

Submitted in partial fulfillment of the
requirements for the degree of
Doctor of Philosophy
in the Graduate School of Arts and Sciences

COLUMBIA UNIVERSITY

2020

© 2020

Charles Rodenkirch

All Rights Reserved

Abstract

Neuromodulation of Thalamic Sensory Processing of Tactile Stimuli

Charles Rodenkirch

Neuromodulatory systems, such as the locus coeruleus (LC) - norepinephrine (NE) system, are integral in the modulation of behavioral state, which in turn exerts a heavy influence on sensory processing, perception, and behavior. LC neurons project diffusely through the forebrain as the sole source of NE. LC tonic firing rate has been shown to correlate with arousal level and behavioral performance. As the LC-NE system innervates sensory pathways and NE has been shown to affect neuronal response, the LC-NE system could potentially allow for state-dependent modulation of sensory processing. However, the precise link between LC activation and sensory processing in the various stages of the sensory pathway that underly perception remained elusive.

It is well established that thalamic relay nuclei play an essential role in gating the flow of sensory information to the neocortex, serving to establish cortical representation of sensory environment. Thalamocortical information transmission has been proposed to be strongly modulated by the dynamic interplay between the thalamic relay nuclei and the thalamic reticular nucleus (TRN). Neurons in the early stages of sensory pathways selectively respond to specific features of sensory stimuli. In the rodent vibrissa pathway, thalamocortical neurons in the ventral posteromedial nucleus (VPM) encode kinetic features of whisker movement, allowing stimuli to be encoded by distinctive, temporally precise firing patterns. Therefore, understanding feature selectivity is crucial to understanding sensory processing and perception. However, whether LC activation modulates this feature selectivity, and if it does, the mechanisms through which this modulation occurs, remained largely unknown.

This work investigates LC modulation of thalamic feature selectivity through reverse correlation analysis of single-unit recordings from different stages of the rat vibrissa pathway. LC activation increased feature selectivity, drastically improving thalamic information transmission. This improvement was dependent on both local activation of α -adrenergic receptors and modulation of T-type calcium channels in the thalamus and was not due to LC modulation of trigeminothalamic feedforward or corticothalamic feedback inputs. LC activation reduced thalamic bursting, but this change in thalamic firing mode was not the primary cause of the improved information transmission as tonic spikes with LC stimulation carried three-times the information than tonic spikes without LC stimulation. Modelling confirmed NE regulation of intrathalamic circuit dynamics led to the improved information transmission as LC-NE modulation of either relay or reticular nucleus alone cannot account for the improvement. These results suggest a new sub-dimension within the tonic mode in which brain state can optimize thalamic sensory processing through modulation of intrathalamic circuit dynamics.

Subsequent computational work was then performed to determine exactly how the encoding of sensory information by thalamic relay neurons was altered to allow for an increase in both information transmission efficiency and rate. The results show that LC-NE induced improvements in feature selectivity are not simply due to an increased signal-to-noise ratio, a shift from bursting to tonic firing, or improvements in reliability or precision. Rather, LC-NE-induced modulation of intrathalamic dynamics changed the temporal response structure thalamic neurons used to encode the same stimuli to a new structure that increased the information carried by both tonic and burst spikes. The shift in event times favors optimal encoding, as more events occur at ideal positions, i.e. when the stimulus most closely matches the neuron's feature selectivity. Further, this work analyzed the ability to reconstruct the original stimulus using the evoked spike

trains of multiple neurons and their recovered feature selectivity from an ideal observer point-of-view. The results showed that LC-activation improved the accuracy of this reconstruction, indicating it may improve the accuracy of perception of whisker stimuli.

Finally, to make this work translatable, the use of vagus nerve stimulation (VNS) was investigated as a potential method for minimally invasive enhancement of thalamic sensory processing. The vagus nerve, which runs through the side of the neck, has long been known to have profound effects on brain-state and VNS has been shown to evoke LC firing. This work elucidates the previously uninvestigated short-term effects of VNS on thalamic sensory processing. Similar to direct LC stimulation, VNS enhanced the feature selectivity of thalamic neurons, resulting in a significant increase in the efficiency and rate of stimulus-related information conveyed by thalamic spikes. VNS-induced improvement in thalamic sensory processing also coincided with a decrease in thalamic burst firing, suggesting the same underlying mechanism as the improvements induced with direct LC stimulation.

Table of Contents

List of Figures	iii
Acknowledgements	vii
Introduction	1
Chapter 1: Locus coeruleus activation enhances thalamic feature selectivity via norepinephrine regulation of intrathalamic circuit dynamics	7
Abstract.....	7
Introduction	8
Methods	10
Results	23
Discussion.....	64
Chapter 2: Locus coeruleus activation optimizes the temporal structure ventral posteromedial nucleus neurons use to encode whisker stimuli	71
Abstract.....	71
Introduction	72
Methods	74
Results	79
Discussion.....	100

Chapter 3: Rapid and transient enhancement of thalamic information transmission induced by
vagus nerve stimulation 102

 Abstract..... 102

 Introduction 103

 Methods 106

 Results 112

 Discussion..... 134

Conclusion..... 139

References 144

List of Figures

Figures

Figure 1-1 White noise reverse correlation analysis for estimation of thalamic feature selectivity during different LC activation conditions.....	24
Figure 1-2 LC activation increased VPm feature selectivity and improved information transmission while decreasing firing rate.	28
Figure 1-3 The LC-activation-induced-increase in thalamic information transmission was not due to modulation of the trigeminothalamic feedforward or corticothalamic feedback inputs....	38
Figure 1-4 The LC-activation-induced-increase in thalamic information transmission was dependent on the action of alpha-adrenergic receptors in the thalamus.	45
Figure 1-5 LC activation modulated intrathalamic circuit dynamics.	49
Figure 1-6 LC activation improved thalamic information transmission through modulation of T-type calcium channel activity.....	57
Figure 1-7 Modelling results indicated that NE action in both the VPm and TRN is optimal for enhancing thalamic information transmission.	61
Figure 2-1 Reverse correlation analysis of the encoding of WGN whisker stimulation by VPm neurons under varying levels of LC activation.	81
Figure 2-2 The temporal structure of response events of a VPm neuron to the same stimulus is altered by LC stimulation.....	86
Figure 2-3 LC-activation induced changes in the temporal structure of VPm response events optimizes feature selectivity.	89
Figure 2-4 LC-activation results in reliable response events occurring being more likely to occur at ideal timepoints for encoding feature selectivity.	94

Figure 2-5 Reconstruction of the stimulus from the responses and feature selectivity of a population of VPM neurons is more accurate with LC-activation.....	98
Figure 3-1 Experimental setup.....	113
Figure 3-2 Standard duty cycle VNS improved thalamic feature selectivity and information transmission while suppressing burst firing.....	115
Figure 3-3 Direct LC activation increased thalamic information transmission in ketamine-anesthetized rats.....	122
Figure 3-4 Standard duty cycled VNS induced a fluctuating thalamic sensory processing state.....	125
Figure 3-5 Fast duty cycle and tonic VNS induce similar improvement in thalamic information transmission as observed with standard duty-cycle VNS.....	127
Figure 3-6 Fast duty cycle VNS cause less fluctuation in improvement in thalamic information transmission.....	128
Figure 3-7 The strength of the effects of fast duty-cycle and tonic VNS on improvement of thalamic sensory increase monotonically with increasing VNS amplitude.....	131
Figure 3-8 The strength of the effects of tonic VNS on improvement of thalamic sensory increase monotonically with increasing VNS frequency.....	134
<u>Supplementary Figures</u>	
Supplementary Figure 1-1 Experimental setup and electrophysiology of VPM neurons.....	26
Supplementary Figure 1-2 LC activation increased thalamic feature selectivity and improved information transmission.....	31
Supplementary Figure 1-3 Optogenetic LC stimulation improved thalamocortical information transmission.....	34

Supplementary Figure 1-4 LC activation improved feature selectivity and information transmission in the awake VPm.....	36
Supplementary Figure 1-5 The LC-activation-induced improvement in thalamic information transmission was not inherited from the PrV.....	40
Supplementary Figure 1-6 Inactivation of the barrel cortex by muscimol injection did not alter LC-activation-induced improvements in thalamic information transmission.	42
Supplementary Figure 1-7 The LC-activation-induced increase in thalamic information transmission was due to the action of NE in the thalamus.	47
Supplementary Figure 1-8 LC activation did not significantly alter the precision of spike timing within events for VPm neurons.....	51
Supplementary Figure 1-9 LC activation modulated intrathalamic circuit dynamics by reducing burst firing in both the TRN and VPm.....	53
Supplementary Figure 1-10 LC-activation-induced increases in thalamic information transmission were inversely correlated with changes in bursting rate in awake rats.....	55
Supplementary Figure 1-11 NE effects on the variance of membrane potential and coefficient of variation of inter-spike-intervals for VPm neurons.....	70
Supplementary Figure 2-1 Electronic and optogenetic LC stimulation produced similar effects on thalamic sensory processing.	83
Supplementary Figure 2-2 LC stimulation slightly reduces event rate and response.....	84
Supplementary Figure 2-3 Removed and new events make up almost half of the total events for their respective conditions	87
Supplementary Figure 2-4 LC-activation-induced changes in the temporal structure of VPm response were not artifacts of event threshold.....	92

Supplementary Figure 2-5 LC-activation increased the directionality of feature selectivity for VPM neurons.....	96
Supplementary Figure 2-6 Stimulus reconstruction using the responses and feature selectivity of a population of VPM neurons is more accurate with LC-activation.....	100
Supplementary Figure 3-1 Summary of information transmission rate (bits/s) with and without standard duty-cycle VNS	117
Supplementary Figure 3-2 VNS enhancement of sensory processing is transient with effects vanishing within 60 s of VNS cessation.	119
Supplementary Figure 3-3 Summary of information transmission rate (bits/s) with and without direct LC stimulation.	123

Acknowledgements

I want to thank my mentor and advisor, Qi Wang, for his guidance, insight, and encouragement. Working closely with him over the last five years has provided me with a wealth of knowledge in the field of neuroscience as well as taught me what it takes to successfully manage a lab. I appreciate someone who leads by example, and the tremendous effort Qi Wang has put in these past years has always encouraged me to put forth my best work as well.

I also want to thank my colleagues with whom I worked with in Qi Wang's lab: Yang Liu, Brian Schriver, Yuxiang Liu, Bina Bansinath, Cody Slater, Nicole Moskowitz, Sophia Zhao, Yue Chang, Shreya Narasimhan, Ioannis Deli, Paulo Eduardo, Zeinab Fazlazi, and Kristen Lawlor. In particular, I want to thank Brian Schriver for the work he contributed to our publication in Nature Neuroscience. I would also like that thank Yang Liu for his advice and training when I first entered the lab.

I would like to thank Jose Manuel Alonso for insightful comments on the development of my research at various points of this work. I would also like to thank Paul Sajda for his comments which helped guide this research. Further, I would like to thank my thesis committee members for their participation in my dissertation and comments on my research.

I would like to thank University of Wisconsin-Madison for providing me with a such a wonderful undergraduate collegiate experience that I decided to stay in college another 5 years. I would also like to thank Columbia for warmly accepting me into their prodigious neuroscience community and providing me with the environment and tools necessary to perform impactful research.

I would like to thank the members of the Columbia University staff who have indirectly supported my research and education. Specifically, the Fairchild Rat Facility for their attentive

care of my research animals and the janitorial staff of Engineering Terrace which made sure our lab and office was always clean.

Finally, I would like to thank my family, especially my parents, for their dedicated efforts to ensure I received the best education as well as sharing their passion for learning with me. Without their unwavering support I could not have made it this far.

Introduction

Locus coeruleus

As the sole source of norepinephrine (NE) to the forebrain, the locus coeruleus (LC)-NE system is integral in the modulation of behavioral states such as attention, arousal, and cognition¹⁻⁵. The tonic firing rate of LC neurons has been shown to correlate with arousal level and behavioral performance⁵⁻⁸. Behavioral state has a strong influence on sensory processing, perception, cognition, and behavioral performance⁶⁻¹⁹. As the LC is a major modulator of behavioral state, understanding how the LC modulates the processing of sensory information will provide further elucidation as to how behavioral states impact cognition¹⁴. Functional connectivity of between the LC and thalamus has been shown to covary with level of arousal in humans²⁰, supporting the hypothesis that the LC plays a role in behavioral-state-linked modulation of thalamic sensory processing. Further support for this theory is provided by research which found that LC activity covaried with false alarm rate on a sensory discrimination task⁵.

The LC has been shown to innervate multiple regions along the sensory pathway, including the thalamocortical relay neurons and the thalamic reticular nucleus (TRN)^{21,22}. NE concentration in the brain increases with LC activation²³ and NE has been shown to increase neuronal excitability by reducing resting potassium conductance¹³, suggesting the LC-NE system may produce state-dependent modulatory effects on sensory processing and thus perception. The LC-NE neuromodulatory system has been proposed as ideally situated to not only regulate the processing of individual networks, but the interaction between different networks as well²⁴. NE released from afferent LC neurons has been implicated in modulating the response of sensory neurons to stimuli across multiple sensory modalities²⁴⁻²⁶. LC activation has also been shown to

sharpen thalamocortical processing resulting in a decrease spike latency and jitter in sensorimotor cortex ²⁷.

Previous work in the rat whisker pathway had shown that increased NE in the sensory thalamus resulted in an improved signal-to-noise ratio stemming from spontaneous firing being suppressed at a higher rate than evoked firing ^{28,29}. Another study had found NE had a cell specific effect of either suppression or facilitation of VPM responses evoked by electrical stimulation of the whiskerpad ³⁰. However, how LC activity modulates neural encoding of complex tactile stimuli in the early stage of sensory pathways remains poorly understood.

Ventral posteromedial nucleus

It is well established that thalamic relay nuclei play an essential role in gating the flow of sensory information to the neocortex ³¹⁻³³. Neurons in the early stages of sensory pathways selectively respond to specific features of sensory stimuli ³⁴⁻³⁹. In the whisker pathway, a selective response for specific kinetic features of whisker stimuli is observed in the principal trigeminal nucleus (PrV) neurons ⁴⁰⁻⁴³ which project to the ventral posteromedial nucleus (VPM) ^{35, 44-47}.

The PrV and VPM are both subdivided into subregions, termed barrelettes and barreloids respectively, with each subregion containing neurons primarily encoding information related to stimuli received by a specific whisker, referred to as the primary whisker ⁴¹. Each VPM neuron exhibits a unique, reliable, sub-millisecond temporally specific variance in its spike-rate response to presentations of certain kinetic features within a stimulus ^{46, 48-51}. High dimensional spatiotemporal stimuli, e.g. continuous WGN whisker deflection, can be encoded by a population of thalamocortical neurons ³⁷⁻³⁹ if the activity of each neuron encodes for the presence/absence of a specific subset of all possible kinetic features ^{35, 44-47}. The relative strength of spiking activity of any VPM neuron at any instant then is relative to the strength of the presence of the features in its

feature set in the incoming stimuli ⁴⁶. This encoding process can be modeled using a linear-nonlinear-Poisson cascade model ^{35,47}. Through reverse correlation analysis of the same neuron's responses to multiple presentations of the same white gaussian noise stimulus that neuron's feature selectivity and corresponding nonlinear tuning functions can be recovered. Through subsequently applying information theory, we can analyze the nonlinear tuning function to quantify the efficiency and rate of information transmitted by the neuron about the absence/presence of that feature in the stimulus.

Thalamocortical neurons do not simply act as just a relay, as their output has been shown to exhibit specific transformations of brainstem signals ⁵². Thalamic activity serves as a strong modulator of cortical activity and has been shown to contribute to learning, memory, inhibitory control, decision-making, control of cortical state, and processing of sensory information ^{18, 52, 53}. Indeed, previous work suggests the thalamus plays a critical role in dynamically regulating thalamocortical information transmission ^{32,33,54,55}. The majority of synapses on thalamic cells are from neuromodulatory systems ⁵⁶, suggesting these systems may play a large role in modulating thalamocortical information transmission.

Thalamic reticular nucleus

Thalamocortical information transmission has been proposed to be strongly modulated by the dynamic interplay between thalamic relay nuclei and the GABAergic thalamic reticular nucleus (TRN) ^{55,57}. The TRN has previously been suggested as playing a role in state-dependent modulatory of thalamic sensory processing ⁵⁷⁻⁶² and has been found to be modulated by NE ⁶³. A brief activation of the TRN has been shown to shift the thalamus into bursting mode ⁶⁴. TRN calcium t-channels responsible for bursting have been found to exhibit a slower inactivation rate and a more depolarized activation range relative to calcium t-channels of VPM neurons ⁶⁵,

potentially indicating the TRN as a driver of bursting activity in the VPm^{66,67}. Accordingly, bursts of TRN spikes have been shown to deeply hyperpolarize thalamic relay neurons, de-inactivating t-type calcium channels and priming them for burst firing⁶⁸⁻⁷⁴. TRN neurons are more likely to burst in response to whisker stimulation than VPm neurons⁷⁵ and following a bursting even tend to exhibit an after-burst hyperpolarization period which often primes the calcium t-channels for another burst⁷⁶, taken together these results suggest that TRN inhibitory influence is indeed a strong driver of thalamic bursting activity^{65-67,77}.

The TRN receives topographically aligned input from the VPm, and in return provides topographically aligned inhibitory input to the VPm^{78,79}, creating a thalamoreticular-thalamo loop. Therefore the TRN exerts a strong modulatory influence over the sensory thalamus⁸⁰⁻⁸² in addition to an influence on other TRN neurons through intra-TRN projections⁸³. Previous work found that TRN firing rate strongly increased with increasing whisker stimulation frequency, while the VPm only exhibited a small increase in firing rate⁸⁴. This suggests that the inhibitory influence of the TRN on the VPm may allow for context-dependent optimization of thalamic sensory processing of high frequency whisker movements⁸⁴.

The TRN has been shown to be modulated by the LC-NE system⁶³. TRN induced hyperpolarization of the VPm has been shown to increase signal to noise ratio, as defined by evoked spike count versus spontaneous spike count^{28,29}. Further, it has been shown that LC-activation results in the TRN switching from bursting to tonic firing^{23,85}, with this shift echoed by the VPm^{64,74,86-90}. TRN neurons have been implicated in gain control and rhythm genesis of thalamocortical neurons, but have been previously thought to only minimally impact the overall temporal structure of their response⁸¹. Finally, the TRN has also been shown to contribute to cross-modal modulation of perception⁹¹⁻⁹⁵.

Thalamic firing modes

Thalamic neurons, including both the VPM and TRN, have been shown to exhibit two distinct firing modes, a tonic steady firing rate and calcium t-channel induced burst firing, which arise from unique intrinsic electrical properties, shared across all sensory thalamic regions, that have been proposed to provide a mechanism for behavioral-state-relative regulation of sensory processing⁹⁶⁻¹⁰³. Burst firing, although previously linked with drowsy states, has been shown to be present in the awake healthy thalamus^{10, 104-108}. It has been proposed that tonic spikes may allow for greater stimulus-relevant information to be encoded, facilitating discrimination, whereas bursts have been proposed to provide a wake-up call by allowing thalamocortical neurons to produce a strong depolarizing effect on their cortical targets^{109, 110}. Burst spikes are not inherently less-informative than tonic spikes as bursts have been proposed to encode complimentary information to tonic spikes¹¹¹⁻¹¹⁴ such as transitions of stimuli state¹¹⁵, saliency¹¹⁶, stimulus optimality¹¹⁷, and naturalistic visual features¹¹⁸. Recent research has proposed that bursts may encode information in aspects of their burst spiking pattern¹¹⁹, such as spike count and relative ISI length¹²⁰⁻¹²³.

Tonic spiking has been shown to faithfully transmit high-frequency stimulation which bursting is unable to track¹²⁴. Interestingly, the same increase in ability to track high frequency stimulation has been shown to be more strongly present in depolarized thalamic states¹²⁵. Tonic firing has been shown to allow for a more linear response to stimulus^{110, 126}, potentially allowing for better discriminability between similar stimuli. Here we find tonic spiking has an improved information transmission efficiency and rate, potentially reducing the metabolic cost of thalamocortical sensory processing¹²⁷. Although individual tonic spikes may not provide reliable

cortical activation, arousal-linked increases in population synchrony may act as a compensatory mechanism^{33, 128-131}.

Burst spikes are defined as any two or more spikes occurring with short ISIs that occur following an extended period of quiescence¹³² and have been shown to be present in the awake thalamus^{104-108, 133-105}. Thalamic bursts generate strong, low-latency, thalamocortical transmissions¹³³⁻¹³⁵ as cortical activation is highly dependent on near coincident excitatory input^{32, 136}. These properties may make bursting more ideal for signal detection¹³⁷. However, burst spiking has been shown to exhibit a more all-or-nothing nonlinear response relative to stimuli^{110, 132, 138}, which may decrease discriminability of similar stimulus. Supporting this theory, a trade-off between reliability of information transfer and increased resolution has been linked to burst and tonic modes, respectively¹³⁹.

LC activation increases extracellular thalamic NE concentration²³, which depolarizes thalamic neurons⁸⁸ including the TRN⁸⁵, shifting them from burst to tonic firing^{87, 140}. Recently, optogenetic depolarization of the VPM has also been shown to shift it from a burst to tonic firing mode¹⁴¹. In this work we find activation of the LC-NE resulted in a decrease of bursting activity within the VPM-TRN circuit, supporting the hypothesis that top-down modulation involves thalamoreticular-thalamo interactions⁵⁵.

Chapter 1: Locus coeruleus activation enhances thalamic feature selectivity via norepinephrine regulation of intrathalamic circuit dynamics

Abstract

The locus coeruleus (LC) - norepinephrine (NE) system modulates behavioral state and innervates thalamic relay nuclei and the thalamic reticular nucleus, which gate transmission of information about stimulus features to the neocortex through dynamic interplay. We investigated locus coeruleus (LC) modulation of thalamic feature selectivity through reverse correlation analysis of single-unit recordings from different stages of the rat vibrissa pathway. LC activation increased feature selectivity, drastically improving thalamic information transmission. We found this improvement was dependent on both local activation of α -adrenergic receptors and modulation of T-type calcium channels in the thalamus and was not due to LC modulation of trigeminothalamic feedforward or corticothalamic feedback inputs. LC activation reduced thalamic bursting, but this change in thalamic firing mode was not the primary cause of the improved information transmission as tonic spikes with LC stimulation carried 3-times the information than tonic spikes without LC stimulation. Modelling confirmed norepinephrine (NE) regulation of intrathalamic circuit dynamics led to the improved information transmission as LC-NE modulation of either relay or reticular nucleus alone cannot account for the improvement. These results suggest a new sub-dimension within the tonic mode in which brain state can optimize thalamic sensory processing through modulation of intrathalamic circuit dynamics.

Introduction

Neuromodulatory systems, such as the locus coeruleus (LC) - norepinephrine (NE) system, are integral in the modulation of behavioral state, which in turn exerts a heavy influence on sensory processing, perception, and behavior^{6-9, 13, 15, 19, 142}. For example, arousal, alertness, and locomotion are typically correlated with significantly elevated sensory evoked neural responses⁶⁻⁸. The LC is the primary source of NE to the forebrain^{1, 14}. LC neurons exhibit constant tonic firing at low frequencies, with frequency correlating with arousal level, behavioral performance⁵ and NE concentration in the brain²³. NE has been shown to alter neuronal excitability¹³, suggesting the LC-NE system produces state-dependent modulatory effects on sensory processing and thus perception. The precise mechanism underlying LC-NE modulation of stimulus feature representation in the various stages of sensory processing that underlies perception, however, remains elusive.

It is well established that the thalamus plays an essential role in gating the flow of sensorimotor information to the neocortex, serving to establish cortical representation of the sensorimotor environment^{31-33, 143}. Thalamocortical information transmission has been proposed to be strongly modulated by the dynamic interplay between the thalamic relay nucleus and the GABAergic thalamic reticular nucleus (TRN)^{55, 57}. Neurons in the early stages of sensory pathways selectively respond to specific features of sensory stimuli³⁴⁻³⁶. In the rodent vibrissa pathway, thalamocortical neurons in the ventral posteromedial nucleus (VPM) encode kinetic features of whisker movement³⁵, allowing stimuli to be represented by distinctive, temporally precise firing patterns. Therefore, understanding feature selectivity is crucial to understanding sensory processing and perception¹⁴⁴.

Here we examine the mechanism underlying LC modulation of thalamic feature selectivity and tactile perception through reverse correlation analysis of single-unit recordings taken from different stages of the rat vibrissa pathway while LC activation conditions were systematically varied. Our results demonstrated an LC-activation-induced decrease in firing rate, coupled with an increase in the feature selectivity of VPM neurons, resulting in a dramatic increase in both information transmission efficiency and rate. Surprisingly, recordings in the projecting primary trigeminal nucleus (PrV) revealed LC activity did not modulate PrV sensory transmission, suggesting the observed increase in thalamic feature selectivity was not trivially inherited from the PrV. Inactivation of the cortical column, topographically aligned with the VPM neuron being recorded, did not affect LC-activation-induced improvement of thalamic feature selectivity, indicating corticothalamic feedback did not play a role in this improvement.

LC activation reduced burst firing for both VPM and TRN neurons. However, VPM tonic spikes without LC stimulation carried only ~30% of the information of those during 5 Hz LC stimulation, suggesting LC-activation-improved information transmission was not a result of simply switching thalamic firing to tonic mode. Blocking thalamic T-type calcium channels suppressed burst firing and eliminated LC-activation-induced improvement of thalamic information transmission, indicating this LC-linked improvement results from suppression of T-channel activity by NE regulation of thalamoreticulo-thalamic circuit dynamics. Modelling results showed that NE effects in solely the VPM or TRN could not account for the dramatic increase in information transmission, suggesting that concurrent LC-NE modulation of both the VPM and TRN is necessary to alter intrathalamic circuit dynamics for optimal thalamic information transmission. Furthermore, we found that LC activation also increased perceptual sensitivity for animals performing a tactile discrimination task. This behavioral improvement was blocked when

NE effects in the thalamus were pharmacologically precluded, confirming that LC-NE modulation of the thalamic sensory processing is critical to the LC-activation-induced improvement in perception. These findings reveal a novel mechanism through which LC activation enhances thalamic sensory processing and perceptual performance and suggest a brain-state-dependent sub-dimension in the tonic mode of thalamic firing.

Methods

Surgery

All procedures performed on animals were approved by the Institutional Animal Care and Use Committees at Columbia University, and were conducted in compliance with guidelines of the National Institutes of Health. Adult female Sprague-Dawley rats weighing between 225 and 300 g (Charles River Laboratories, Wilmington, MA) were used.

Acute procedures were similar to those described previously^{33, 145}. Briefly, rats were sedated with 5% vaporized isoflurane in the home cages before being transported to the surgery suite. Once mounted on a stereotaxic frame, the anesthetic was switched to sodium pentobarbital (intravenously through tail vein, initial dose 30 mg/kg) which was maintained throughout the surgery via a syringe pump. Body temperature was maintained at 37 °C by a servo-controlled heating pad and blood-oxygen saturation level and heart rate were continuously monitored using a non-invasive monitor (Nonin Medical Inc, Plymouth, MN). The animal was mounted on a custom-modified stereotaxic frame (RWD Life Science, China) on top of a floating air table in preparation for surgery, subsequent LC microstimulation (electrical or optogenetic), and VPM, PrV, TRN, or Barrel cortex recording. To allow for placement of a microelectrode within the LC, a small craniotomy was made over the left LC. A second craniotomy was then created above either the PrV, VPM, or TRN representing the right whiskers to allow for recording. On a subset of

surgeries, a third craniotomy was made to allow access to the left barrel cortex. Any exposed brain surface was then covered in warm saline, contained by retaining wells created around the craniotomies.

Electrophysiology

Single, sharp tungsten microelectrodes (75 μm in diameter, impedance of $\sim 3\text{ M}\Omega$, FHC Inc, Bowdoin, ME) were used to record extracellular single-unit activity. Extracellular neural signals were referenced to a ground screw in contact with the dura, band-pass filtered (300-8k Hz), and digitized at 40 kHz using a Plexon recording system (OmniPlex, Plexon Inc., Dallas, TX). Spike sorting of single units was performed using commercially available software (Offline Sorter, Plexon Inc.). Only large, easily isolatable units with a minimum refractory period greater than 1 ms and a stable waveform throughout the entire recording were used. A hydraulic micropositioner (David Kopf, Tujunga, CA) allowed for slow, controlled positioning of the electrode adjacent to recorded neurons.

All regions recorded from were targeted using their stereotaxic coordinates as per the rat brain atlas¹⁴⁶. Identification of LC neurons was described in detail previously¹⁴⁵, and was based on LC neuron hallmarks: wide action potential waveform ($>1.8\text{ ms}$) and elevated firing rate in response to paw or tail pinch followed by a brief suppression period (**Fig. 1-1b**). VPM neurons were verified by their depth (greater than 5 mm), response to a half-sinusoid whisker deflection (10 ms duration), and ability to continuously respond to continuous whisker stimulation³³. When recording from the PrV, to ensure we did not accidentally record from the caudally adjacent SpV, the initial penetration was done rostral of the PrV ($\sim 3\text{ mm}$ caudal to lambda), then subsequent penetrations were performed, moving 100 μm posterior between each penetration, until neurons responding to whisker stimulation were found, thus ensuring we were recording from the rostral

edge of the PrV, located away from the SpV⁴². PrV identity was further confirmed by short-latency response to a half-sinusoid whisker deflection (**Supplementary Fig. 1-5a**). TRN neurons were identified by their narrow waveform, and response to a half-sinusoid whisker deflection (**Supplementary Fig. 1-9c**). Barrel cortex columns were mapped based on responses to manual stimulation of individual whiskers.

Following completion of the experiment, in a subset of experiments for each recorded location, the recording system was disconnected and an electrical microstimulator (Multi Channel Systems, Reutlingen, Germany) was used to pass a DC current (200 μ A, 10 s) through the stimulating electrode, at points located every 500 μ m during retraction, which created lesions visible in histology. The animal was subsequently transcardially perfused with 4% paraformaldehyde, and the brain was harvested for post-experiment histological analysis, allowing the recording location to be further confirmed.

Locus coeruleus activation

After electrophysiologically confirming the microelectrode was within the LC, the electrode was disconnected from the recording system and connected to a calibrated electrical microstimulator (S88, Grass Instrument, Warwick, RI), which was then triggered by an xPC target real-time system (Mathworks, MA) running at 1 kHz. During periods of microstimulation-induced LC activation, cathode-leading biphasic current pulses (200 μ s per phase, 60 μ A) were continuously delivered at either 2 or 5 Hz, beginning 5 s before whisker stimulation and lasting throughout the entire period of whisker stimulation for a total length of 165 s. This microstimulation did not produce any visible jaw twitching, indicating current was not spreading to the neighboring mesencephalic trigeminal nucleus¹⁴⁷, thus indicating an accurate stimulation of only the LC without activating surrounding nuclei. 95 s of dead time was inserted between each

stimulation period to allow for the system to return to baseline conditions. For each recording, 3-13 repetitions (average 5.64 ± 0.62 repetitions) of each LC condition were delivered in a random order.

For optogenetic LC activation, during the initial aseptic surgery, a craniotomy was created above the LC and the LC was mapped using the stereotaxic coordinates and electrophysiological characteristics listed above. We then injected a lentivirus, which selectively transfects noradrenergic LC neurons, resulting in these neurons expressing Channelrhodopsin2 (pLenti-PRSx8-hChR2(H134R)-mCherry, the UNC vector core, $\sim 7 \times 10^9$ vp/ml). The virus was injected through a pulled glass pipette using a pico-injector (PLI100, Harvard Apparatus, 100 nl/min). 4 weeks following the initial injection, a second surgery was performed during which a fiber optic cannula (200 μ m diameter, 0.39 NA) was positioned targeting the LC. Animals that were used for acute recordings had the fiber optic cannula simply held in place using a micropositioner, and the acute experiments were performed directly after insertion of the fiber optic cannula. This transfection and fiber optic cannula implantation allowed us to selectively activate the LC using photostimulation (493 nm wavelength). LC stimulation patterns were identical to those used with electrical microstimulation, with the biphasic current pulse simply replaced by a pulse of blue light (20 mW/mm², pulse length 5 ms).

Whisker stimulation

A custom modified galvomotor (galvanometer optical scanner model 6210H, Cambridge Technologies) controlled by a closed-loop system (micromax 67145 board, Cambridge Technology) was used to deliver precise, high-frequency mechanical whisker stimulations. The galvo motor's position was controlled via the same real-time system controlling LC activation and verified by sending the galvo motor's output analog position signal into the same Plexon recording

system used to record the neuron's response. Whiskers were cut to a length of ~10 mm, and inserted into the deflecting arm so that the arm was positioned ~5 mm from the skin. During each block of an LC stimulation condition, following a 5 s period allowing the system to adjust to the new condition, the galvo motor was used to continuously deliver whisker deflection following a signal consisting of 8 repetitions of a 20 s clip of frozen white Gaussian noise (WGN). Two versions of frozen WGN were used (standard deviation of 1.4 or 1.2 degrees deflection) and both yielded similar results. All WGN was low pass filtered (butterworth, 10th order) at 250 Hz (**Supplementary Fig. 1-1b**). This resulted in 24-104 repetitions (average 45.09 ± 4.92) of the WGN during each LC stimulation condition per neuron. As our aim was to determine if neurons had similar or altered responses to identical stimuli under varying conditions of LC activation, the direction of whisker deflection was initially chosen to be the direction which elicited the strongest response from the recorded neuron, then remained fixed for the remainder of the recording.

Pharmacological manipulation

In a subset of experiments, the barrel columns of the barrel cortex were mapped. We then injected muscimol (2 μ L, 5 mM, injected at 100 nl/min) directly into the center of the cortical craniotomy, through a pulled glass pipette (20 μ m opening) using a pico-injector (PLI100, Harvard Apparatus). These injections silenced any responses of barrel cortex neurons, in the injected or adjacent columns, to whisker deflections as evidenced by the disappearance of an LFP response (**Supplementary Fig. 1-6b**). This effectively removed the Barrel cortex's influence on the thalamus as previously shown¹⁴⁸. VPM recordings following these injections were then taken from the barreloid topographically aligned with the barrel column into which we injected muscimol, confirmed by the VPM neurons' response to the same primary whisker.

On another subset of experiments, phentolamine, an α -adrenergic receptor antagonist (~2 μ l 10 mM injected at 100 nl/min), ML-218 Hydrochloride, a selective inhibitor of T-type calcium channels ¹⁴⁹ (~2 μ L, dissolved in DMSO at 25 mM, diluted with saline to 5 mM, injected at 100 nl/min), TTA-P2, another selective inhibitor of T-type calcium channels ¹⁵⁰ (~2 μ l, dissolved in DMSO at 25 mM, diluted with saline to 5 mM, injected at 100 nl/min) or Saline (~2 μ l, as a control, injected at 100 nl/min) was directly injected into the thalamus. This was accomplished using a pulled glass pipette using a pico-injector (PLI100, Harvard Apparatus) for acute animals and through an implanted cannula targeting the thalamus for chronic behaving animals.

Awake, head-fixed electrophysiology

After a post-surgery recovery period, animals were trained to tolerate head fixation. Rats bodies were wrapped in a stretchable sleeve to immobilize and calm them and then placed within a hard tube which provides a sense of safety to the rats ¹⁵¹. The rat's heads were then fixed in place on a stereotaxic frame using the surgically implanted head plate. After recovery from the implantation of a recording window ¹⁵¹, animals were trained daily to tolerate head fixation until all signs of stress during head fixation disappeared (e.g. teeth chattering, porphyrin staining, vocalization, and physically resisting fixation) at which point we began collecting recordings of VPm neurons in response to WGN whisker stimulus under varying levels of LC activation. The recordings were performed in a light and sound attenuation chamber.

Data analysis

Both PrV and VPm neurons can be modeled by the linear-nonlinear-Poisson model (LNP) ^{35, 47}. Therefore, by analyzing the neuron's spiking response to a repeated delivery of a frozen 20 s clip of WGN whisker deflection, we can recover the neurons' feature selectivity in terms of a linear filter set and the corresponding set of nonlinear tuning functions. Here we recovered each

neuron's first significant feature using a spike triggered average (STA) to calculate the average whisker displacement in a 20 ms window preceding a spike. We then used a spike triggered covariance (STC) matrix to recover the remaining set of significant features for any neurons which selectively responded to more than one kinetic feature^{35,47}.

$$STA = \frac{1}{N} \sum_{n=1}^N \vec{S}(t_n)$$

$$STC = \frac{1}{N-1} \sum_{n=1}^N [\vec{S}(t_n) - STA][\vec{S}(t_n) - STA]^T$$

Where t_n is the time of the n^{th} spike, $\vec{S}(t_n)$ is a vector representing the stimulus during the temporal window preceding that spike, and N is the total number of spikes.

Statistical significance of STAs was determined using a bootstrap procedure (1000 bootstrap trials). Any recovered STAs whose amplitude fell within the 99.9 percentile of the bootstrap displacement range were considered insignificant. The significance of STC recovered filters was determined using nested bootstrapping of the eigenvalues corresponding to the STC recovered filters. If a recovered eigenvalue exceeded the 99.9 percentile of its corresponding bootstrap range its filter was considered significant. Neurons without significant feature selectivity were excluded from further analysis.

To quantify the modulation of the recovered features by LC activation, we defined a feature modulation factor as:

$$\text{feature modulation factor} = \frac{\text{control feature} \cdot \text{conditional feature}}{\text{control feature} \cdot \text{control feature}}$$

Alternatively, feature amplitude was also calculated as the peak-to-peak displacement amplitude of the feature.

To estimate the nonlinear tuning functions corresponding to the significant recovered features, we calculated the feature coefficient, defined as the dot product between a neuron's linear filter and a stimulus feature, preceding each spike, from which the probability distribution of feature coefficient values k given a spike (i.e. $\text{Prob}(k|\text{spike})$) was generated. All possible feature coefficients were then found for the stimulus used, calculated by sliding a 20 ms window through the 20 s WGN stimulus, from which a probability distribution of all feature coefficient values (i.e. $\text{Prob}(k)$) was generated. Then by dividing $\text{Prob}(k|\text{spike})$ by $\text{Prob}(k)$, we generated the nonlinear tuning function value which maps firing rate to feature coefficient value.

To quantify the information the spike train conveys about the absence/presence of a feature under varying LC activation conditions, we calculated mutual information between the presence or absence of a feature and the observation of a spike as ^{35, 152}

$$Info(k; spike) = \int dk * Prob(k|spike) * \log_2\left(\frac{Prob(k|spike)}{Prob(k)}\right)$$

Where k is the feature. Information transmission rate, i.e. bits/second, was calculated by multiplying bits/spike by the average firing rate of the neuron in response to WGN stimulus.

To facilitate event based analysis, the peristimulus time histogram (PSTH) of the neuron's responses was binned (2 ms bins) and convolved with an adaptive boxcar kernel ¹⁵³, whose size was dynamically increased from 1 at each bin until the bins spanned by that kernel contained at least 10 spikes, to produce a spike density function (SDF). Any points where the SDF crossed a threshold set at 3 times the mean firing rate was defined as an event, as previously suggested by Mainen and Sejnowski ¹⁵³. Spikes which fell within events were considered reliable while spikes outside of events were classified as unreliable spikes. Precision was calculated as the average standard deviation of spike times within each event.

Burst spiking was defined as any two or more spikes occurring with an ISIs of 4 ms or less and following at least 100 ms of quiescence¹³². Coefficient of variation (CV) of inter-spike-intervals was calculated as the standard deviation of inter-spike-intervals divided by the mean inter-spike-interval.

To test whether reduction in gain or increased reliability could explain the increase in information transmission by VPM neurons in response to LC activation, we computationally manipulated recorded spike trains. To simulate firing rate reduction, we randomly deleted spikes from the 0 Hz LC stimulation spike train, for each recording, until its firing rate matched that of the neurons 5 Hz LC stimulation spike train. To match the reliability of the recorded control VPM spike train to that of the VPM spike train with 5 Hz LC stimulation, we first calculated the reliability of the VPM spike train with 5 Hz LC stimulation. We then estimated the amount of unreliable or reliable spikes which would need to be deleted from the control VPM spike train to make its reliability match that of the 5 Hz LC stimulation VPM spike train. For the majority of recordings (18 of 22 cells), the LC 5 Hz spike train was more reliable than the control VPM spike train, and a set of random chosen unreliable spikes was deleted. However, for a minority of recordings (4 of 22) in which the 5 Hz LC stimulation spike train was less reliable than the control spike train, a randomly selected set of reliable spikes were deleted. Once the computationally modified control VPM spike train was generated, its new reliability was calculated. If the new reliability did not closely match that of the 5 Hz LC stimulation VPM spike train (as changes in event threshold produced by change in firing rate affect reliability calculations), the estimation of unreliable or reliable spikes needed to be removed was incremented or decremented as necessary and the above manipulations were again applied to the original control VPM spike train. This process was repeated until the reliability of computationally modified control spike train was

accurately matched to that of the corresponding 5 Hz LC stimulation spike train. We then calculated the feature selectivity and information transmission of these reliability-matched spike trains. For each recording, the above computational manipulation was performed 1000 times, with information transmission being calculated for each of the 1000 simulations. The average of the resulting 1000 information transmission values was then found and used for each recording.

Modelling

To facilitate our investigation of how the LC-NE system modulates feature selectivity in the VPM we created a simplified model of the intrathalamic circuit consisting of a single VPM and a single TRN neuron (**Fig. 1-7a**). The TRN neuron received excitatory input from the VPM neuron and in turn provided inhibitory input back to the VPM neuron as well as to itself. An integrate-and-fire-or-burst (IFB) model was used to simulate the TRN and VPM neurons.

The input of the VPM model neuron was randomly drawn from a collection of responses of an experimentally recorded PrV neuron to repeated frozen WGN whisker stimulus. For each of the 100 simulated responses of the model neuron, the input was a summation of 5 randomly selected trials from the set of recorded PrV neurons responses. We then performed reverse correlation analysis of the resulting VPM response relative to the WGN whisker stimulus.

The modeled VPM and TRN neurons were constructed using a single compartment that contained 4 membrane currents and 3 synaptic currents.

$$\tau \left(\frac{dV}{dt} \right) = R_m \left(\sum I_{membrane} + \sum I_{synaptic} \right)$$

With time constant $\tau = 5 \text{ ms}$, and membrane resistance $R_m = 20 \text{ M}\Omega$. When the modeled neuron's membrane potential crossed a threshold (spike threshold potential = -40 mV) a spike was generated, and membrane potential was reset (reset potential = -48 mV). Membrane currents were modeled using differential equations and exponential integration methods¹⁵⁴. The magnitude of

each of the membrane currents was calculated at each time step. The current contributed by the potassium leak channel was calculated as: $I_{leak} = G_{leak} * (E_{leak} - V)$ with $E_{leak} = -85$ mV and G_{leak} being set for each neuron at a level which resulted in firing and bursting rates comparable to those observed in-vivo (average G_{leak} of 1.5 ± 0.4 nS for VPM neurons and 4.5 ± 0 nS for TRN neurons). The fast and slow potassium channels currents were calculated as $I_{K_i} = G_K * D_{K_i} * (E_K - V)$ with $E_K = -85$ mV. Where G_K limits the max conductance and is equal to 0.5 nS. Whenever the model neuron fired a spike, potassium conductance factor (D_{K_i}) was increased by a fixed amount A_{K_i} and decayed with time constant T_{K_i} using the following equation:

$$\frac{dD_{K_i}}{dt} = \frac{-D_{K_i} + A_{K_i} * H_K}{T_{K_i}}$$

Where H_K equals 1 if a spike has been fired and 0 at all other times. For the fast potassium channels which acted as a delayed rectifier $A_{K_1} = 20$ and $T_{K_1} = 5$ ms. For the slow potassium channels $A_{K_2} = 5$ and $T_{K_2} = 100$ ms¹⁵⁴. In addition, the neurons have a voltage dependent calcium T-channel¹⁵⁵ with current $I_T = G_T * B_T * H_T * (E_T - V)$ with $E_T = 120$ mV and G_T set for each neuron at a level which resulted in a physiological relevant bursting rate (average G_T of 28 ± 0.5 nS for both TRN and VPM neurons). H_T is set to 1 if the neuron's membrane potential is greater than the hyperpolarization threshold (hyperpolarization threshold = -50 mV) or 0 at all other times. B_T represents the fraction of calcium T-channels that are de-inactivated at any instant and varies between 0 and 1, with value increasing when the neuron's membrane potential is beneath the hyperpolarization threshold as $\frac{dB_t}{dt} = \frac{1-B}{T_{B_{increasing}}}$ and value decreasing when the neuron's membrane potential is above the hyperpolarization threshold as $\frac{dB_t}{dt} = \frac{B}{T_{B_{decreasing}}}$. $T_{B_{increasing}}$ was set to 60 ms which results in ~80% of calcium T-channels being de-inactivated after 100 ms of

hyperpolarization and $T_{B_{decreasing}}$ was set to 3 ms which results in inactivation of 99% of calcium T-channels after 10 ms of membrane potential exceeding the hyperpolarization threshold.

Currents due to PSPs were calculated as: $I_{PSP} = G_{PSP} * C_{PSP} * (E_{PSP} - V)$ where G_{PSP} is the max possible conductance for that PSP type and C_{PSP} represents the strength of conductance relative to the last occurrence of a input spike. For glutamate EPSPs $E_{EPSP} = 0$ mV and G_{EPSP} was set for each neuron at a level which resulted in a physiological relevant firing rate (average $G_{EPSP} = 120 \pm 28$ nS for VPm neurons and 1010 ± 85 nS for TRN neurons). For both GABA_A and GABA_B IPSPs $E_{IPSP} = -85$ mV and G_{IPSP} was set for each neuron at a level which resulted in a physiological relevant firing rate (average GABA_A $G_{IPSP} = 13230 \pm 430$ nS for both VPm neurons and TRN neurons, average GABA_B $G_{IPSP} = 810 \pm 270$ nS for VPm neurons and 550 ± 180 nS for TRN neurons). For all PSPs, the time course of C_{PSP} strength was modeled using dual-alpha function equations¹⁵⁴ with the value of C_{PSP} following a spike calculated as:

$$C_{PSP} = \frac{1}{T_{C_1} - T_{C_2}} * (e^{-\frac{t}{T_{C_1}}} - e^{-\frac{t}{T_{C_2}}})$$

Where t is the time post input spike received. For glutamate EPSPs $T_{C_1} = 0.9$ ms and $T_{C_2} = 2.5$ ms which results in a EPSP with a max conductance at ~1-2 ms following input which decays in ~15 ms. For GABA_A IPSPs $T_{C_1} = 2.5$ ms and $T_{C_2} = 15$ ms which results in an IPSP with a max conductance at ~5 ms following input which decays in ~100 ms. For GABA_B IPSPs $T_{C_1} = 90$ ms and $T_{C_2} = 100$ ms which results in an IPSP with a max conductance at ~205 ms following input which decays in ~300 ms. Whenever a PSP was generated due to an incoming spike, a dual-alpha function as described above was added into the vector of C_{PSP} which allowed for PSPs for to be temporally summed.

These parameters above resulted in a population of VPm neurons on which we can simulate the effects of NE. In this model, to simulate the effects of increased NE concentration, we decreased the strength of the hyperpolarizing leak current to simulate the depolarizing effects of NE (average G_{leak} with NE of 0.5 ± 0.02 nS for both VPm and TRN neurons) and increased the amplitude of post synaptic potentials to simulate NE-induced increased efficacy of neurotransmitters glutamate (average G_{EPSP} with NE = 370 ± 45 nS for VPm neurons and 1610 ± 190 nS for TRN neurons), GABA_A (average GABA_A G_{IPSP} with NE = 15230 ± 200 nS for VPm neurons and 15040 ± 70 nS for TRN neurons), and GABA_B (average GABA_B G_{IPSP} with NE = 23460 ± 660 nS for both VPm and TRN neurons)¹⁵⁴. Further, we were able to use the model to investigate the effects of NE selectively in the VPm only or the TRN only by selectively changing these parameters for the modelled VPm or TRN neuron only. Finally, we also investigated the effects of removing calcium T-channels in the VPm only, TRN only, or both which allowed us to tease apart their effects on thalamic feature selectivity.

Histology

The animal's brain was fixed in 4% paraformaldehyde in phosphate buffered saline (PBS) for up to 24 hours at 4°C and cryoprotected in increasing concentrations of sucrose (10%, 20%, 30%) for 24 hours each or until the tissue sank to the bottom of the container. Brain tissue was sectioned coronally at 20 μm using a freezing microtome (Leica Microsystems Inc, Buffalo Grove, IL). Slides used for confirming electrode placement were either Nissl stained or stained for cytochrome oxidase. Slides used for confirmation of selective lentiviral expression were immunohistochemically analyzed for the expression of tyrosine hydroxylase (expressed in LC neurons, sheep anti-tyrosine hydroxylase primary antibody, EMD Millipore, Alexa Fluor 488 Donkey anti-sheep IgG secondary antibody, Jackson Immuno Research) and mCherry (reporter

protein, Mouse Living Colors DsRed polyclonal primary antibody, Clontech, Alexa Fluor 594 Donkey Anti-Mouse IgG, Jackson Immuno Research). Slides were then coverslipped with Permount mounting medium (ThermoFischer Scientific, Waltham, MA), and were examined using an Olympus CKX41 inverted microscope (Center Valley, PA). Images were stitched together with Microsoft Image Composite Editor.

Statistics

All statistical tests were two-sided. A one-sample Kolmogorov-Smirnov test was used to assess the normality of data before performing statistical tests. If the samples were normally distributed, a paired or unpaired t-test was used. Otherwise, the two-sided Mann-Whitney U-test was used for unpaired samples or the two-sided Wilcoxon signed-rank test for paired samples. Bonferroni correction was used for multiple comparisons. No statistical methods were used to predetermine sample sizes, but our sample sizes are similar to those in prior reports and are typical for the field. Stimulus randomization was generated by using Matlab random number generators. Data collection and analysis were not performed blind to the conditions of the experiments.

Results

We microstimulated the LC of pentobarbital-anesthetized rats while recording single-unit activity from the VPm in the rat vibrissa pathway (**Fig. 1-1a,b,c**). VPm neurons were identified by their depth, waveform, and their reliable, short latency response to a brief deflection of their principal whisker³³ (**Fig. 1-1d**). On a subset of experiments, correct placement of the stimulating and recording electrodes was further confirmed by post mortem histological analysis (**Fig. 1-1c,e**).

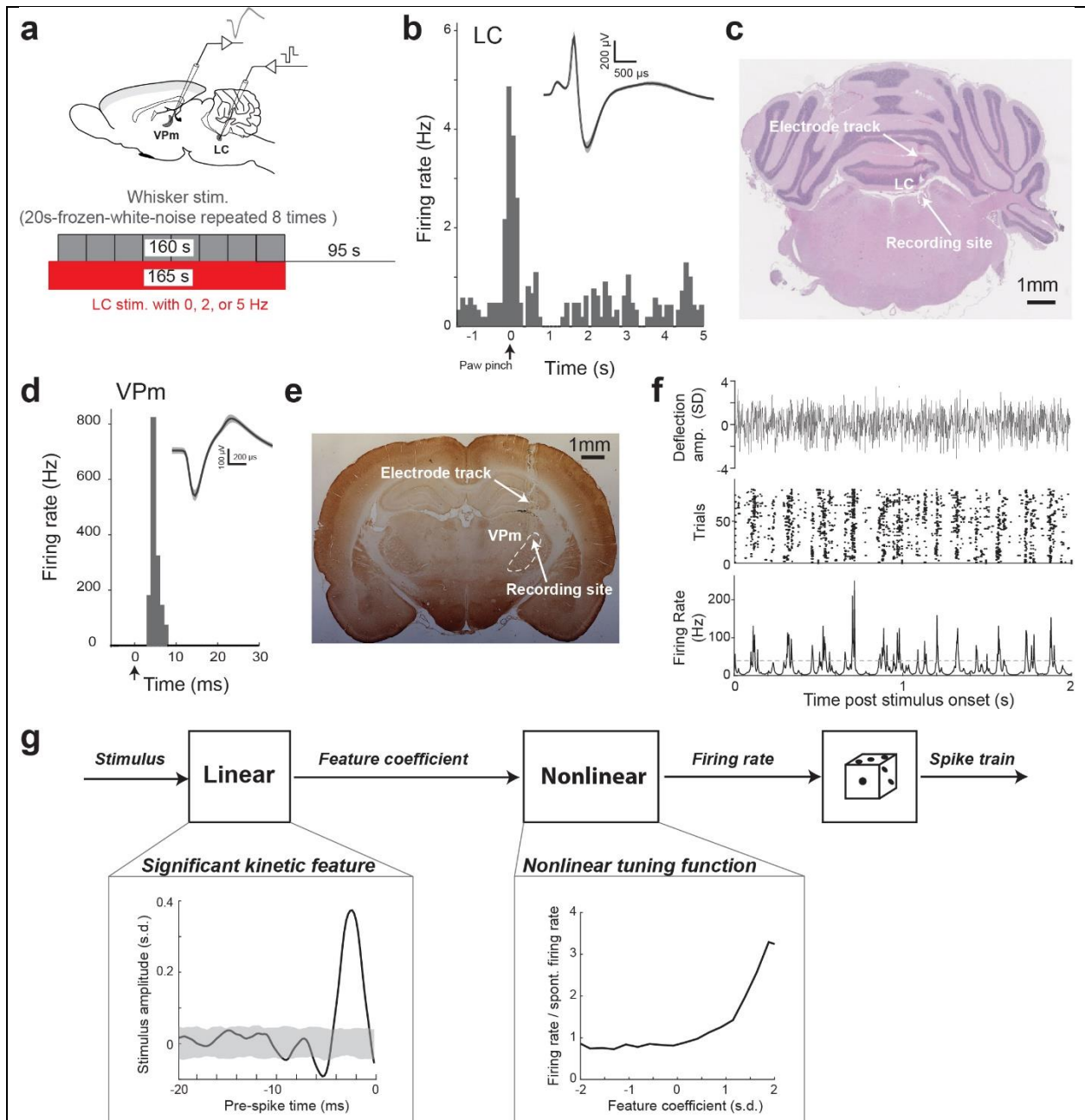


Figure 1-1 White noise reverse correlation analysis for estimation of thalamic feature selectivity during different LC activation conditions.

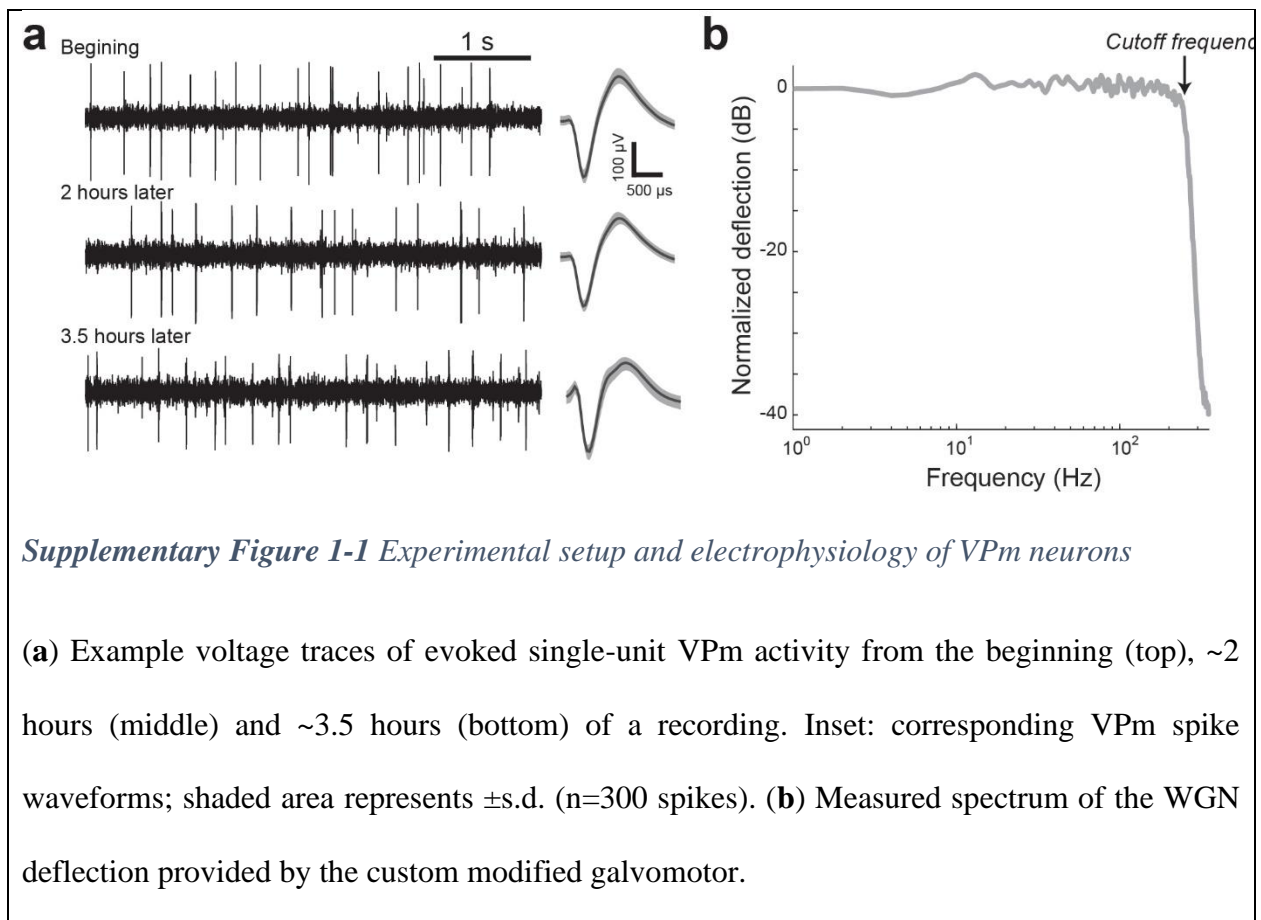
(a) Schematic illustration of experimental setup and stimulation paradigm (adapted from a rat brain atlas). (b) Example of phasic LC firing followed by inhibition in response to tail pinch.

Inset: example wide LC waveform; shaded area represents \pm s.d (n=70 spikes). (c) Histological confirmation of correct electrode placement in the LC. (d) Example single-unit VPm response to a punctate stimulation of its principal whisker, with arrow marking stimulation onset. Inset: example VPm waveform; shaded area represents \pm s.d. (n=48 spikes) (e) Histological confirmation of correct electrode placement in the VPm. (f) Top: clip from one of the frozen WGN stimuli used for reverse correlation analysis. Middle: example raster plot of the response of a VPm neuron to the whisker stimulation shown above. Bottom: spike density function (SDF) created from the response of the same VPm neuron. Dashed line: threshold used to define events. (g) A diagram of the Linear-Nonlinear-Poisson cascade model used to characterize thalamic feature selectivity. Boxes: example kinetic feature and corresponding nonlinear tuning function for a VPm neuron recovered using white Gaussian noise reverse correlation analysis. Shaded area indicates 99.9% confidence interval.

LC activation improved VPm feature selectivity while decreasing firing rate

To study how the LC-NE system modulates the coding properties of thalamic relay neurons and the information they transmit, single-unit extracellular recordings of VPm neurons, lasting ~2 hours, were acquired (**Supplementary Fig. 1-1a**). During these recordings we randomly cycled through 3 varying conditions of LC activation: 0 (i.e. no LC stimulation, as a control), 2, and 5 Hz and mechanically stimulated the principal whisker with low-pass filtered frozen white Gaussian noise (WGN) (**Fig. 1-1a, Supplementary Fig. 1-1b**, see **Methods**). Each LC activation condition was typically repeated multiple times throughout each recording (range of 3-13 repetitions, average of 5.6 ± 0.6 repetitions, mean \pm s.e.m. reported for all results unless otherwise stated). During control conditions, VPm neurons were highly responsive to WGN whisker stimulation,

firing in a reliable, temporally-precise fashion at certain events in the stimulus¹⁵³ (**Fig. 1-1f**). White noise reverse correlation analysis allowed us to recover the kinetic features of the whisker movement to which VPM neurons were significantly sensitive to (**Fig. 1-1g**, see **Methods**). A VPM neuron's feature selectivity can be represented by a set of kinetic features it is sensitive to, coupled with a corresponding set of nonlinear tuning functions which map the neuron's firing rate response versus how similar the stimulus is to that feature (i.e. the 1st and 2nd component of **Fig. 1-1g**, respectively). Consistent with previous work, VPM neurons in our dataset were found to be selective for 1-3 features, with the majority being selective for 2 features³⁵.



When we examined the effects of LC activation on thalamic response to stimuli, we found that LC activation significantly reduced the firing rate of VPM neurons in response to WGN

whisker stimulation (**Fig. 1-2a**). LC activation did not induce changes in the shape of the kinetic features for which a neuron was selective; however, we did find the amplitude of the recovered features increased in an LC-activation-frequency dependent manner (**Fig. 1-2b**). To quantify this modulation of the recovered features we computed the feature modulation factor, defined as the dot product of a feature recovered under control conditions with that from LC activation conditions normalized by the dot product of the control condition recovered feature with itself (see **Methods**). A feature modulation factor of 1 would indicate that LC activation had no effect on the recovered features. If the amplitude of the recovered feature increased, then the feature modulation factor would also increase. Indeed, we found that 2 and 5 Hz LC activation resulted in significantly increased feature modulation factors of approximately 15% and 47%, respectively (**Fig. 1-2c**). We also calculated the average peak-to-peak amplitude of the features that the VPM encoded. Consistent with the feature modulation factor, the average peak-to-peak amplitude also increased with the frequency of LC activation (**Supplementary Fig. 1-2a**).

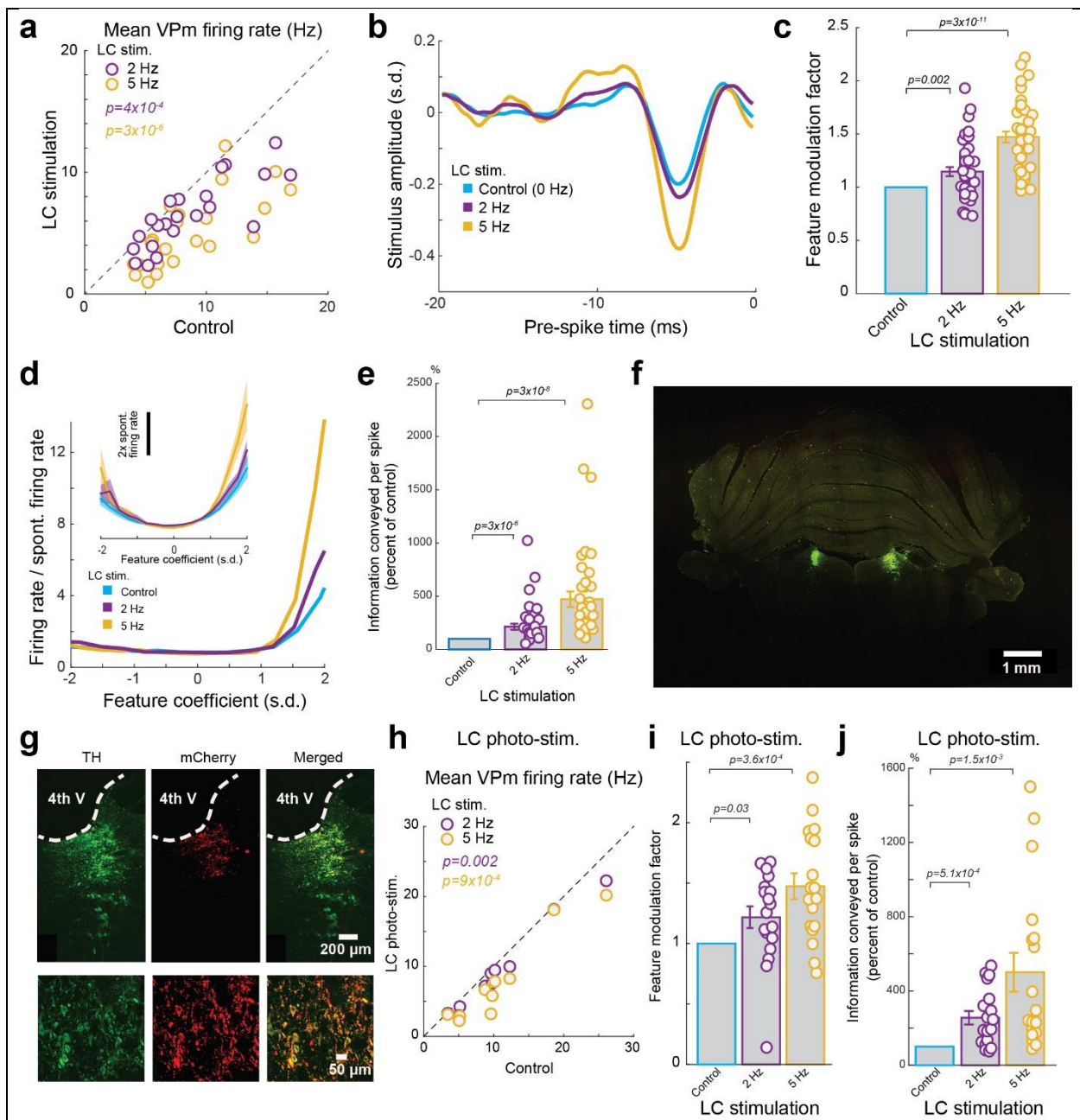


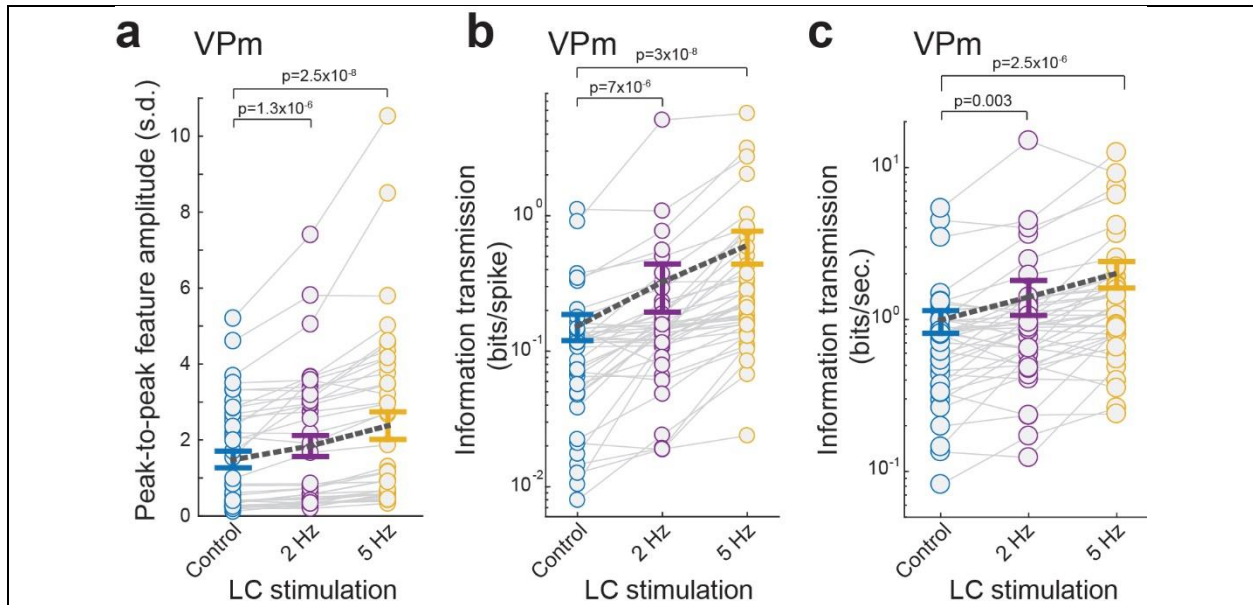
Figure 1-2 LC activation increased VPM feature selectivity and improved information transmission while decreasing firing rate.

(a) Summary of VPM firing rate in response to WGN whisker stimulation under varying LC stimulation conditions. Each circle represents a VPM neuron (8.5 ± 0.8 Hz without LC

stimulation vs 6.4 ± 0.6 Hz during 2 Hz LC stimulation and 5.0 ± 0.6 Hz during 5 Hz LC stimulation, $n=22$ neurons across 15 animals, Bonferroni corrected $\alpha=0.025$, $p=3.1 \times 10^{-4}$ and $=2.5 \times 10^{-6}$ respectively, paired t-test) **(b)** Example of a recovered feature of a VPm neuron under varying LC stimulation conditions. **(c)** Population average of feature modulation factor for VPm neurons under varying LC stimulation conditions. Each circle represents a significant feature (1 without LC stimulation vs 1.15 ± 0.04 during 2 Hz LC stimulation and 1.47 ± 0.05 during 5 Hz LC stimulation, $n=41$ features across 22 neurons across 15 animals, Bonferroni corrected $\alpha=0.025$, $p=1.5 \times 10^{-3}$ and $=2.3 \times 10^{-11}$ respectively, paired t-test). **(d)** Example of nonlinear tuning functions, corresponding to the features shown in Fig. 1-2a. Inset: the population average nonlinear tuning functions under varying LC stimulation conditions. **(e)** Normalized changes in information transmission efficiency (bits/spike) for VPm neurons under varying LC stimulation conditions. Each circle represents a significant feature ($213 \pm 29\%$ of the control during 2 Hz LC stimulation and $469 \pm 72\%$ of the control during 5 Hz LC stimulation, $n=41$ features across 22 neurons across 15 animals, Bonferroni corrected $\alpha=0.025$, $p=2.9 \times 10^{-6}$ and $=2.5 \times 10^{-8}$ respectively, Wilcoxon signed-rank test). **(f)** LC locations were confirmed by tyrosine hydroxylase (TH) immunoreactivity (green) in a coronal section. **(g)** Histological confirmation of selective transgene expressions in LC neurons. Left: TH labels LC neurons. Middle: viral mCherry reporter expression. Right: Merged image shows colocalization. Similar results were observed in 2 other animals. **(h)** Summary of VPm firing rate in response to WGN whisker stimulation under varying LC photostimulation conditions. Each circle represents a VPm neuron (10.9 ± 2.2 Hz without LC stimulation vs 9.4 ± 2.0 Hz during 2 Hz LC stimulation and 7.8 ± 2.0 Hz during 5 Hz LC stimulation, $n=10$ neurons across 4 animals, Bonferroni corrected $\alpha=0.025$, $p=2.1 \times 10^{-3}$ and $=9.0 \times 10^{-4}$ respectively, paired t-test). **(i)** Population average of feature

modulation factor for VPm neurons under varying LC photostimulation conditions. Each circle represents a significant feature (1 without LC stimulation vs 1.22 ± 0.09 during 2 Hz LC stimulation and 1.47 ± 0.11 during 5 Hz LC stimulation, $n=18$ features across 10 neurons across 4 animals, Bonferroni corrected $\alpha=0.025$, $p=2.7 \times 10^{-2}$ and $=3.6 \times 10^{-4}$ respectively, paired t-test).

(j) Normalized changes in information transmission efficiency (bits/spike) for VPm neurons under varying LC photostimulation conditions. Each circle represents a significant feature ($256 \pm 36\%$ of the control during 2 Hz LC stimulation and $501 \pm 104\%$ of the control during 5 Hz LC stimulation, $n=18$ features across 10 neurons across 4 animals, Bonferroni corrected $\alpha=0.025$, $p=5.1 \times 10^{-4}$ and $=1.4 \times 10^{-3}$ respectively, paired t-test). Error bars and shaded area indicate \pm s.e.m.



Supplementary Figure 1-2 LC activation increased thalamic feature selectivity and improved information transmission.

(a) Population average of peak-to-peak amplitude of significant features for VPM neurons under varying LC stimulation conditions (1.49 ± 0.22 without LC stimulation vs 1.85 ± 0.28 during 2 Hz LC stimulation and 2.38 ± 0.36 during 5 Hz LC stimulation, $n=41$ features across 22 neurons across 15 animals, Bonferroni corrected $\alpha=0.025$, $p=1.3 \times 10^{-6}$ and $=2.5 \times 10^{-8}$ respectively, Wilcoxon signed-rank test). Each circle represents a significant feature. (b) Population average of information transmission efficiency (bits/spike) for VPM neurons under varying LC stimulation conditions (0.15 ± 0.03 bits/spike without LC stimulation vs 0.32 ± 0.12 bits/spike during 2 Hz LC stimulation and 0.60 ± 0.16 bits/spike during 5 Hz LC stimulation, $n=41$ features across 22 neurons across 15 animals, Bonferroni corrected $\alpha = 0.025$, $p=6.7 \times 10^{-6}$ and $=2.5 \times 10^{-8}$ respectively, Wilcoxon signed-rank test). Each circle represents a significant feature. (c) Population average of information transmission rate (bits/second) for VPM neurons under varying LC stimulation conditions (0.97 ± 0.17 bits/sec without LC stimulation vs 1.43 ± 0.37

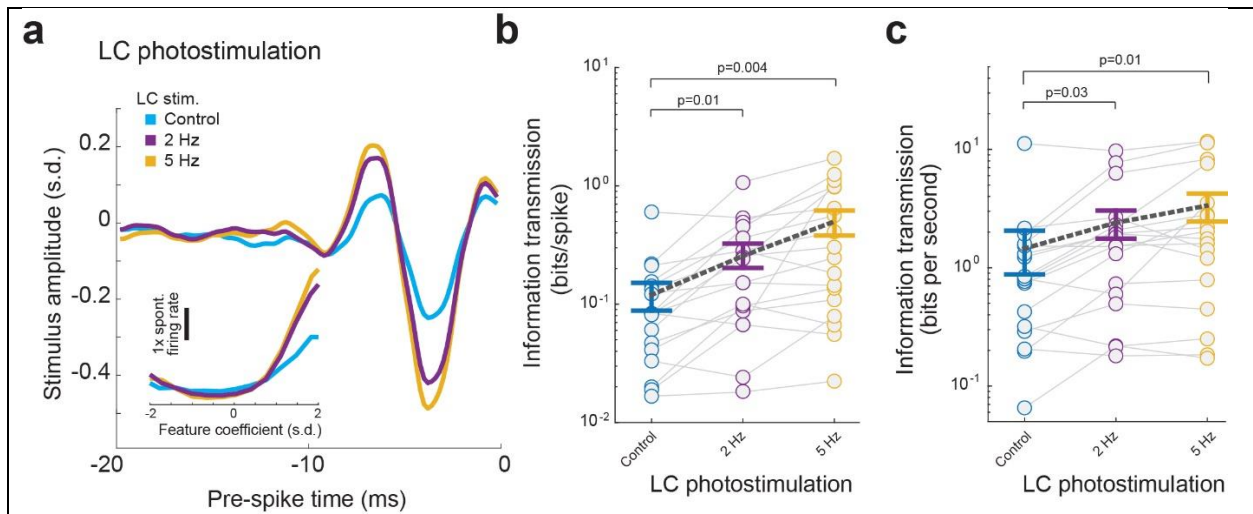
bits/sec during 2 Hz LC stimulation and 2.0 ± 0.40 bits/sec during 5 Hz LC stimulation, $n=41$ features across 22 neurons across 15 animals, Bonferroni corrected $\alpha = 0.025$, $p=3.0 \times 10^{-3}$ and $=2.5 \times 10^{-6}$ respectively, Wilcoxon signed-rank test). Each circle represents a significant feature. Error bars indicate \pm s.e.m.

Having determined the encoded feature set for each VPm neuron under each LC activation condition, we were then able to calculate the corresponding nonlinear tuning functions³⁵. Interestingly, we found that LC activation resulted in a change in the nonlinear tuning functions of VPm neurons that indicated an increased selectivity of response to the specific features encoded by the VPm neurons (**Fig. 1-2d**). This is manifested as an increased firing probability in response to timepoints in the stimulus with relatively high feature coefficient values (**Fig. 1-2d**), as a feature coefficient at any given time point represents the similarity between the stimulus and a feature.

The findings detailed above necessitated an information theoretic approach to quantify the effects of the LC-activation on thalamic transmission of information about the absence/presence of the encoded kinetic feature(s), we use an information theoretic approach^{35, 152}. 2 and 5 Hz LC stimulation drastically increased the information that each spike conveyed (**Fig. 1-2e**, **Supplementary Fig. 1-2b**). Interestingly, despite the reduction in VPm firing rate, LC activation also resulted in over a twofold increase in information transmission rate (bits/sec) (**Supplementary Fig. 1-2c**).

To rule out the possibility that the observed phenomenon was due to inadvertent stimulation of brainstem nuclei adjacent to the LC, optogenetic LC stimulation was used on a subset of experiments. We selectively expressed ChR2 in LC neurons by injecting a lentivirus with a PRSx8 promoter that is selective for LC-NE neurons (pLenti-PRSx8-hChR2(H134R)-mCherry)

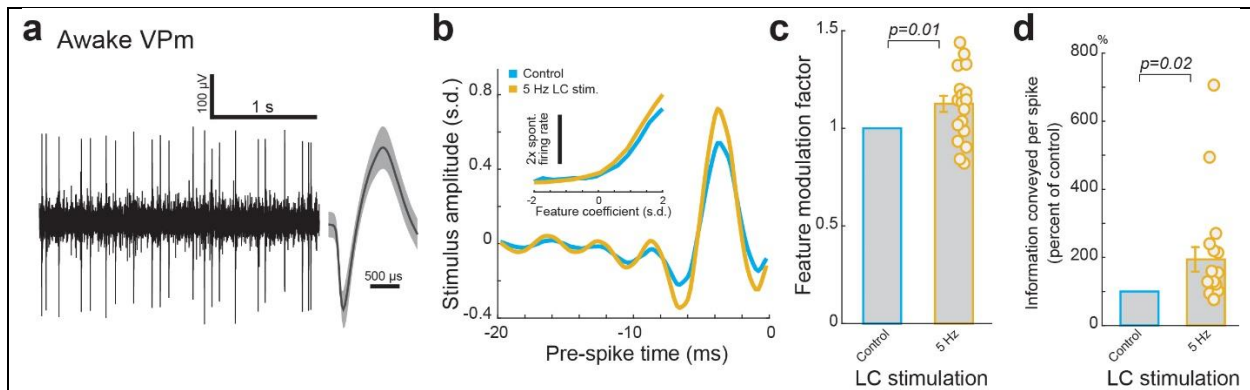
into the LC ¹⁵⁶. On a subset of animals we validated the selectivity with post-mortem immunohistological analysis (**Fig. 1-2f,g**). 4 weeks after transfection, we performed the same white noise reverse correlation experiment while varying LC activation condition, as detailed above, except photostimulation was used to activate the LC instead of electrical microstimulation. These experiments showed an LC-photoactivation-dependent-decrease in firing rate (**Fig. 1-2h**), increase in feature selectivity (**Supplementary Fig. 1-3a**), increase in feature modulation factor (**Fig. 1-2i**), increase in information transmission (**Fig. 1-2j, Supplementary Fig. 1-3b**), and increase in information transmission rate (**Supplementary Fig. 1-3c**). This confirmed the effects of electrical microstimulation of the LC on thalamic information transmission were due to selective LC activation and unlikely due to the inadvertent activation of the adjacent nuclei or axons of passage.



Supplementary Figure 1-3 Optogenetic LC stimulation improved thalamocortical information transmission.

(a) Example of a recovered feature for a VPM neuron under varying LC photostimulation conditions. Inset: the nonlinear tuning functions of the same neuron. (b) Population average of information transmission efficiency (bits/spike) for VPM neurons under varying LC photostimulation conditions (0.12 ± 0.03 bits/spike without LC stimulation vs 0.26 ± 0.06 bits/spike during 2 Hz LC stimulation and 0.50 ± 0.12 bits/spike during 5 Hz LC stimulation, $n=18$ features across 10 neurons across 4 animals, Bonferroni corrected $\alpha=0.025$, $p=0.012$ and $=3.7 \times 10^{-3}$ respectively, paired t-test). Each circle represents a significant feature. (c) Population average of information transmission rate (bits/second) for VPM neurons under varying LC photostimulation conditions (1.47 ± 0.59 bits/sec without LC stimulation vs 2.40 ± 0.64 bits/sec during 2 Hz LC stimulation and 3.34 ± 0.88 bits/sec during 5 Hz LC stimulation, $n=18$ features across 10 neurons across 4 animals, Bonferroni corrected $\alpha=0.025$, $p=0.033$ and $=0.013$ respectively, paired t-test). Each circle represents a significant feature. Error bars indicate \pm s.e.m.

To rule out the possibility that the observed phenomenon was an artifact of anesthesia and to ensure the observed phenomenon generalizes to awake animals, we recorded the response of VPM neurons to repeated WGN stimulation of their principle whisker in awake, head-fixed rats (**Supplementary Fig. 1-4a**, see **Methods**) while modulating LC activity either electrically or optogenetically. In awake rats we found that LC-activation still induced an increase in feature selectivity (**Supplementary Fig. 1-4b**) as well as an increase in the feature modulation factor (**Supplementary Fig. 1-4c**). Further we observed a similar LC-activation-induced increase in information transmission (**Supplementary Fig. 1-4d**), confirming that LC activation enhancing thalamic information transmission is a general phenomenon. Although LC-activation-induced improvements in information transmission were present in the awake thalamus, these improvements were less drastic when compared to that observed in anesthetized rats. This less-strong improvement of information transmission during awake states was probably due to interplay between the LC-NE system and other neuromodulatory systems which were dampened by anesthesia but were active in the awake state.



Supplementary Figure 1-4 LC activation improved feature selectivity and information transmission in the awake VPM.

(a) Example single-unit activity in awake VPM. Shaded area represents \pm s.d. ($n=500$ spikes) (b) Example of a recovered feature for a VPM neuron with and without LC stimulation. Inset: corresponding nonlinear tuning functions. (c) Population average of feature modulation factor for VPM neurons with and without LC stimulation in awake rats (1 without LC stimulation vs 1.11 ± 0.04 during 5 Hz LC stimulation, $n=19$ features across 13 neurons across 4 animals, $\alpha=0.05$, $p=0.013$, paired t-test). Each circle represents a significant feature. (d) Normalized changes in information transmission efficiency (bits/spike) for VPM neurons with and without LC stimulation in awake rats ($194 \pm 36\%$ of the control during 5 Hz LC stimulation, $n=19$ features across 13 neurons across 4 animals, $\alpha=0.05$, $p=1.8 \times 10^{-3}$, paired t-test). Each circle represents a significant feature. Error bars indicate \pm s.e.m.

Improved thalamic feature selectivity and information transmission by LC activation was not inherited from the projecting trigeminal input

Although LC activation resulted in a strong modulation of VPM neurons' coding properties, it was not clear if the mechanism underlying this modulation was occurring directly in

the thalamus, or at previous stages of the pathway. To investigate this possibility, we recorded single-unit activity in the principal trigeminal nucleus (PrV) of the vibrissa system, which projects and provides direct feedforward excitatory input to the VPM in the vibrissa pathway (**Fig. 1-3a, Supplementary Fig. 1-5a**).

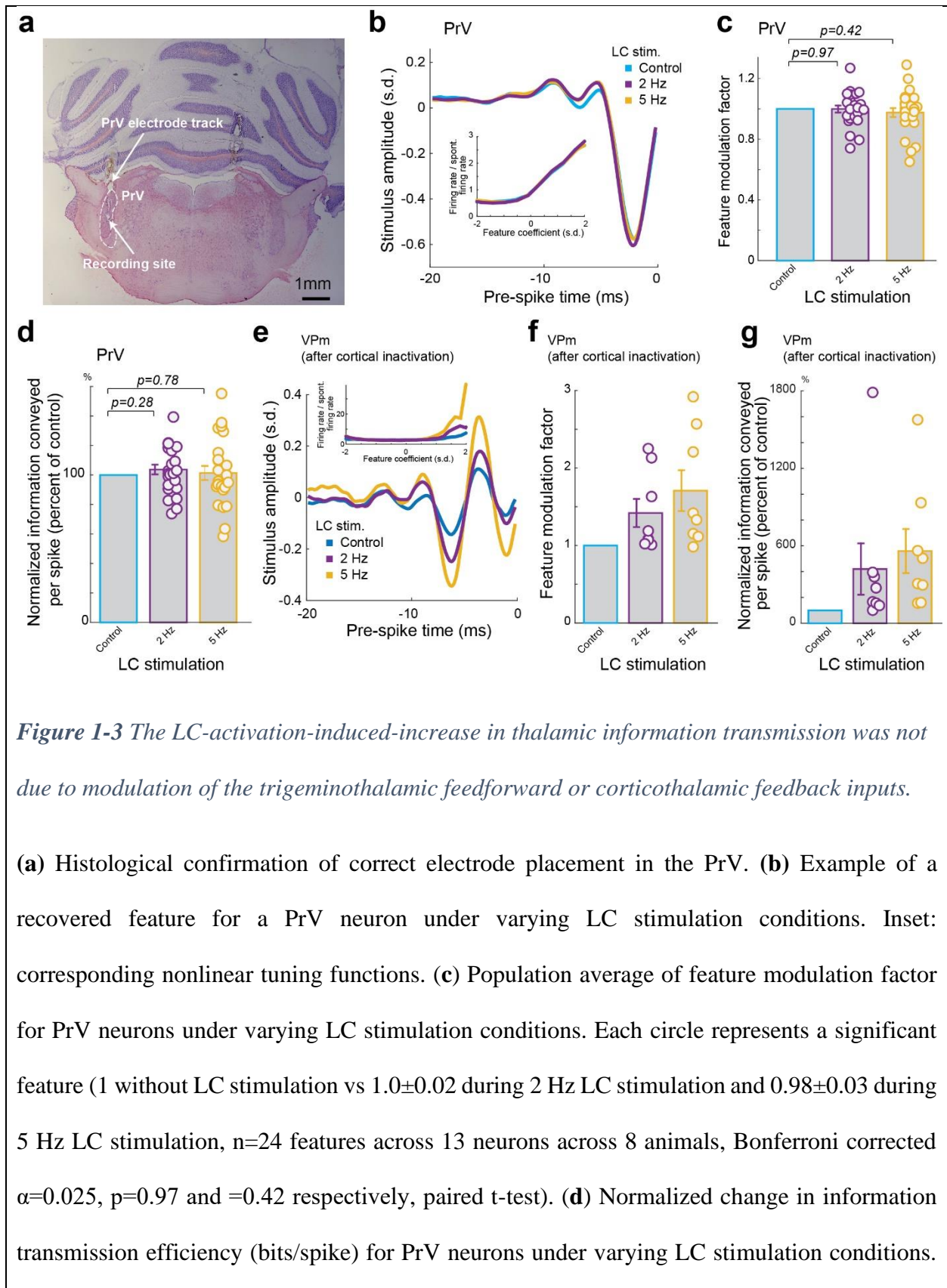
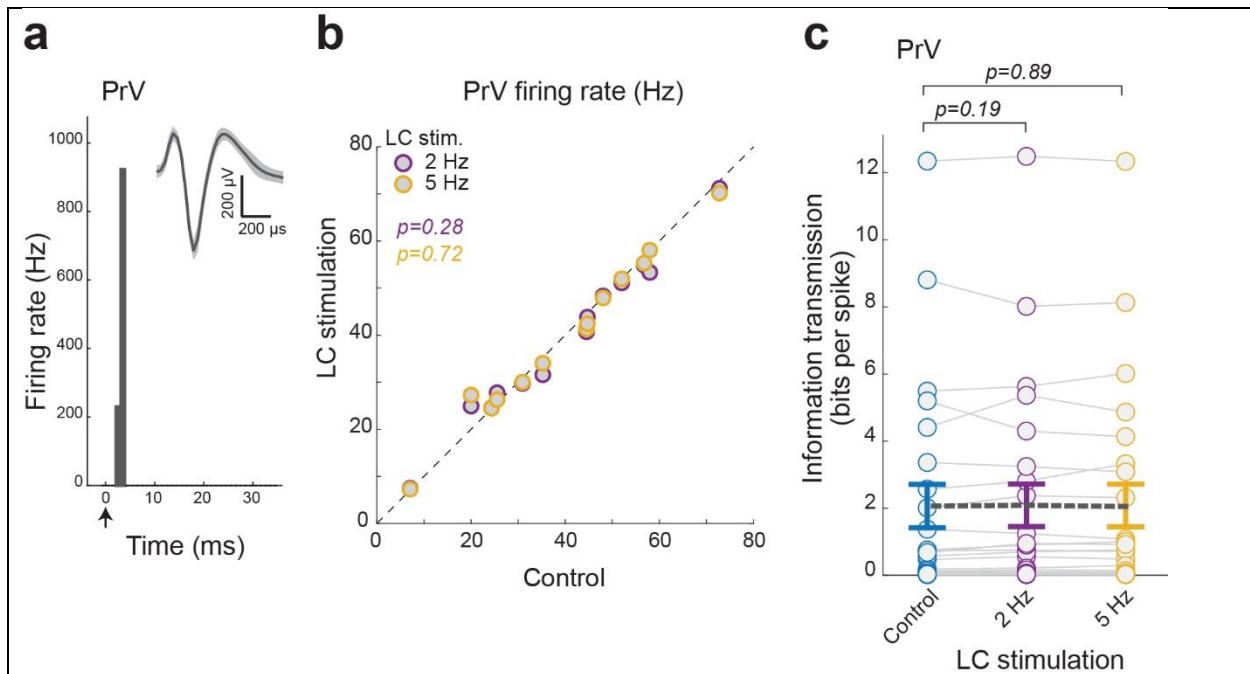


Figure 1-3 The LC-activation-induced-increase in thalamic information transmission was not due to modulation of the trigeminothalamic feedforward or corticothalamic feedback inputs.

(a) Histological confirmation of correct electrode placement in the PrV. **(b)** Example of a recovered feature for a PrV neuron under varying LC stimulation conditions. Inset: corresponding nonlinear tuning functions. **(c)** Population average of feature modulation factor for PrV neurons under varying LC stimulation conditions. Each circle represents a significant feature (1 without LC stimulation vs 1.0 ± 0.02 during 2 Hz LC stimulation and 0.98 ± 0.03 during 5 Hz LC stimulation, $n=24$ features across 13 neurons across 8 animals, Bonferroni corrected $\alpha=0.025$, $p=0.97$ and $=0.42$ respectively, paired t-test). **(d)** Normalized change in information transmission efficiency (bits/spike) for PrV neurons under varying LC stimulation conditions.

Each circle represents a significant feature ($104 \pm 3\%$ of the control during 2 Hz LC stimulation and $101 \pm 5\%$ of the control during 5 Hz LC stimulation, $n=24$ features across 13 neurons across 8 animals, Bonferroni corrected $\alpha=0.025$, $p=0.28$ and $=0.78$ respectively, paired t-test). (e) Example of a recovered feature for a VPM neuron, post cortical inactivation, under varying LC stimulation conditions. Inset: corresponding nonlinear tuning functions. (f) Population average of feature modulation factor for VPM neurons, post cortical inactivation, under varying LC stimulation conditions. Each circle represents a significant feature (1 without LC stimulation vs 1.42 ± 0.18 during 2 Hz LC stimulation and 1.71 ± 0.26 during 5 Hz LC stimulation, $n=8$ features across 7 neurons across 4 animals, Bonferroni corrected $\alpha=0.025$, $p=0.055$ and $=0.031$ respectively, paired t-test). (g) Population average of information transmission efficiency (bits/spike) for VPM neurons, post cortical inactivation, under varying LC stimulation conditions. Each circle represents a significant feature ($430 \pm 199\%$ of the control during 2 Hz LC stimulation and $560 \pm 171\%$ of the control during 5 Hz LC stimulation, $n=8$ features across 7 neurons across 4 animals, Bonferroni corrected $\alpha=0.025$, $p=0.15$ and $=0.031$ respectively, paired t-test). Error bars indicate \pm s.e.m.

Interestingly, we found that LC activation did not have any significant effect on the feature selectivity of PrV neurons (**Fig. 1-3b**). Further we observed no LC-activation-induced difference in PrV firing rate (**Supplementary Fig. 1-5b**) or change in feature modulation factor (**Fig. 1-3c**). Consequently, there was no LC-activation-induced increase in information transmission efficiency (**Fig. 1-3d, Supplementary Fig. 1-5c**).



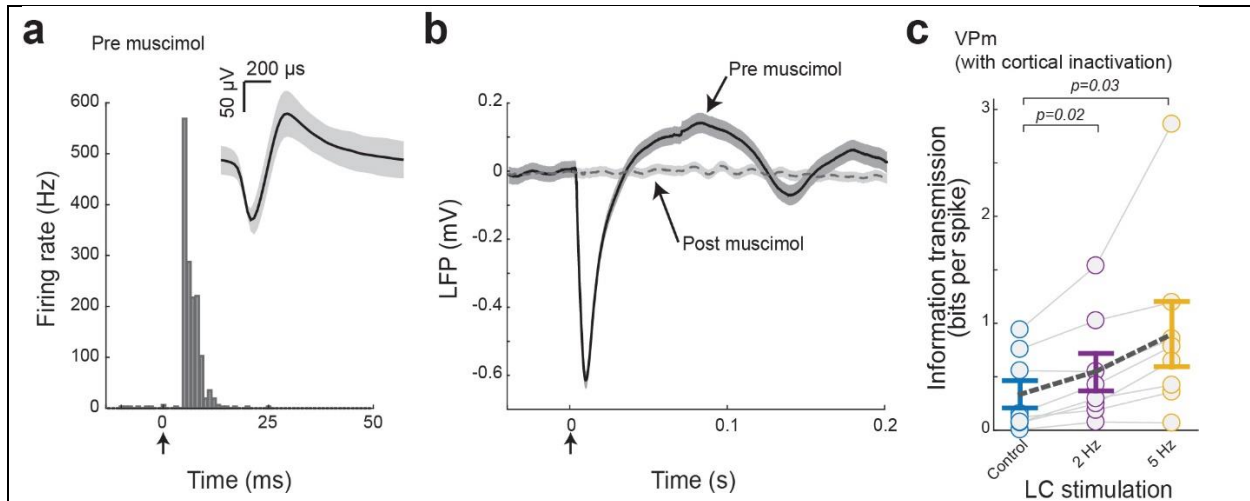
Supplementary Figure 1-5 The LC-activation-induced improvement in thalamic information transmission was not inherited from the PrV.

(a) Example single-unit PrV response to a punctate stimulation of its principal whisker, with arrow marking stimulation onset. Inset: example PrV waveform; shaded area represents \pm s.d. (n=56 spikes) (b) PrV firing rate in response to WGN whisker stimulation under varying LC stimulation conditions (40 ± 5 Hz without LC stimulation vs 39 ± 5 Hz during 2 Hz LC stimulation and 40 ± 5 Hz during 5 Hz LC stimulation, n=13 neurons across 8 animals, Bonferroni corrected $\alpha=0.025$, $p=0.28$ and $=0.72$ respectively, paired t-test). Each circle represents a PrV neuron. (c) Population average of information transmission efficiency (bits/spike) for PrV neurons under varying LC stimulation conditions (2.06 ± 0.65 bits/spike without LC stimulation vs 2.09 ± 0.64 bits/spike during 2 Hz LC stimulation and 2.08 ± 0.63 bits/spike during 5 Hz LC stimulation, n=24 features across 13 neurons across 8 animals, Bonferroni corrected $\alpha=0.025$, $p=0.19$ and

=0.89 respectively, Wilcoxon signed-rank test). Each circle represents a significant feature. Error bars indicate \pm s.e.m.

LC-activation-induced improvement of thalamic feature selectivity and information transmission was not due to corticothalamic feedback

Previous studies have found that the deep cortical layers send dense projections to the thalamus¹⁵⁷. As the LC also innervates the cortex, it could be possible that LC activation alters corticothalamic feedback in a way which results in an increase in the information transmitted by thalamocortical neurons. To test the extent to which corticothalamic feedback plays a role in the LC-activation-induced increase in VPM feature selectivity, we silenced the cortex in a subset of rats to remove its possible influence on LC-activation-induced changes in thalamic processing. We initially mapped the barrel columns (**Supplementary Fig. 1-6a**), then injected muscimol into the center of the cortical craniotomy. In two animals we confirmed intracortical muscimol silenced the cortex as we observed no evoked spiking activity or LFP response in the central column nor adjacent columns (**Supplementary Fig. 1-6b**). We then performed single-unit recording in the VPM barreloid topographically aligned with the barrel column in which the injection was made.



Supplementary Figure 1-6 Inactivation of the barrel cortex by muscimol injection did not alter LC-activation-induced improvements in thalamic information transmission.

(a) Example single-unit barrel cortex response to a punctate stimulation of its principal whisker, with arrow marking stimulation onset. Inset: example barrel cortex waveform; shaded area represents \pm s.d. ($n=1398$ spikes) **(b)** Example average LFP response in barrel cortex to a punctate stimulation of the cortical barrel column's principal whisker before and after muscimol injection. Shaded area represents \pm s.e.m ($n=313$ and $n=308$ trials respectively). **(c)** Population average of information transmission efficiency (bits/spike) for VPM neurons, post cortical inactivation, under varying LC stimulation conditions (0.33 ± 0.13 bits/spike without LC stimulation vs 0.54 ± 0.18 bits/spike during 2 Hz LC stimulation and 0.90 ± 0.31 bits/spike during 5 Hz LC stimulation, $n=8$ features across 7 neurons across 4 animals, Bonferroni corrected $\alpha=0.025$, $p=0.017$ and $p=0.028$ respectively, paired t-test). Each circle represents a significant feature. Error bars indicate \pm s.e.m.

Interestingly, we found that cortical inactivation also had no effects on the LC-activation-induced increase in thalamic feature selectivity and information transmission. We still observed

the same LC-activation-induced increase in feature sensitivity following muscimol injection to the cortex (**Fig. 1-3e**) as well as an LC-activation-induced increase in feature modulation factors (**Fig. 1-3f**) and increase in information transmission (**Fig. 1-3g, Supplementary Fig. 1-6c**).

LC-activation-induced improvement of thalamic information transmission resulted from the action of NE on alpha-adrenergic receptors in the thalamus

As the LC projects to other neuromodulatory systems¹⁵⁸, it is unclear whether direct (NE action in the thalamus), or indirect (action of other neuromodulators indirectly released by LC activation) effects of LC activation, or a combination of both, was responsible for the improved thalamic information transmission. To test the extent to which noradrenergic receptor activation was involved in enhancing thalamic information transmission by LC activation, we blocked alpha-adrenergic receptors in the thalamus by injecting phentolamine¹⁵⁹. LC electrode position was confirmed by a VPm recording prior to phentolamine injection that showed an LC-activation dependent increase in feature selectivity (**Fig. 1-4a**). Prior to phentolamine injection, the same trend of increase was present for feature modulation factors (**Fig. 1-4b**) and information transmission (**Fig. 1-4d, Supplementary Fig. 1-7a**).

We then slowly injected the alpha-adrenergic receptor antagonist phentolamine (2 μ L, 100 nl/min, 10 mM) into the thalamus. Following phentolamine injection into the thalamus, LC-activation no longer had any effect on feature selectivity (**Fig. 1-4c**), indicating that alpha-adrenergic receptor activation is primarily responsible for the observed effects of LC-activation on thalamic processing. With phentolamine we saw no LC-stimulation-induced change in the feature modulation factor (**Fig. 1-4b**), and no change in information transmission (**Fig. 1-4d, Supplementary Fig. 1-7b**). Moreover, we tested the effects of LC activation following saline injection and found the same LC-activation-induced improvement of information transmission in

the VPm, confirming that the disappearance of LC effects on thalamic information processing with phentolamine injection was not due to possible damage inflicted by the injection (**Supplementary Fig. 1-7c**).

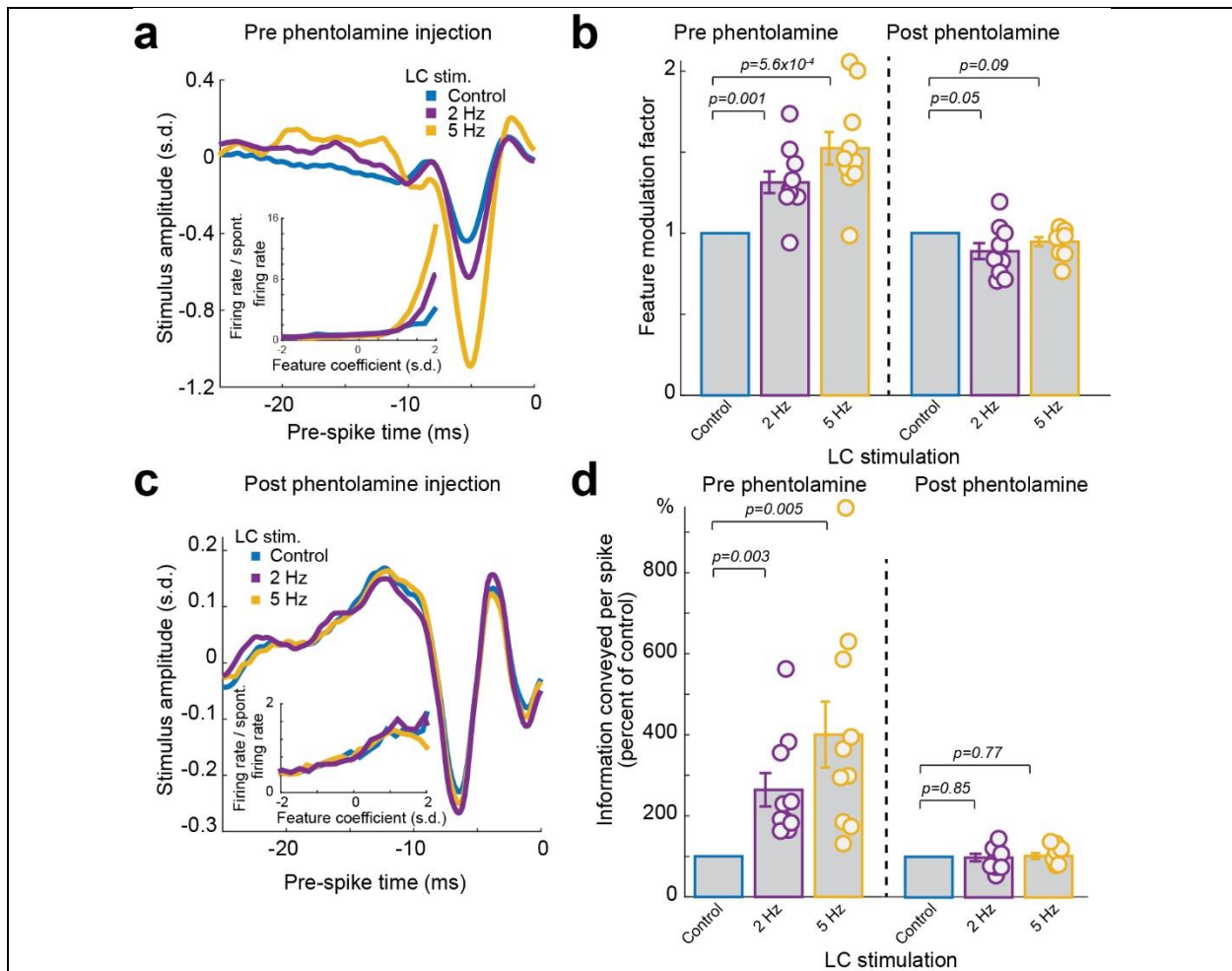
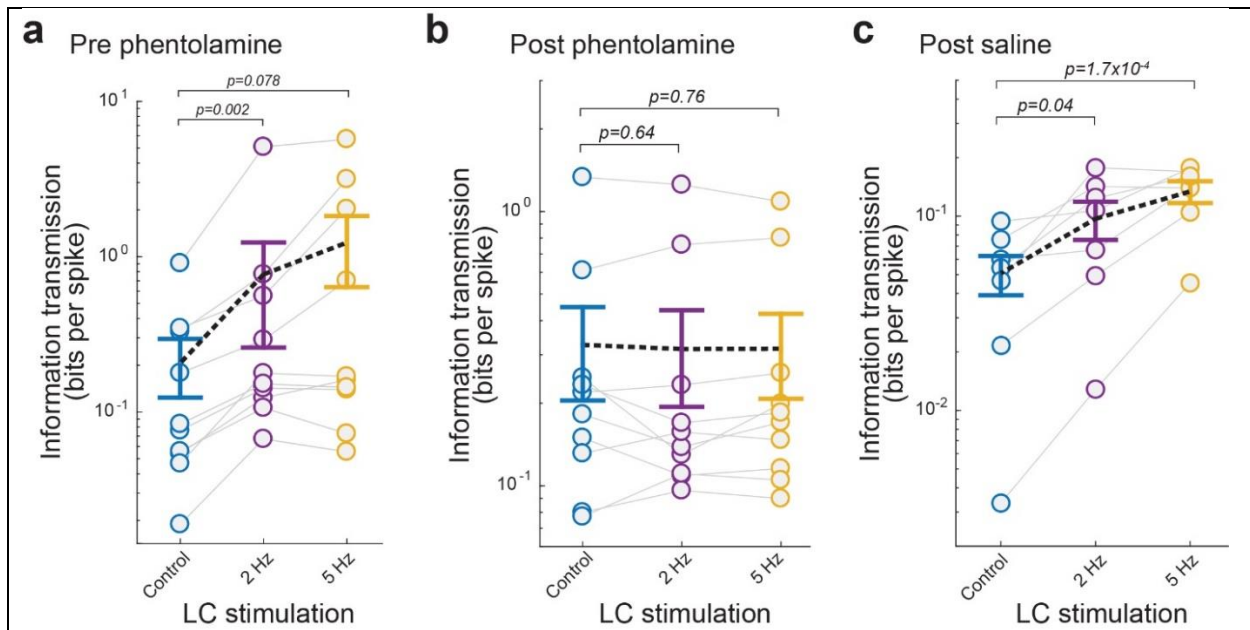


Figure 1-4 The LC-activation-induced-increase in thalamic information transmission was dependent on the action of alpha-adrenergic receptors in the thalamus.

(a) Example of recovered features for a VPM neuron, prior to phentolamine injection, under varying LC stimulation conditions. Inset: corresponding example nonlinear tuning functions.

(b) Population average of feature modulation factor under varying LC stimulation conditions. Each circle represents a significant feature. Left: VPM neurons, prior to phentolamine injection (1 without LC stimulation vs 1.31 ± 0.07 during 2 Hz LC stimulation and 1.52 ± 0.10 during 5 Hz LC stimulation, $n=10$ features across 6 neurons across 4 animals, Bonferroni corrected $\alpha=0.025$,

$p=1.1 \times 10^{-3}$ and $=5.6 \times 10^{-4}$ respectively, paired t-test). Right: VPm neurons, post phentolamine injection (1 without LC stimulation vs 0.89 ± 0.05 during 2 Hz LC stimulation and 0.95 ± 0.03 during 5 Hz LC stimulation, $n=10$ features across 5 neurons across 4 animals, Bonferroni corrected $\alpha=0.025$, $p=0.05$ and $=0.09$ respectively, paired t-test). (c) Example of a recovered feature for a VPm neuron, post phentolamine injection, under varying LC stimulation conditions. Inset: corresponding nonlinear tuning functions. (d) Population average of information transmission efficiency (bits/spike) under varying LC stimulation conditions. Left: VPm neurons, prior to phentolamine injection ($264 \pm 41\%$ of the control during 2 Hz LC stimulation and $401 \pm 81\%$ of the control during 5 Hz LC stimulation, $n=10$ features across 6 neurons across 4 animals, Bonferroni corrected $\alpha=0.025$, $p=3.1 \times 10^{-3}$ and $=5.0 \times 10^{-3}$ respectively, paired t-test). Right: VPm neurons, post phentolamine injection. Each circle represents a significant feature ($98 \pm 9\%$ of the control during 2 Hz LC stimulation and $102 \pm 7\%$ of the control during 5 Hz LC stimulation, $n=10$ features across 5 neurons across 4 animals, Bonferroni corrected $\alpha=0.025$, $p=0.84$ and $=0.77$ respectively, paired t-test). Error bars indicate \pm s.e.m.



Supplementary Figure 1-7 The LC-activation-induced increase in thalamic information transmission was due to the action of NE in the thalamus.

(a) Population average of information transmission efficiency (bits/spike) for VPM neurons, prior to phentolamine injection, under varying LC stimulation conditions (0.21 ± 0.09 bits/spike without LC stimulation vs 0.75 ± 0.49 bits/spike during 2 Hz LC stimulation and 1.23 ± 0.60 bits/spike during 5 Hz LC stimulation, $n=10$ features across 6 neurons across 4 animals, Bonferroni corrected $\alpha=0.025$, $p=0.002$ and $=0.076$, respectively, paired t-test). Each circle represents a significant feature. (b) Population average of information transmission efficiency (bits/spike) for VPM neurons, post phentolamine injection, under varying LC stimulation conditions (0.33 ± 0.12 bits/spike without LC stimulation vs 0.32 ± 0.12 bits/spike during 2 Hz LC stimulation and 0.32 ± 0.11 bits/spike during 5 Hz LC stimulation, $n=10$ features across 5 neurons across 4 animals, Bonferroni corrected $\alpha=0.025$, $p=0.64$ and $=0.76$ respectively, paired t-test). Each circle represents a significant feature. (c) Population average of information transmission efficiency (bits/spike) for VPM neurons, post saline injection, under

varying LC stimulation conditions (0.05 ± 0.01 bits/spike without LC stimulation vs 0.10 ± 0.02 bits/spike during 2 Hz LC stimulation and 0.13 ± 0.02 bits/spike during 5 Hz LC stimulation, $n=7$ features across 4 neurons across 4 animals, Bonferroni corrected $\alpha=0.025$, $p=0.037$ and $=1.7 \times 10^{-4}$ respectively, paired t-test). Each circle represents a significant feature. Error bars indicate \pm s.e.m.

Increased information transmission did not result from gain reduction or changes in signal-to-noise ratio

When investigating how the LC-activation-induced change in VPm response leads to increased feature selectivity and information transmission, we first asked whether suppression of VPm firing rate could provide an explanation. To test this, a computational control was conducted in which we randomly deleted spikes from the control VPm spike raster until the average firing rate of each spike raster was equalized to their corresponding 5 Hz LC stimulation spike raster's firing rate. We then computed the information that the firing-rate-matched spike train transmitted and found that simulated suppression of firing rate did not result in any significant increase in information transmission (**Fig. 1-5a**), ruling out gain reduction as a mechanism.

All VPm neurons produced a reliable response to specific kinetic features occurring at specific temporal locations in the WGN stimulus, resulting in many temporal response events present in the generated SDF. These events, defined by thresholding the SDF of the neurons response (**Fig. 1-1f**, see **Methods**), allowed us to quantify the reliability and precision of neural responses¹⁵³. We found that LC activation increased reliability (**Fig. 1-5b**), but not precision (**Supplementary Fig. 1-8**).

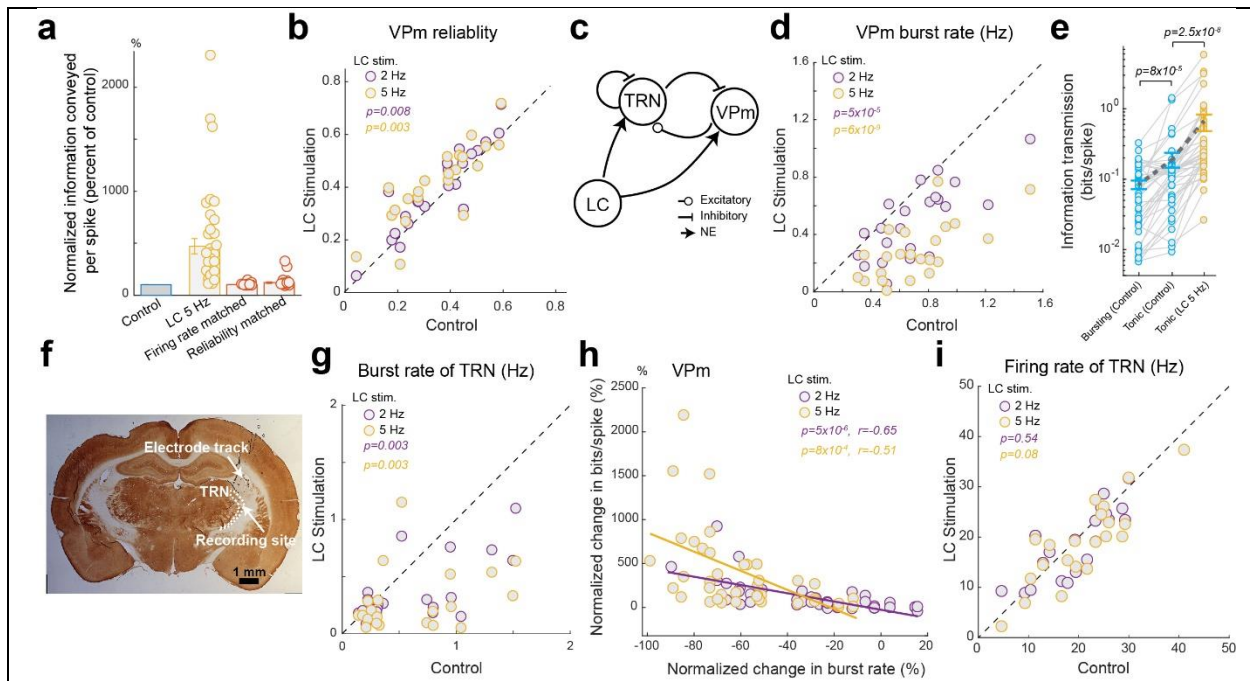


Figure 1-5 LC activation modulated intrathalamic circuit dynamics.

a) Population average of information transmission efficiency (bits/spike) for VPM neurons under varying LC stimulation conditions compared with simulated reductions in firing rate ($102 \pm 1\%$ of the control, $n=41$ features across 22 neurons across 15 animals, $\alpha=0.05$, $p=0.55$, Wilcoxon signed-rank test) and increases in reliability ($121 \pm 7\%$ of the control, $n=41$ features across 22 neurons across 15 animals, $\alpha=0.05$, $p=3.7 \times 10^{-6}$, Wilcoxon signed-rank test). **(b)** LC activation significantly improved the reliability of the VPM response to WGN whisker stimulation. Each circle represents a VPM neuron (0.35 ± 0.03 without LC stimulation vs 0.39 ± 0.03 during 2 Hz LC stimulation and 0.41 ± 0.03 during 5 Hz LC stimulation, $n=22$ neurons across 15 animals, Bonferroni corrected $\alpha=0.025$, $p=8.0 \times 10^{-3}$ and $=2.6 \times 10^{-3}$ respectively, paired t-test). **(c)** Diagram of the reciprocal connection between the VPM and TRN, both of which are recipient of LC projections. **(d)** Summary of VPM burst rate in response to WGN whisker stimulation under varying LC stimulation conditions. Each circle

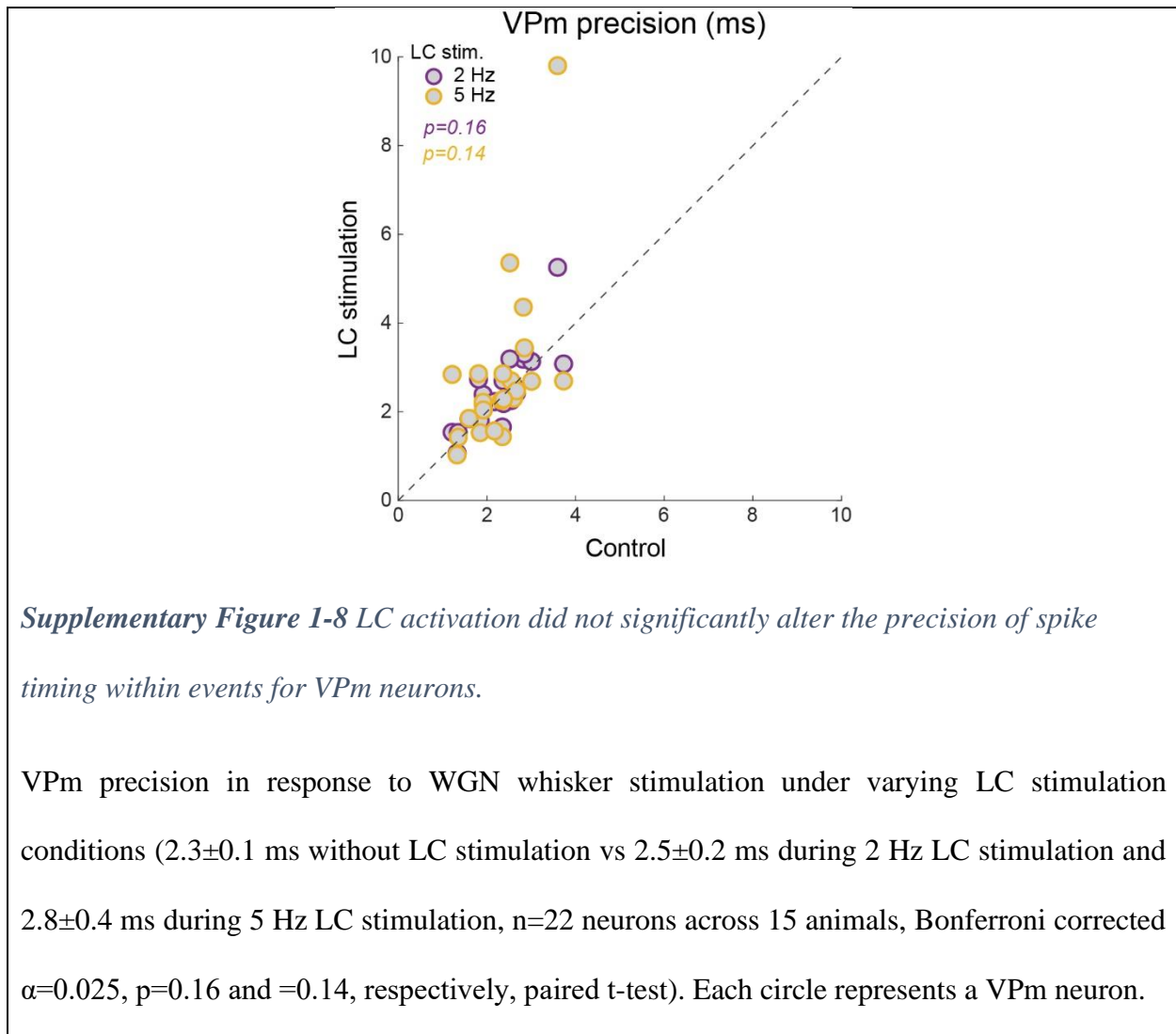
represents a VPM neuron (0.71 ± 0.06 Hz without LC stimulation vs 0.48 ± 0.05 Hz during 2 Hz LC stimulation and 0.28 ± 0.04 Hz during 5 Hz LC stimulation, $n=22$ neurons across 15 animals, Bonferroni corrected $\alpha=0.025$, $p=4.3 \times 10^{-5}$ and $=6.0 \times 10^{-9}$ respectively, paired t-test).

(e) Comparison of information carried by bursting and tonic spikes without LC stimulation (0.08 ± 0.01 bits/spike vs 0.19 ± 0.05 bits/spike, $n=41$ features across 22 neurons across 15 animals, Bonferroni corrected $\alpha=0.025$, $p=8.0 \times 10^{-5}$, Wilcoxon signed-rank test) as well as information carried by tonic spikes with and without LC stimulation (0.19 ± 0.05 bits/spike without LC stimulation vs 0.65 ± 0.17 bits/spike with 5 Hz LC stimulation, $n=41$ features across 22 neurons across 15 animals, $\alpha=0.05$, $p=2.5 \times 10^{-8}$, Wilcoxon signed-rank test).

(f) Histological confirmation of correct electrode placement in the TRN. (g) Summary of TRN burst rate in response to WGN whisker stimulation under varying LC stimulation conditions. Each circle represents a TRN neuron (0.62 ± 0.10 Hz without LC stimulation vs 0.37 ± 0.06 Hz during 2 Hz LC stimulation and 0.29 ± 0.06 Hz during 5 Hz LC stimulation, $n=22$ neurons across 10 animals, Bonferroni corrected $\alpha=0.025$, $p=2.6 \times 10^{-3}$ and $=2.2 \times 10^{-3}$ respectively, paired t-test).

(h) Percent change in information transmission efficiency is inversely correlated with percent change in burst rate for VPM neurons during LC activation ($r=-0.65$ and $=-0.51$ respectively, Pearson's coefficient).

(i) Summary of TRN firing rate in response to WGN whisker stimulation under varying LC stimulation conditions. Each circle represents a TRN neuron (20.7 ± 1.9 Hz without LC stimulation vs 20.1 ± 2.0 Hz during 2 Hz LC stimulation and 18.9 ± 1.8 Hz during 5 Hz LC stimulation, $n=22$ neurons across 10 animals, Bonferroni corrected $\alpha=0.025$, $p=0.54$ and $=0.08$ respectively, paired t-test). Error bars indicate \pm s.e.m.

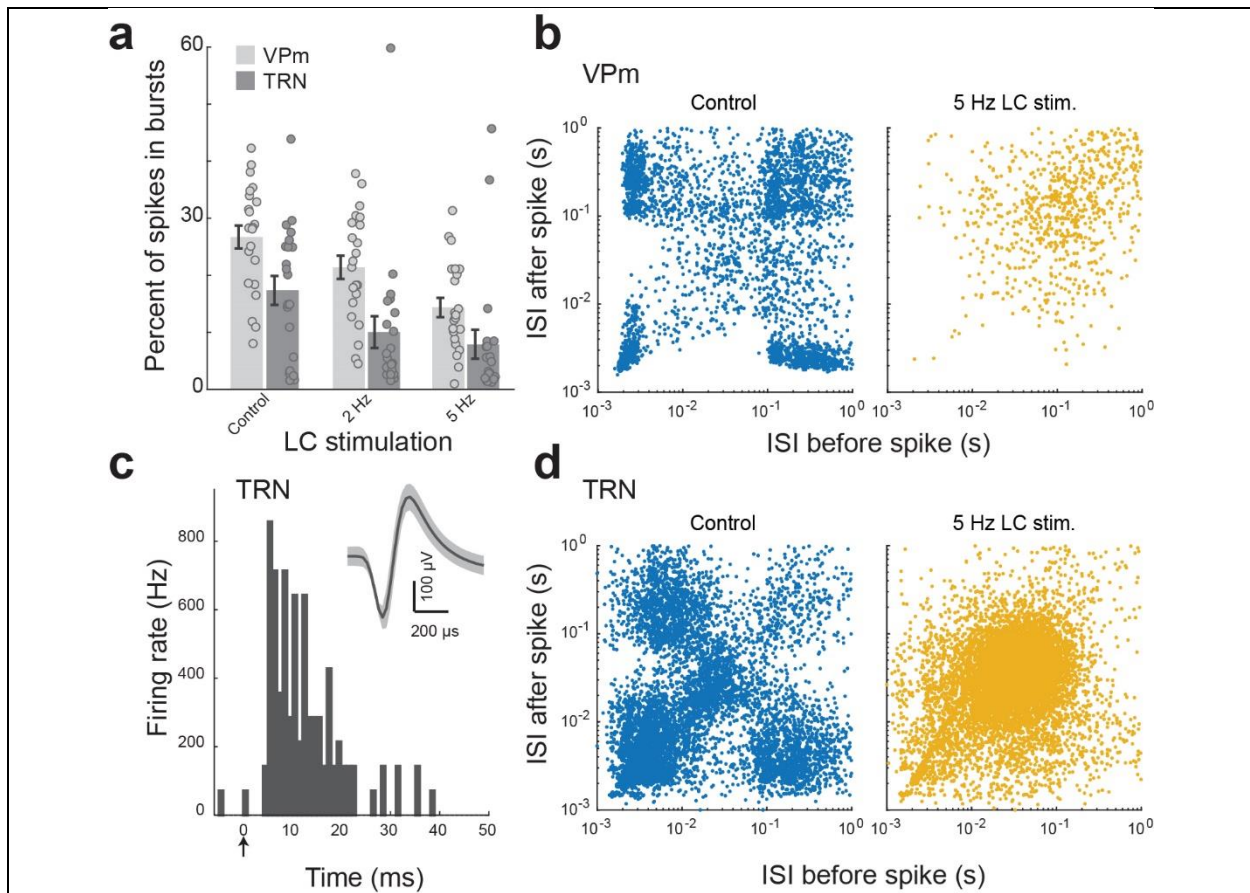


Previous work suggested that NE improves sensory processing by increasing signal (i.e. evoked responses) to noise (i.e. spontaneous responses) ratio (SNR). For temporally extended stimuli, reliability is likely a more appropriate measure for SNR than the ratio of evoked to spontaneous firing rate (see **Discussion**). As we observed an increase in reliability with LC activation, we then examined the extent to which an increase in reliability could contribute to increases in feature selectivity and information transmission. To this end, we randomly deleted or added unreliable spikes from the VPM control spike raster until the reliability of the responses was equal to that of the responses under 5 Hz LC stimulation (see **Methods**). We then compared the

information transmitted by the original spike train and the reliability-matched spike train. Interestingly, we found that this simulated increase in reliability only resulted in a significant, but moderate, increase in information transmission (**Fig. 1-5a**). However, this increase was drastically smaller than that observed with 5 Hz LC stimulation (i.e. 469% of the control during 5 Hz LC stimulation). This suggests LC-activation-induced increase in reliability is not likely the primary mechanism underlying the increase in thalamic information transmission.

LC modulation of thalamoreticulo-thalamic circuit dynamics improved feature selectivity and information transmission.

We have demonstrated that trigeminothalamic feedforward and corticothalamic feedback input had no roles in LC modulation of thalamic information transmission (**Fig. 1-3**), indicating the locus of the mechanism underlying the observed phenomena is in the thalamus. In the sensory thalamus, the dynamic interplay between the relay nuclei and the TRN (**Fig. 1-5c**) plays an essential role in gating information to the cortex^{55,57}. The percent of spikes in bursts for VPm cells was comparable to that found in the awake somatosensory thalamus¹⁰⁸ (**Supplementary Fig. 1-9a**) and we found that LC activation resulted in a shift from burst to tonic firing mode for VPm neurons as both burst rate and percent of spikes in bursts decreased during LC activation (**Fig. 1-5d, Supplementary Fig. 1-9b**). Decreased firing rate during LC activation suggests that the suppression of VPm bursts was not simply due to the depolarizing effect of NE.



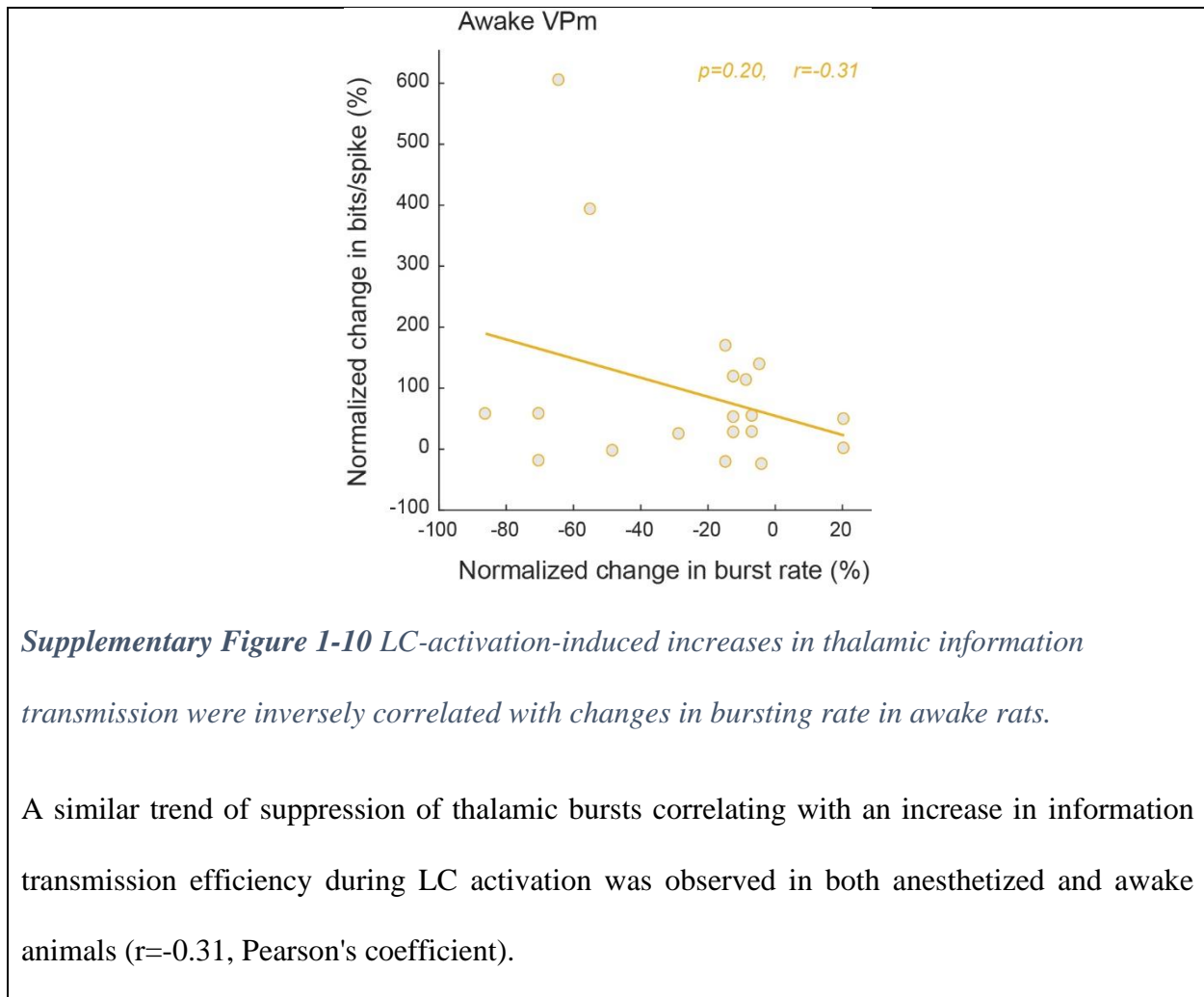
Supplementary Figure 1-9 LC activation modulated intrathalamic circuit dynamics by reducing burst firing in both the TRN and VPM.

(a) Population average of percent of spikes in bursts for VPM and TRN neurons under varying LC stimulation conditions (VPM: $26 \pm 2\%$ without LC stimulation vs $21 \pm 2\%$ during 2 Hz LC stimulation and $14 \pm 2\%$ during 5 Hz LC stimulation, $n=22$ neurons across 15 animals, Bonferroni corrected $\alpha=0.025$, $p=3.8 \times 10^{-4}$ and $=1.1 \times 10^{-7}$, respectively, paired t-test; TRN: $17 \pm 3\%$ without LC stimulation vs $10 \pm 3\%$ during 2 Hz LC stimulation and $8 \pm 3\%$ during 5 Hz LC stimulation, $n=21$ neurons across 10 animals, Bonferroni corrected $\alpha=0.025$, $p=0.031$ and $=0.007$, respectively, paired t-test). **(b)** Example plots from the same VPM neuron showing inter-spike-intervals (ISIs) before vs after each spike in response to WGN whisker stimulation. Left: without

LC stimulation. Right: with 5 Hz LC stimulation. (c) Example single-unit TRN response to a punctate stimulation of its principal whisker, with arrow marking whisker stimulation onset. Inset: example TRN waveform; shaded area represents \pm s.d. (n=220 spikes) (d) Example plots from the same TRN neuron showing ISIs before and after each spike in response to WGN whisker stimulation. Left: without LC stimulation. Right: with 5 Hz LC stimulation. Error bars indicate \pm s.e.m.

Consistent with previous work¹⁶⁰, we found that, during control conditions, bursting spikes carried less than half of the information carried by tonic spikes (**Fig. 1-5e**). Surprisingly, tonic spikes carried significantly more information with LC activation than without LC activation (**Fig. 1-5e**). This difference between tonic spikes with and without LC stimulation suggests a sub-dimension in the tonic mode, influenced by the LC, which can be modulated to allow for more efficient information transmission.

Single-unit recordings from the TRN (**Fig. 1-5f, Supplementary Fig. 1-9c**) revealed that LC activation also decreased TRN burst firing in response to WGN whisker stimulation, indicating an LC-activation-induced change in thalamoreticulo-thalamic circuit dynamics (**Fig. 1-5g, Supplementary Fig. 1-9a,d**). More interestingly, the suppression of VPm bursts was correlated with the increase in information transmission efficiency seen during LC activation (**Fig. 1-5h**). Importantly, this trend also holds in awake animals (**Supplementary Fig. 1-10**). Although LC activation reduced TRN bursting, it did not significantly alter TRN firing rate (**Fig. 1-5i**), resulting in sustained, tonic TRN inhibition being delivered to the VPm during LC activation as compared to the bursting inhibition the TRN provides without LC activation.

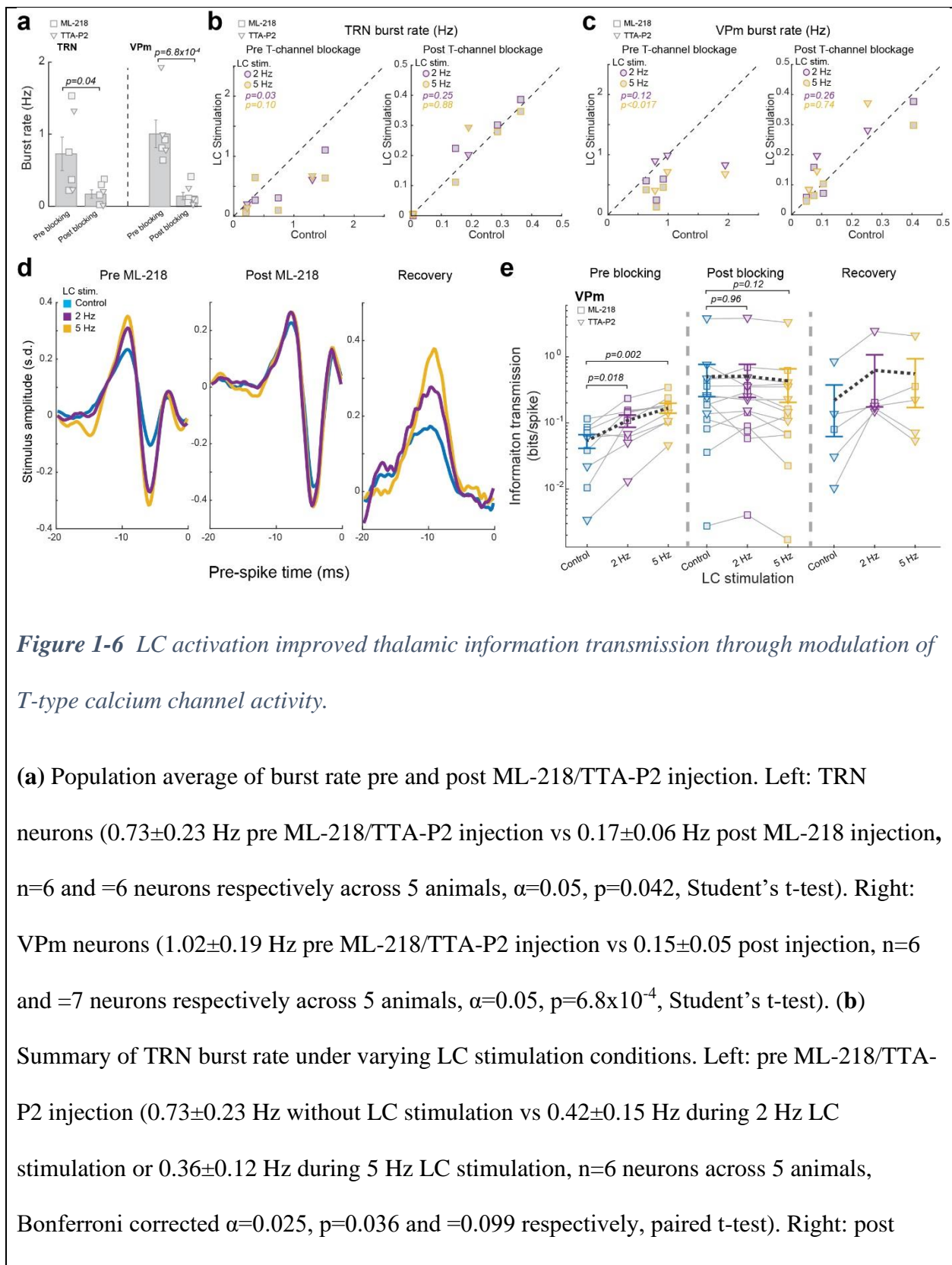


LC modulation of thalamic information transmission is through modulation of T-type calcium channels

We found LC activation simultaneously enhanced thalamic information transmission and reduced thalamic burst firing, which is mediated by T-type calcium channels. Yet our analyses suggested that LC-activation-improved information transmission was not simply due to VPM neurons switching from burst mode to tonic mode. However, LC regulation of intrathalamic circuit dynamics still could explain the improved tonic information transmission due to the suppressive

effects of LC-activation on T-type calcium channel activities involved in the subthreshold processes underlying spike generation and therefore information transmission (see **Discussion**).

To test the causal relationship between T-type calcium channel activity and LC-activation-induced enhancement of information transmission, we injected ML-218 hydrochloride or TTA-P2, both selective T-type calcium channel antagonists, into the thalamus to pharmacologically block these channels. Following the injection of ML-218/TTA-P2, bursting was decreased for VPM and TRN neurons, indicating ML-218/TTA-P2 effectively blocked calcium T-channels throughout the thalamus (**Fig. 1-6a**). Further, although LC activation had a suppressive effect on VPM and TRN burst firing in recordings prior to the injection of ML-218/TTA-P2 (**Fig. 1-6b,c**), it failed to reduce burst rate following injection of ML-218/TTA-P2 (**Fig. 1-6b,c**).



ML-218/TTA-P2 injection (0.17 ± 0.06 Hz without LC stimulation vs 0.18 ± 0.06 Hz during 2 Hz LC stimulation and 0.17 ± 0.06 Hz during 5 Hz LC stimulation, $n=6$ neurons across 5 animals, Bonferroni corrected $\alpha=0.025$, $p=0.25$ and $=0.88$ respectively, paired t-test). (c) Summary of VPM burst rate under varying LC stimulation conditions. Left: pre ML-218/TTA-P2 injection (1.02 ± 0.19 Hz without LC stimulation vs 0.67 ± 0.11 Hz during 2 Hz LC stimulation and 0.45 ± 0.08 Hz during 5 Hz LC stimulation, $n=6$ neurons across 5 animals, Bonferroni corrected $\alpha=0.025$, $p=0.12$ and $=0.017$ respectively, paired t-test). Right: post ML-218/TTA-P2 injection (0.15 ± 0.05 Hz without LC stimulation vs 0.17 ± 0.05 Hz during 2 Hz LC stimulation and 0.16 ± 0.05 Hz during 5 Hz LC stimulation, $n=7$ neurons across 5 animals, Bonferroni corrected $\alpha=0.025$, $p=0.26$ and $=0.74$ respectively). (d) Example of recovered features from a VPM neuron, under varying LC stimulation conditions. Left: pre ML-218 injection. Center: post ML-218 injection. Right: recovery from ML-218. (e) Population average of information transmission efficiency (bits/spike) for VPM neurons under varying LC stimulation conditions. Left: pre ML-218/TTA-P2 injection (0.05 ± 0.01 bits/spike without LC stimulation vs 0.11 ± 0.02 bits/spike during 2 Hz LC stimulation and 0.17 ± 0.03 bits/spike during 5 Hz LC stimulation, $n=9$ features across 6 neurons across 5 animals, Bonferroni corrected $\alpha=0.025$, $p=0.018$ and $=2.3 \times 10^{-3}$ respectively, paired t-test). Center: post ML-218/TTA-P2 injection (0.51 ± 0.26 bits/spike without LC stimulation vs 0.51 ± 0.26 bits/spike during 2 Hz LC stimulation or 0.43 ± 0.23 bits/spike during 5 Hz LC stimulation, $n=14$ features across 7 neurons across 5 animals, Bonferroni corrected $\alpha=0.025$, $p=0.96$ and $=0.12$ respectively, paired student's t-test). Right: recovery from ML-218/TTA-P2 (~4 hours after the injection, 0.22 ± 0.16 bits/spike without LC stimulation vs 0.64 ± 0.46 bits/spike during 2 Hz LC stimulation and 0.56 ± 0.39 bits/spike during 5 Hz LC stimulation, $n=5$ features across 4

neurons across 4 animals, Bonferroni corrected $\alpha=0.025$, $p=0.24$ and $=0.22$ respectively, paired student's t-test). Each marker represents a significant feature. Error bars indicate \pm s.e.m.

In recordings taken prior to ML-218/TTA-P2 injection, we found the same LC-activity-dependent increase in feature selectivity (**Fig. 1-6d**) and enhanced thalamic information transmission efficiency (**Fig. 1-6e**). However, following the inactivation of T-type calcium channels by ML-218/TTA-P2, we found the LC-activity-dependent increase in feature selectivity was no longer present (**Fig. 1-6d**). Accordingly, ML-218/TTA-P2 also blocked the LC-activity-induced increase in information transmission efficiency (**Fig. 1-6e**). The trend of LC activation effects on thalamic information transmission re-emerged after ML-218/TTA-P2 wore off (**Fig. 1-6d,e**), indicating that the observed changes resulted from reversible pharmacological blocking of T-type calcium channels by ML-218/TTA-P2.

Modelling confirmed that LC-NE modulation of intrathalamic circuit dynamics enhances information transmission.

Isolating the effects of NE in only the VPm or TRN as compared to the effects of NE in both the VPm and TRN would allow us to elucidate the mechanism behind how LC-NE modulation of intrathalamic circuit dynamics affects sensory processing. However, as it is currently technically impossible to selectively block NE effects only in the VPm or TRN in-vivo due to the adjacent proximity of the VPm and TRN, we constructed a simple network model of the intrathalamic circuit (see **Methods**) to examine the effects of NE action in intrathalamic circuit. Thalamic neuron properties were modeled using an integrate-and-fire-or-burst (IFB) model and the effects of NE on neurotransmitter efficacy and leak current were simulated¹⁵⁴. The modelled

intrathalamic circuit consists of a VPm IFB neuron and a TRN IFB neuron, with the VPm neuron projecting excitatory input to the TRN neuron which provides inhibitory feedback to both the VPm neuron and itself (**Fig. 1-7a**). We used experimentally recorded PrV spike responses to WGN whisker stimulation as the input to the intrathalamic model circuit (see **Methods**). The spikes of the VPm model neurons could then be compared to the whisker stimulation, allowing for reverse correlation analysis and quantification of thalamic feature selectivity and information transmission of the modeled VPm neuron's outputs. As seen in-vivo, the simulated effects of NE on the modelled intrathalamic circuit resulted in an increase in feature selectivity (**Fig. 1-7b**), leading to a significant improvement in information transmission (**Fig. 1-7c**). Further we found that the simulated effects of NE on the modelled intrathalamic circuit also resulted in the same decrease in VPm and TRN bursting rate as we observed in-vivo (**Fig. 1-7d**).

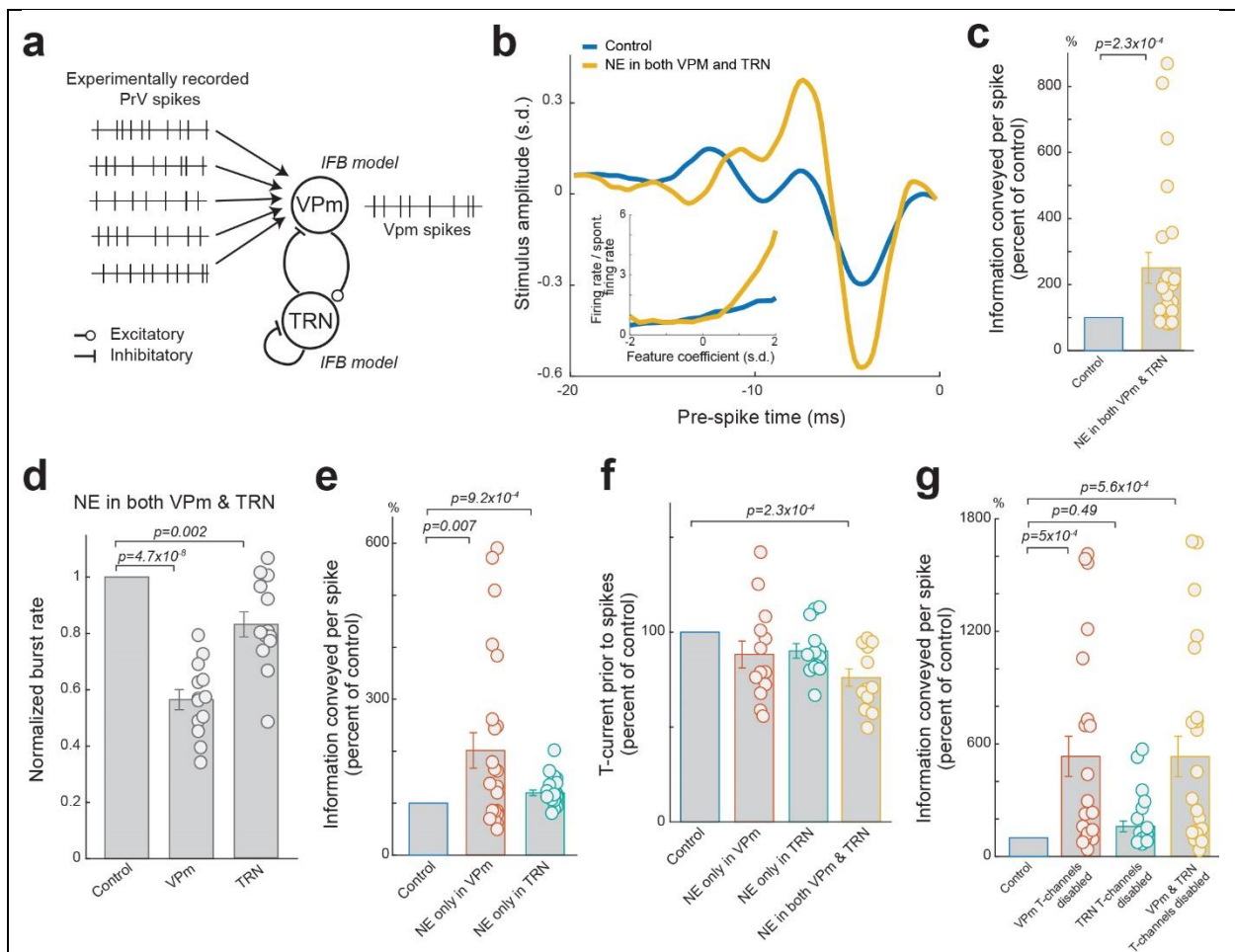


Figure 1-7 Modelling results indicated that NE action in both the VPM and TRN is optimal for enhancing thalamic information transmission.

(a) Diagram of the simple network model consisting of a VPM and a TRN IFB neuron. **(b)** Example of recovered features of a VPM model neuron with and without NE effects on the intrathalamic circuitry. Inset: corresponding nonlinear tuning functions. **(c)** Normalized changes in information transmission efficiency (bits/spike) for VPM model neurons with and without NE effects in the thalamus. Each circle represents a significant feature ($251 \pm 46\%$ of the control during simulated NE effects, $n=24$ features across 13 modelled VPM neurons, $\alpha=0.05$, $p=2.3 \times 10^{-4}$, Wilcoxon signed-rank test). **(d)** NE action in the intrathalamic circuitry

also suppressed burst rate of both modelled VPm and TRN neurons (VPm: $56\pm 4\%$ of control, TRN: $83\pm 4\%$ of control, $n=13$ modeled VPm and TRN neurons, Bonferroni corrected $\alpha=0.025$, $p=4.7\times 10^{-8}$ and $=2.4\times 10^{-3}$ respectively, paired t-test.). (e) Normalized changes in information transmission efficiency (bits/spike) for VPM model neurons when NE only affects the VPm or TRN. Each circle represents a significant feature ($202\pm 34\%$ of the control during simulated NE effects on VPm only, $120\pm 5\%$ of the control during simulated NE effects on TRN only, $n=24$ features across 13 modelled VPm neurons, Bonferroni corrected $\alpha=0.025$, $p=7\times 10^{-3}$ and $=9.2\times 10^{-4}$, respectively, paired t-test). (f) Normalized T-current contributing to VPm spikes when NE acts in VPm, TRN, or both VPm and TRN ($88\pm 7\%$ of control for NE in VPm, $90\pm 4\%$ of control for NE in TRN, $76\pm 5\%$ of control for NE in both VPm and TRN, $n=13$ modelled VPm neurons, Bonferroni corrected $\alpha=0.016$, $p=0.12$ and $=0.024$ and $=2.3\times 10^{-4}$ respectively, paired t-test). (g) Normalized changes in information transmission efficiency (bits/spike) for modelled VPm neurons when T-type Ca^{2+} channels were disabled in VPm, TRN, or both VPm and TRN (VPm T-type channels disabled: $533\pm 107\%$, TRN T-type channels disabled: $160\pm 29\%$ of the control, VPm and TRN T-type channels disabled: $533\pm 108\%$ of the control, $n=24$ features across 13 modelled VPM neurons, Bonferroni corrected $\alpha=0.016$, $p=5\times 10^{-4}$ and $=0.49$ and $=5.6\times 10^{-4}$ respectively, paired t-test and Wilcoxon signed-rank test and paired t-test respectively). Each circle represents a significant feature. Error bars indicate \pm s.e.m.

Next, we used our model to investigate the effects of NE only in the VPm or only in the TRN. Simulating NE effects isolated in the VPm also resulted in an increase in information transmission (**Fig. 1-7e**); however, the increase resulting from NE effects in both VPm and TRN

was significantly larger, approximately $40\pm 16\%$, than that resulting from simulated NE effects in only the VPm (n=24 features across 13 modelled VPm neurons, $\alpha=0.05$, $p=0.028$, paired t-test). Further we found simulating NE effects isolated in the TRN also resulted in a slight improvement in information transmission (**Fig. 1-7e**), which was also significantly less than the improvement seen when NE affected both VPm and TRN (i.e. $120\pm 5\%$ vs $251\pm 46\%$, n=24 features across 13 modelled VPm neurons, $\alpha=0.05$, $p=4.7\times 10^{-3}$, Wilcoxon signed-rank test). Although these results suggest the direct actions of NE on the VPm or TRN alone could improve thalamic information transmission, we found LC modulation of both the VPm and the TRN (i.e. intrathalamic circuit dynamics) is optimal for improving thalamic feature selectivity and information transmission.

We have demonstrated in-vivo that blocking T-channels in the thalamus also blocked LC modulation of thalamic information transmission, suggesting T-channels play an important role in LC-NE modulation of thalamic feature selectivity. As we hypothesized that T-current resulting from the all-or-none nature of T-channel activations is suboptimal for transmitting information about stimulus features (see **Discussion**), we calculated the average calcium T-channel current prior to spikes in our model to investigate the presumed contribution of T-channels to spike generation. As we expected, NE effects in the thalamus decreased average T-current prior to spikes (**Fig. 1-7f**), confirming NE improves information processing through reduction of T-channel activity as suggested by our in-vivo experiments.

To elucidate the exact effects of VPm and TRN T-channels on thalamic information transmission, we removed calcium T-channels from either the VPm, TRN, or both the VPm and TRN within our model. As expected, disabling T-channels in both the VPm and TRN model neurons resulted in a dramatic improvement in information transmission (**Fig. 1-7g**). However, this improvement was not significantly different than when calcium T-channels were disabled only

in the modelled VPm neuron. Further, we found that disabling calcium T-channels in only the TRN neuron resulted in a relatively small and not significant improvement in VPm information transmission (**Fig. 1-7g**).

The results from our model suggest that the main mechanism behind the experimentally observed LC-NE-induced improvement in information transmission is the reduction of calcium T-channel currents in the VPm. However, we also found that the effects of LC-NE on both the TRN and VPm in concert generates the strongest reduction in VPm calcium T-channel activity through NE's effects on intrathalamic dynamics. Taken together, these simulation results indicate that NE modulation of VPm neurons' T-channels, presumably through regulation of the interplay between the VPm and TRN, is the main source of LC-induced improvements in thalamic information transmission.

Discussion

Elevated LC activity has been associated with increased arousal and an attentive behavioral state^{1, 158}. The LC is the primary source of adrenergic projections to the forebrain¹⁴ and innervates the sensory pathways, suggesting a role in state-dependent modulation of sensory processing and perception. Through direct activation of the LC-NE system, we found that elevated LC-NE activity causes a dramatic increase in thalamic feature selectivity and improvement in information transmission.

Our results strongly suggest that LC-activation-induced improvement of thalamocortical information transmission is primarily mediated by NE regulation of intrathalamic circuit dynamics via the direct action of NE on α -adrenergic receptors in both the VPm and TRN. LC activation improved thalamic information transmission in both anesthetized and awake animals, suggesting LC-NE improvement of thalamic information transmission is a general phenomenon. However,

the improvement in information transmission was significantly greater in anesthetized than awake animals, likely due to the interplay in awake animals between the LC-NE system and other arousal-contributing neuromodulators, which are probably more active in the awake state^{13, 28, 31, 161}. Importantly, we found photostimulation of the LC in awake, head-fixed rats improved behavioral performance on a perceptual discrimination task and this enhancement of behavior was due to NE regulation of intrathalamic circuit dynamics. This suggests LC modulation of sensory processing in the early stage of sensory pathways is critical to perception.

Recent studies have demonstrated that LC activation elicits frequency-dependent pupil dilation^{145, 162}. Taken together, these results and our results presented here are consistent with several previous studies that have shown a relationship between pupil size and sensory processing^{8, 15, 17}. While these previous studies have demonstrated that pupil-linked arousal, presumably mediated by the LC-NE system, is tightly correlated with improved cortical encoding of sensory signals, our data suggest that pupil-linked improvement in sensory processing could already occur in first-order thalamic neurons.

Alert, aroused states and locomotion have both been linked to increased neuronal response to sensory input^{6-8, 163}, indicating gain increases with heightened behavioral states. This increased responsiveness, however, did not alter sensory neurons' sensitivity to stimuli^{6, 163}. We found LC activation decreased the overall response of VPM neurons to continuous whisker stimulation. Surprisingly, this decreased gain was coupled with a drastic improvement in information transmission that cannot be explained by the reduction in gain (**Fig. 1-5a**). Our isolation of the effects of the LC-NE system may lend an explanation for this surprising result. In awake, behaving animals, behavioral state is modulated by a complex interplay between multiple neuromodulatory systems, including the noradrenergic and cholinergic systems^{13, 161}. Indeed, activation of either

the LC or the cholinergic basal forebrain desynchronizes cortical EEG ^{145, 164}. Cholinergic system activation increases firing rate for neurons in the visual cortex ¹⁶⁵, suggesting cholinergic systems may potentially counterbalance the suppressive effects of the LC-NE system observed in this study. Indeed, the cholinergic system is activated by locomotion and plays a role in locomotion-linked visual sensory processing ^{166, 167}. Our findings are, nevertheless, consistent with the notion that norepinephrine boosts the effective salience of incoming sensory signals ^{5, 14}. Increased selectivity of the response of thalamocortical neurons during LC-mediated arousal may provide the cortex with a more accurate representation of stimuli. This may lead to more effective functional reorganization of cortical representation of behaviorally important sensory signals, possibly through noradrenergic plasticity in concert with other top-down/bottom-up mechanisms ^{9, 32, 159}.

Local application of norepinephrine in the somatosensory thalamus has been shown to suppress spontaneous activity while slightly increasing isolated-punctate-whisker-deflection-evoked responses, resulting in an increased signal-to-noise ratio (SNR), defined as the ratio of evoked to spontaneous firing rate ²⁸. This led to an NE induced increase in SNR to be initially hypothesized as the mechanism underlying LC-activity-induced improved thalamic sensory processing. Most complex sensory guided behavior involves naturalistic, temporally extended stimuli (e.g. whisking against a textured surface), for which evoked and spontaneous spikes cannot be easily identified; however, reliability can be used as a measure of SNR for these responses ¹⁵³. During continuous whisker stimulation, reliable and unreliable spikes are analogous to evoked and spontaneous spikes, respectively, as reliable spikes carry significantly more stimulus-related information than unreliable spikes (data not shown). Although LC activation increased the

reliability of thalamic responses, we found increased SNR, as measured by reliability, could not explain the drastically improved thalamocortical encoding (**Fig. 1-5a**).

Previous work has shown thalamic relay neurons fire in two modes: tonic and bursting⁹⁰,¹³². Although burst firing is shown to be present in the awake thalamus^{10, 108, 133}, it is believed to serve as a “wake-up call” to the cortex. Tonic mode, on the other hand, is thought to be more ideal for transmission of detailed information about stimuli¹⁶⁰. When de-inactivated, a weak incoming EPSP could activate T-type calcium channels to generate powerful low-threshold calcium spikes, which in turn trigger sodium spikes^{90, 132}. This all-or-none nature of T-channel activation may result in VPM spikes that are less selective to a specific encoded feature as due to the facilitative action of T-channels, weak EPSPs from non-encoded features could produce the same spiking activity as strong EPSPs produced by encoded features.

During low arousal, thalamic neurons are relatively hyperpolarized³¹, which increases the likelihood of T-type calcium channels being de-inactivated. Due to the reciprocal connection between the VPM and TRN, a burst of TRN spikes has been shown to hyperpolarize thalamocortical neurons, and thus increase the portion of de-inactivated T-channels, indicated by increases in burst firing⁶⁴. TRN neurons also exhibit a stereotyped after-burst hyperpolarization lasting ~100-120 ms⁷⁶. This hyperpolarization is long enough to de-inactivate T-type calcium channels in the TRN, enabling TRN neurons to burst again after a moderate depolarization resulting from VPM spikes. Larger fluctuations of VPM membrane potential caused by this bursting activity within the thalamoreticulo-thalamic circuitry may increase the portion of time T-channels are de-inactivated, which would be detrimental to unbiased, linear transformation of feedforward PrV synaptic inputs to suprathreshold activity. In line with this notion, our experimental and simulation data demonstrated the detrimental role of T-type calcium channel

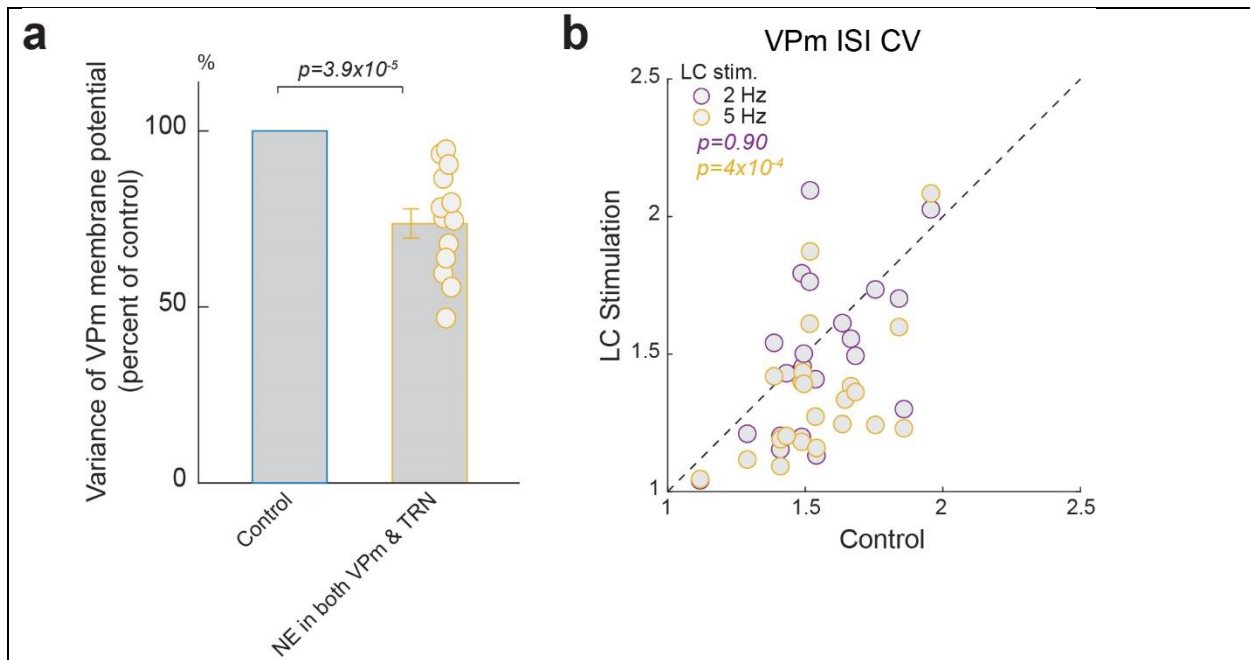
activity to information transmission as blocking T-type calcium channels drastically improved information transmission (**Fig. 1-6&7**).

Our data showed that LC activation reduced bursting for VPM neurons, which, at first glance, suggested that the observed LC-activation-improved information transmission was merely a result of an LC-induced switch to a tonic firing mode. However, to our surprise, further analyses showed that this is not the case as information carried by tonic spikes with LC stimulation was approximately 3-fold that of tonic spikes from the same VPM neuron without LC stimulation (**Fig. 1-5e**), suggesting that tonic mode during LC activation was not functionally equivalent to tonic mode without LC activation.

What then is the difference between the tonic mode with and without LC stimulation? An explanation to why tonic spikes during LC activation are informative may come from a recent finding that a small portion of T-type channels are de-inactivated even during relatively depolarized states ¹⁵⁰. Although small, due to the strength of T-type channel conductance, this population may still significantly contribute to tonic spiking. These results showed graded activation of T-channels facilitated the generation of tonic spikes, and improved the input-output gain of thalamic relay neurons, presumably making them more optimal for detecting sensory input than discriminating between different features within the sensory input ^{33, 150}. During LC activation, NE altered intrathalamic circuit dynamics, which resulted in steady TRN tonic inhibition of the VPM (**Fig. 1-5g**). VPM neurons then experienced both the steady depolarizing effects of NE and the tonic hyperpolarizing effects of TRN inhibition, perhaps creating concurrent push-pull forces on membrane potential which may buffer against fluctuations ¹³. As previous experimental evidences suggested that even short periods of hyperpolarization had statistically significant effects on recruiting more T-channels in thalamocortical cells ¹⁶⁸, the collective effects

described above likely diminish the overall contribution of T-channel current to tonic spikes, thus improving information transmission about the encoded features.

In support of this notion, recent studies showed a reduction in the variance of membrane potential during high arousal indexed by pupil size and locomotion^{8, 163, 169}. Consistent with these previous works, our modelling results showed a decrease in the variance of VPM membrane potential during simulated NE action in the thalamus (**Supplementary Fig. 1-11a**). Further, our in-vivo data demonstrated a decrease in the coefficient of variance (CV) of inter-spike-intervals during LC activation (**Supplementary Fig. 1-11b**), quantitatively indicating a decrease in fluctuation of VPM membrane potential during LC activation¹⁷⁰. Therefore, we suggest a new brain-state-dependent-sub-dimension within the tonic mode, in which the LC, and perhaps other neuromodulatory systems, can optimize thalamocortical information transmission through modulating intrathalamic circuit dynamics. Future studies combining whole-cell recording and LC manipulation are necessary to definitively test this potential cellular mechanism.



Supplementary Figure 1-11 NE effects on the variance of membrane potential and coefficient of variation of inter-spike-intervals for VPm neurons.

(a) NE activation in the modelled intrathalamic circuit decreased the variance of membrane potential of VPm neurons ($74 \pm 4\%$ of the control for NE in both VPm and TRN, $n=13$ modelled VPm neurons, $\alpha=0.05$, $p=3.9 \times 10^{-5}$, paired t-test). (b) Coefficient of variation of VPm inter-spike-intervals under varying LC stimulation conditions (1.56 ± 0.04 without LC stimulation vs 1.57 ± 0.10 during 2 Hz LC stimulation and 1.36 ± 0.05 during 5 Hz LC stimulation, $n=22$ neurons across 15 animals, Bonferroni corrected $\alpha=0.025$, $p=0.90$ and $=4.0 \times 10^{-4}$ respectively, Wilcoxon signed-rank test). Each dot represents a VPm neuron. Error bars indicate \pm s.e.m.

Chapter 2: Locus coeruleus activation optimizes the temporal structure ventral posteromedial nucleus neurons use to encode whisker stimuli

Abstract

Previous work has shown that locus coeruleus – norepinephrine (LC-NE) induced improvements in ventral posteromedial nucleus (VPm) feature selectivity are not simply due to an increased signal-to-noise ratio or a shift from burst to tonic firing. Here we find that LC-NE modulation of intrathalamic dynamics optimized the temporal structure of the reliable response events VPm neurons used encode the same stimuli. This change in response temporal structure is not simply form an improvement in reliability or precision, instead LC-NE activation resulted in a removal of certain events observed during the control response coupled with the emergence of new events. Through analyzing the feature selectivity of the spikes falling within each event type we were able to discern that the emerged events had a greater feature selectivity and were more informative than the removed events, indicating the LC-activation-induced changes in the temporal response structure of VPm neurons was beneficial for information transmission. Indeed, when we compared the temporal response structures observed with and without LC stimulation to a computationally generated ideal event structure for each feature, we found that LC stimulation resulted in more events being observed to occur at ideal timepoints. Finally, we looked at how LC activation affects the ability to decode a stimulus given only the feature selectivity and spike trains of a population of thalamocortical neurons. Here, we confirmed that LC-activation-induced improved information transmission improved the accuracy of the decoded stimulus.

Introduction

The locus coeruleus – norepinephrine (LC-NE) system is a major neuromodulatory system of attention, arousal, and cognition³. It has long been suggested that the LC exerts a strong influence on sensory processing and therefore perception^{29, 158}. Indeed, many different publications have shown that NE affects the response properties of thalamic neurons in-vitro^{85, 87, 88}. It has also been shown that LC activation affects the response properties of thalamocortical sensory neurons in-vivo^{28, 30, 158}. However, until recently it was still unclear how LC-NE modulation affected the ability of neurons of the ventral posteromedial nucleus (VPM) of the thalamus to encode information about complex spatiotemporal whisker stimuli. Our recent publication has shown that LC activation enhances the selectivity of the response of VPM neurons to specific features in the WGN whisker stimulation¹⁰⁵. This enhancement of feature selectivity was shown to occur due to direct action of NE on noradrenergic receptors in the thalamus which led to a change in intrathalamic dynamics that minimized calcium t-channel activity. The enhanced feature selectivity was shown to result in increased transmission efficiency and rate of stimulus-related information. Finally, we found that LC stimulation in awake rats improved their perceptual sensitivity, suggesting that LC optimization of thalamic sensory processing improves accuracy of perception^{105, 171}.

How do LC-mediated changes in intrathalamic dynamics change the way in which a VPM neuron encodes for the absence/presence of specific kinetic features in stimuli? Our previous work had found that changes in the gain of VPM neuron's responses was not a plausible explanation¹⁰⁵. In addition, it was determined LC-induced removal of burst spikes could also not explain the dramatic improvement in feature selectivity, as tonic spikes with LC stimulation carried more information than tonic spikes without LC stimulation¹⁰⁵. Rather there is a more complex shift in

intrathalamic dynamics, resulting from a reduction in calcium t-channel activity, which optimizes the thalamus for transmitting information about stimulus details. This is supported by recent research which has shown calcium t-channels are also involved in tonic thalamic firing^{150, 172, 173} and that thalamic bursting has been shown to be associated with increased noise in synaptic background activity¹⁶⁸. These results suggest that LC-modulation of intrathalamic states may reduce the subthreshold membrane potential fluctuations shown to be present in thalamocortical neurons¹⁷⁴. If these membrane potential fluctuations are not stimulus related, they would act as noise which may degrade the ability of VPm neurons to respond selectively to specific features.

To investigate further, we analyzed the events used by each VPm neuron to encode a stimulus, e.g. the timepoints in the stimulus at which the VPm neuron reliably responded for most presentations of the stimulus. Our previous work had shown that an LC-induced increase in reliability (i.e. more spikes within events vs outside events) could not explain the dramatic enhancement in information transmission¹⁰⁵. Further, we observed no LC-induced increase in precision (jitter of spike times within events). Here, by comparing the temporal structure of events used to encode the same stimulus with and without LC stimulation, we find a surprising occurrence, LC activation alters the temporal structure of events. Through comparing the feature selectivity of the spikes falling within events that were removed by LC stimulation to that of spikes falling within events that were newly emerged during LC stimulation, we find that this LC-induced removal and emergence of events favors enhanced feature selectivity as newly emerged events were more informative than removed events. Further, we compared the temporal event structure used to encode a stimulus with and without LC stimulation to a computationally generated, ideal temporal event structure and found that LC stimulation increased the percent of events occurring at ideal times. Finally, when we examined the ability to decode the original stimulus from the spike

trains and feature selectivity of a population of VPm neurons we found the reconstruction was more accurate with LC stimulation than without. Taken together, this research sheds light on how the LC-NE systems is able to optimize thalamic sensory processing for accurate encoding of stimuli details.

Methods

Electrophysiology

All experimental data analyzed in this study were previously published in a study investigating how LC activation affects thalamic feature selectivity ¹⁰⁵. Detailed surgical and electrophysiological methods behind the generation of the data can be found in ¹⁰⁵. Briefly, rats were anesthetized with sodium pentobarbital and mounted to a stereotaxic frame to allow for craniotomies which gave access to the LC and VPm or TRN. For rats which underwent electronic LC microstimulation, a recording electrode was advanced into the LC, with LC location being confirmed by the characteristic response of LC neurons to paw pinch ¹⁴⁵. The recording system was then disconnected, and the electrode was connected to an electrical microstimulator (S88, Grass Instrument, Warwick, RI). For rats that underwent optogenetic LC stimulation, 4 weeks prior to the experiment, a lentivirus was injected directly into the rat's LC which allowed for selective transfection of noradrenergic neurons to express Channelrhodopsin2 (pLenti-PRsX8-hChR2(H134R)-mCherry, the UNC vector core, ~7e9 vp/ml). At the beginning of optogenetic LC stimulation experiments, a fiber optic cannula was advanced so as to be positioned against the LC, and then was attached to an LED driver (Plexon, 493 nm wavelength). For all experiments, a recording electrode was then advanced into the VPm or TRN, with VPm/TRN neurons being identified by their stereotaxic coordinates, waveforms, and response to punctate whisker deflection

Experimental paradigm

The experimental procedures briefly described here are discussed in more detail in the original publication of this data set ¹⁰⁵. Briefly, a frozen block of WGN whisker deflection was repeatedly delivered to the primary whisker via a custom modified galvomotor ¹⁷⁵ (galvanometer optical scanner model 6210H, Cambridge Technologies) controlled by a closed-loop system (micromax 67145 board, Cambridge Technology). Single-unit recordings of VPM neurons' responses to multiple repetitions of the stimulus were then captured via a Plexon recording system (OmniPlex, Plexon Inc., Dallas, TX). During each recording, LC activation condition was varied. Each recording then consisted of multiple responses of the same VPM neuron to the same frozen WGN stimulus for each condition of LC activation. This allowed us to analyze how LC activation changes the way in which each VPM neuron selectively encodes for information about the absence/presence of kinetic features in the stimulus.

Reverse Correlation Analysis

Here we model the response of both VPM and TRN neurons using the linear-nonlinear-Poisson cascade model (LNP) ^{35,47}. Through analyzing multiple responses of a neuron to the same frozen WGN stimulus, we can identify the kinetic features in the stimulus to which the neuron selectively responds. Here we recovered each neuron's significant features by first calculating the spike-triggered-average (STA) followed by calculating the spike-triggered-covariance (STC) matrix to recover the remaining set of significant features for any neurons which selectively responded to more than one kinetic feature ^{35,47}.

$$STA = \frac{1}{N} \sum_{n=1}^N \vec{S}(t_n)$$

$$STC = \frac{1}{N-1} \sum_{n=1}^N [\vec{S}(t_n) - STA][\vec{S}(t_n) - STA]^T$$

Where t_n is the time of the n^{th} spike, $\vec{S}(t_n)$ is a vector representing the stimulus during the temporal window preceding that spike, and N is the total number of spikes. Statistical significance of features was determined using bootstrap procedures⁴⁷. To quantify the change in amplitude of features recovered during different LC activation conditions, we used a feature modulation factor previously defined as¹⁰⁵:

$$\text{feature modulation factor} = \frac{\text{control feature} \cdot \text{conditional feature}}{\text{control feature} \cdot \text{control feature}}$$

Once the linear portion of the LNP model was recovered, i.e. the kinetic features the neuron selectively responded to, the corresponding nonlinear tuning functions for each feature can be calculated by dividing the probability distribution of feature coefficients given a spike by the probability distribution of all possible feature coefficients found in the stimulus:

$$\text{Nonlinear tuning function} = \frac{\text{Prob}(k|\text{spike})}{\text{Prob}(k)}$$

Where k is feature coefficient values, i.e. the dot product between the linear filter and the preceding stimulus.

The strength of the directionality of the selective response to a specific feature was quantified via analyzing the symmetry of the nonlinear tuning function as follows:

$$\text{directionality alpha value} = \frac{G(B) - G(-B)}{G(B)}$$

Where G is the nonlinear tuning function and B is equal to 2 standard deviations of feature coefficient value.

Information conveyed by VPM neurons about the features they selectively responded to were quantified as^{35, 152}:

$$Info(k; spike) = \int dk * Prob(k|spike) * \log_2\left(\frac{Prob(k|spike)}{Prob(k)}\right)$$

Where k is the feature coefficient and the resulting bits/spike value indicates the mutual information between the absence/presence of that kinetic feature in the stimulus and the occurrence of a spike by this neuron.

To allow for identification of reliable events in the response of neurons to the same WGN whisker stimulus, the peristimulus time histogram (PSTH) of the neuron's responses was binned (2 ms bins) and convolved with an adaptive boxcar kernel¹⁵³, with kernel size being dynamically increased at each bin until the bins spanned by the kernel contained at least 10 spikes, to produce a spike density function (SDF). A threshold (3 times the mean firing rate unless otherwise stated) was then used to identify peaks in the SDF which were then considered events¹⁵³.

Decoding ventral posteromedial nucleus responses

To reconstruct an approximation of the original stimulus from the VPM responses we first calculated the average temporal response pattern of each neuron to the incoming stimulus (e.g. the peristimulus time histogram) as well as the features that neuron encoded for. For neurons that were selective for multiple features, each feature-PSTH pair was considered unique. We then selected only the directionally selective feature-PSTH pairs to use for the initial reconstruction. This was done as from an ideal observer viewpoint the non-directionally selective features cannot be decoded until the directionality of the stimulus is determined.

For each directionally selective feature-PSTH pair, at each timepoint in the PSTH the preceding strength of the feature in the stimulus was assumed to be relative to the PSTH value in that bin (i.e. average spike count/trial at that timepoint). The reconstructed vector at each point for a directionally selective feature-PSTH pair was therefore calculated as:

$$reconstruction_{directional\ feature}(t) = \sum_{i=1}^{T-1} feature(T-i) * PSTH(t+i)$$

Where the bin size for both the PSTH and feature are equal to the sampling frequency of the original stimulus (i.e. 5000 Hz, 0.2 ms bins) and T is the length of the feature. We then summed all reconstruction vectors corresponding to each directional feature-PSTH pair and took the z-score of the resulting vector to generate a reconstruction of the original stimulus.

$$directional\ reconstruction = z\ score(\sum reconstruction_{directional\ feature})$$

Using the directional-feature generated reconstruction to approximate the original stimulus direction at any timepoint, we were then able to improve the reconstruction further using the non-directionally selective feature-PSTH pairs. To this end, for each non-directionally selective feature-PSTH pair we generated a reconstruction which was at each point equal to:

$$reconstruction_{non-directional\ feature}(t) = \sum_{i=1}^{T-1} A * feature(T-i) * PSTH(t+i)$$

$$A = 1\ if\ dot(directional\ reconstruction(t-T:t),\ feature) \geq 0$$

$$A = -1\ if\ dot(directional\ reconstruction(t-T:t),\ feature) < 0$$

The value of A effectively flips the feature at any timepoint so that its direction is chosen to be the direction which best matches the reconstruction generated from directional features only.

Once we had then calculated a reconstructed stimulus vector for each non-directionally selective feature-PSTH pair we were then able to generate a reconstruction of the stimulus using both directional and non-directional feature-PSTH pair reconstructions as

complete reconstruction

$$= z \text{ score} \left(\sum \text{reconstructions}_{\text{directional feature}} \right. \\ \left. + \sum \text{reconstructions}_{\text{non-directional feature}} \right)$$

Statistics

All statistical tests were two-sided. A one-sample Kolmogorov-Smirnov test was used to assess the normality of data before performing statistical tests. If the samples were normally distributed, a paired or unpaired t-test was used. Otherwise, the two-sided Mann-Whitney U-test was used for unpaired samples or the two-sided Wilcoxon signed-rank test for paired samples. Bonferroni correction was used for multiple comparisons.

Results

We recorded single-unit activity of VPM neurons in response to repeated presentations of a frozen WGN whisker deflection pattern while varying activation condition of the LC-NE system in pentobarbital-anesthetized rats¹⁰⁵ (**Fig. 2-1a**). Here, we model the encoding of the high dimensional spatiotemporal whisker deflection signal into a neuron's spike train using the linear-nonlinear-Poisson cascade model^{35,47} (**Fig. 2-1b**). In response to multiple presentations of the same WGN whisker stimulation, VPM neurons respond reliably at specific timepoints which correspond to sections of the stimulus which closely match the kinetic features the neuron selectively encodes for (**Fig. 2-1c**). These timepoints at which a reliable response occurs, called events, were identified through using a threshold (3x mean firing rate) to identify peaks in the spike density function (SDF). Once multiple responses of a neuron to the same frozen stimulus had been recorded, the SDF was generated by first collapsing the perievent raster into a peristimulus time histogram (PSTH), then smoothing the PSTH by convolving it with an adaptive

kernel (**see methods**). Through reverse correlation analysis, we were able to recover the kinetic feature(s) to which each VPM neuron selectively responded to and then calculate the corresponding nonlinear tuning function(s), which illustrate the sensitivity of the neuron's response to how closely the stimulus resembles that feature. We were then able to use an information theoretic approach (**see methods**) to quantify the mutual information between a neuron's spike response and the absence/presence of the features the neuron selectivity encodes for in the stimulus ¹⁰⁵.

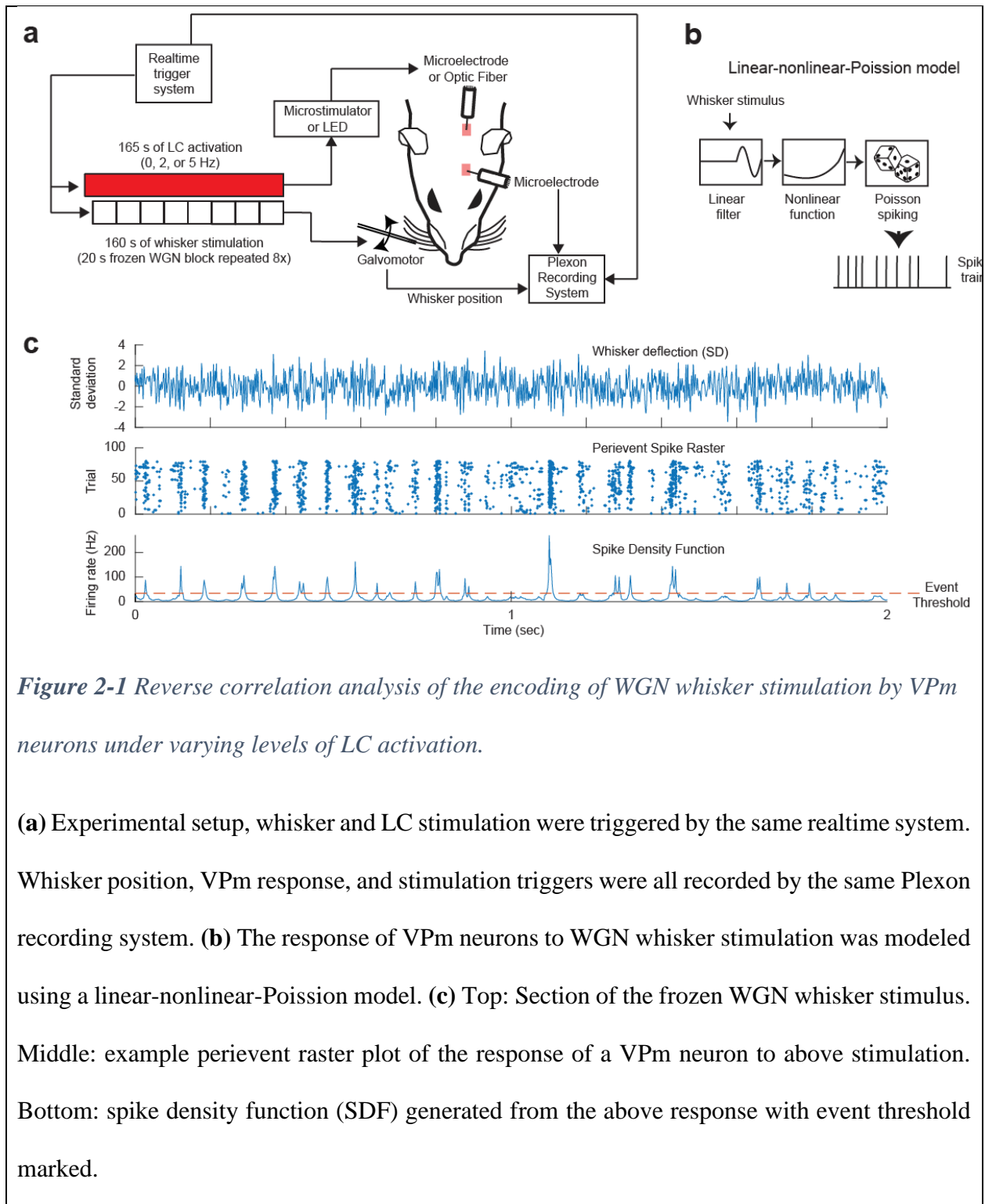
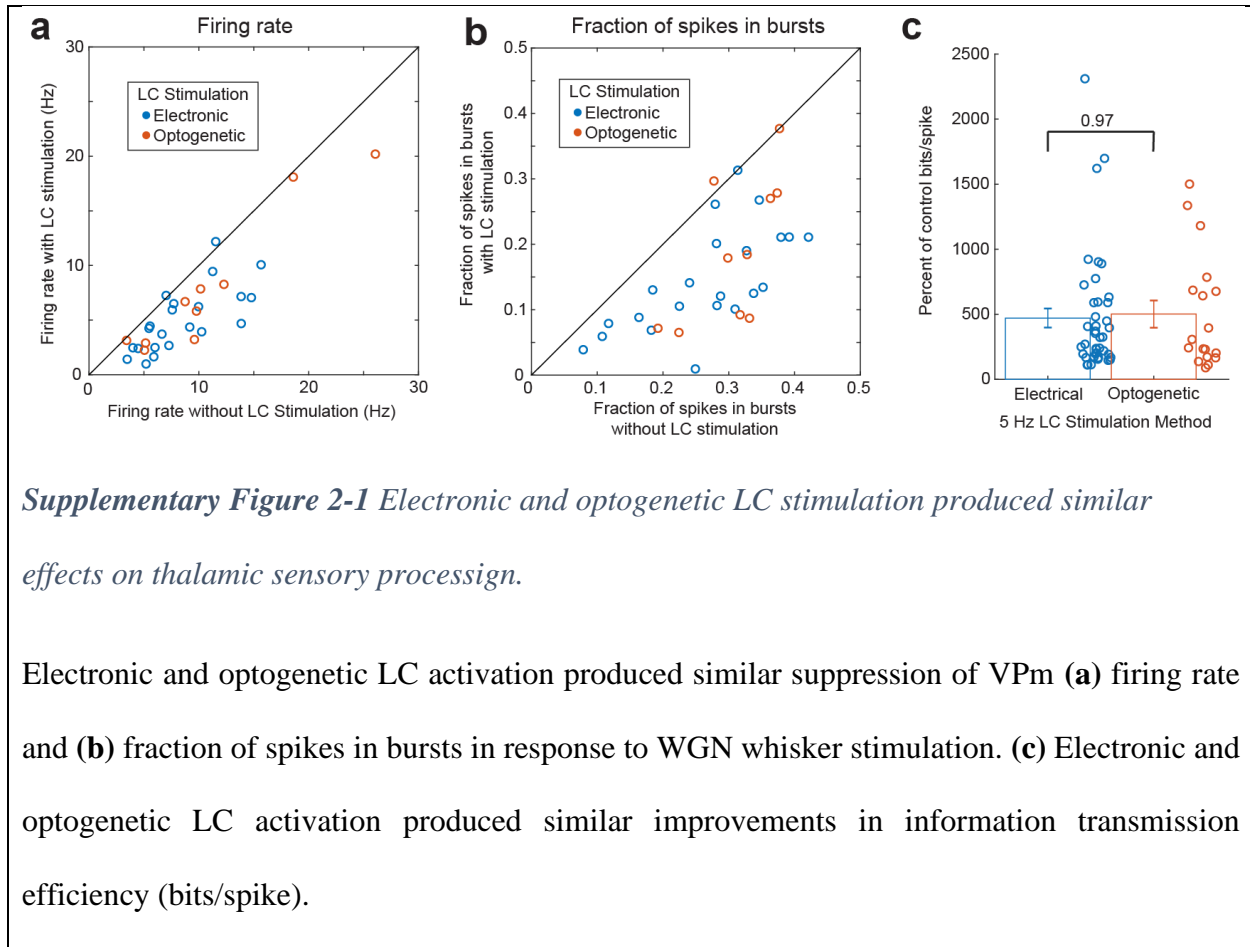


Figure 2-1 Reverse correlation analysis of the encoding of WGN whisker stimulation by VPM neurons under varying levels of LC activation.

(a) Experimental setup, whisker and LC stimulation were triggered by the same realtime system. Whisker position, VPM response, and stimulation triggers were all recorded by the same Plexon recording system. **(b)** The response of VPM neurons to WGN whisker stimulation was modeled using a linear-nonlinear-Poisson model. **(c)** Top: Section of the frozen WGN whisker stimulus. Middle: example perievent raster plot of the response of a VPM neuron to above stimulation. Bottom: spike density function (SDF) generated from the above response with event threshold marked.

For the purpose of this analysis we combined two data sets, one in which the LC was activated with electrical microstimulation and another in which the LC was optogenetically

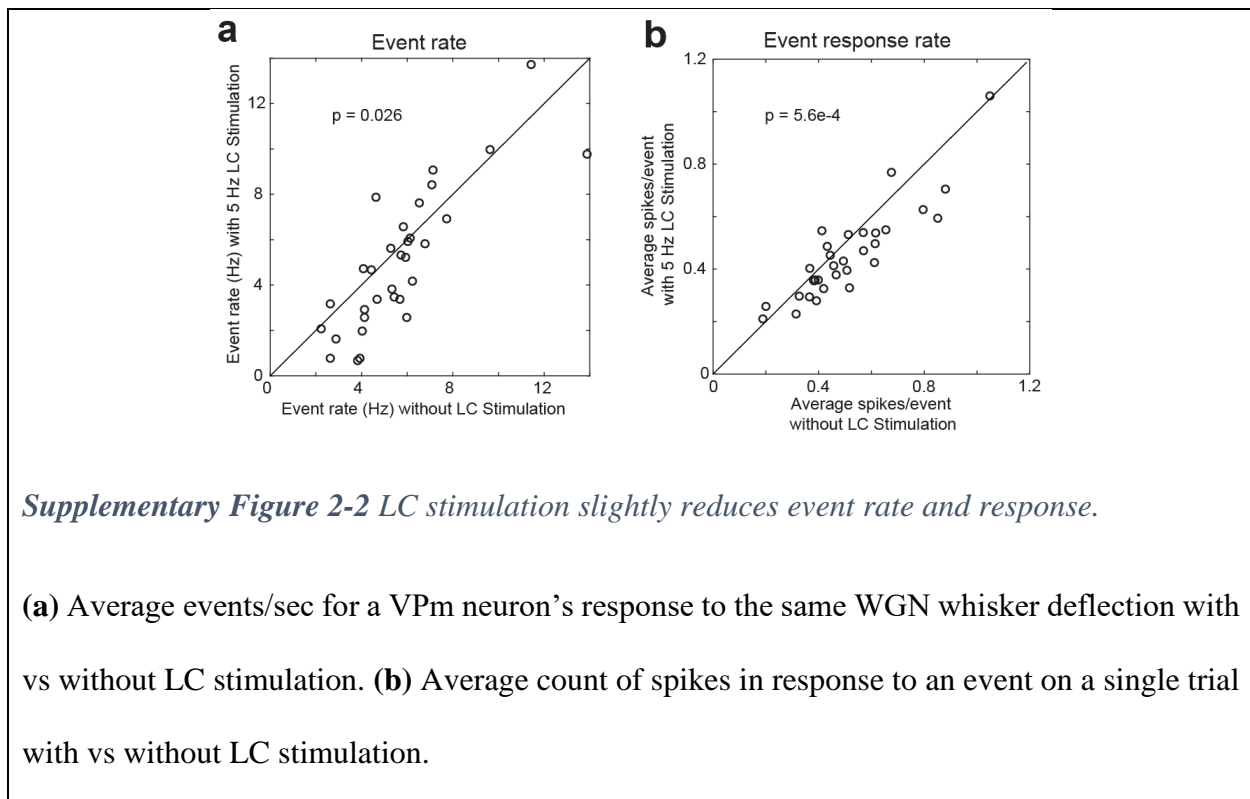
activated. Electrical and optogenetic stimulation were both delivered at 5 Hz and produced similar observed suppressive effects on VPM firing rate (**Supplementary Fig. 2-1a**, 58 ± 5 percent of control firing rate with 5 Hz electrical LC stimulation vs. 67 ± 6 percent during 5 Hz optogenetic LC stimulation, 22 neurons across 15 rats vs. 10 neurons across 4 rats respectively, $p = 0.29$, unpaired t-test) and bursting rate (**Supplementary Fig. 2-1b**, 39 ± 5 percent of control bursting rate with 5 Hz electrical LC stimulation vs. 48 ± 10 percent during 5 Hz optogenetic LC stimulation, 22 neurons across 15 rats vs. 10 neurons across 4 rats respectively, $p = 0.31$, unpaired t-test) and enhancement effects on information transmission (**Supplementary Fig. 2-1b**, 471 ± 73 percent of control bits/spike with 5 Hz electrical LC stimulation vs. 502 ± 105 percent during 5 Hz optogenetic LC stimulation, 22 neurons across 15 rats vs. 10 neurons across 4 rats respectively, $p = 0.97$, Mann-Whitney U-test).



LC modulation of thalamoreticulo-thalamic circuit dynamics altered the temporal structure VPM neurons used to encode the same WGN whisker stimulus.

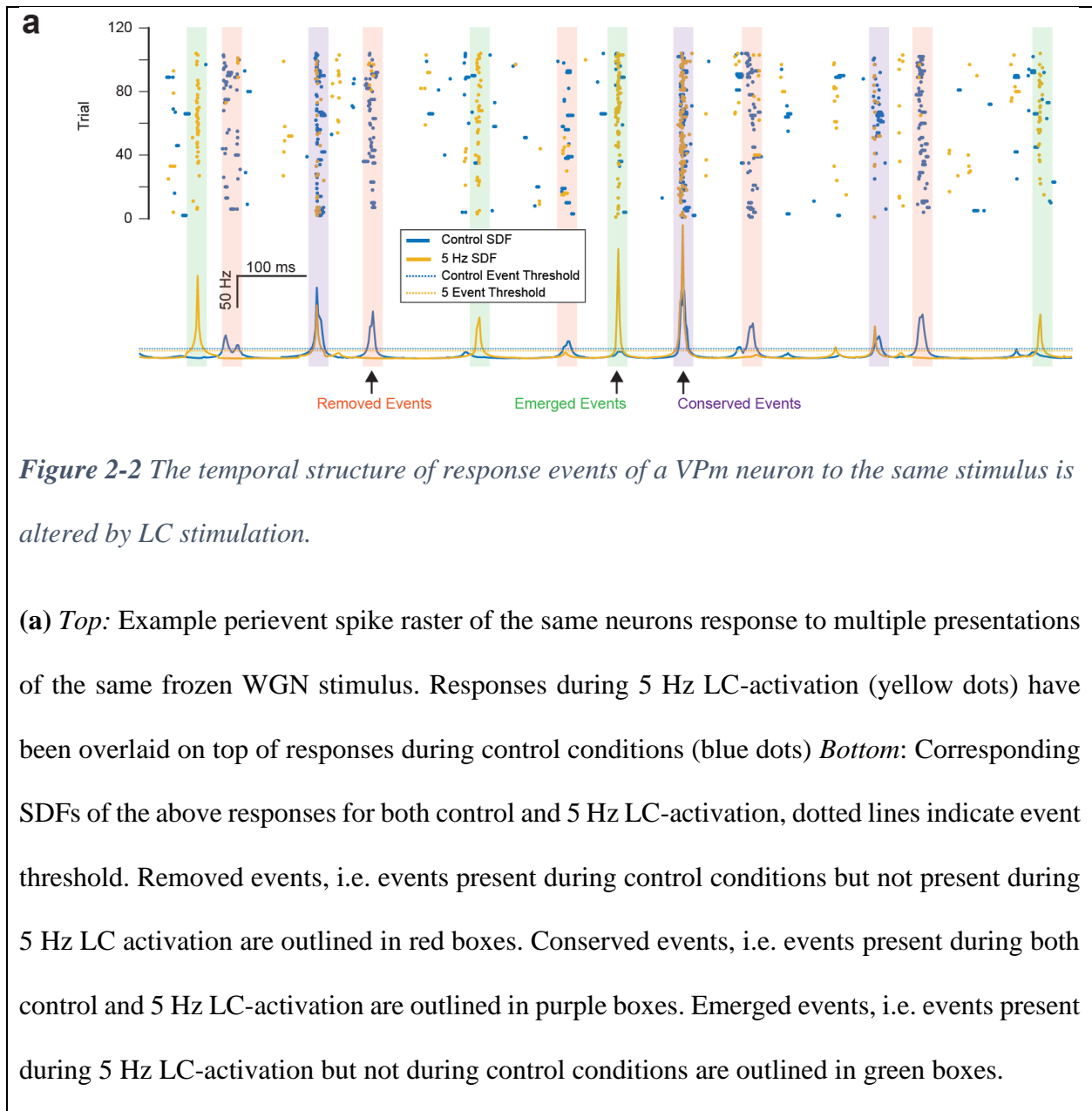
Comparing the number of events between VPM responses under different LC activation conditions, we found LC activation resulted in a slight decrease in event rate (**Supplementary Fig. 2-2a**, 5.7 ± 0.4 Hz without LC stimulation vs 5.0 ± 0.5 with 5 Hz LC stimulation, 32 neurons across 19 rats, $p = 0.026$, paired t-test). Looking at the average spiking response of a VPM neuron during an event we find that most events only encompass a single spike (as average spikes/event < 1) and that LC activation slightly reduced the average spikes in response to an event (**Supplementary Fig. 2-2b**, 0.51 ± 0.03 spikes/event without LC stimulation vs 0.45 ± 0.03 spikes/event with 5 Hz LC stimulation, 32 neurons across 19 rats, $p = 5.6e-4$, paired t-test). This slight reduction in both event

rate and strength of event response is expected given the observed LC-activation-induced suppression of VPM firing rate. Interestingly, our previous work showed that neither the LC-induced general reduction in firing rate nor the LC-activation-induced improvement in reliability could be responsible for the observed LC-activation-induced improvement in information transmission efficiency and rate¹⁰⁵. Further, our previous work had also found that removal of bursting spikes could also not explain the observed LC-activation-induced enhancement of sensory processing, as tonic spikes during LC activation carried significantly more information than tonic spikes without LC activation¹⁰⁵. How then is the temporal pattern of the VPM response, used to encode the absence/presence of features in the incoming stimulus, changed in such a way that improves the efficiency and rate of the information transmitted?



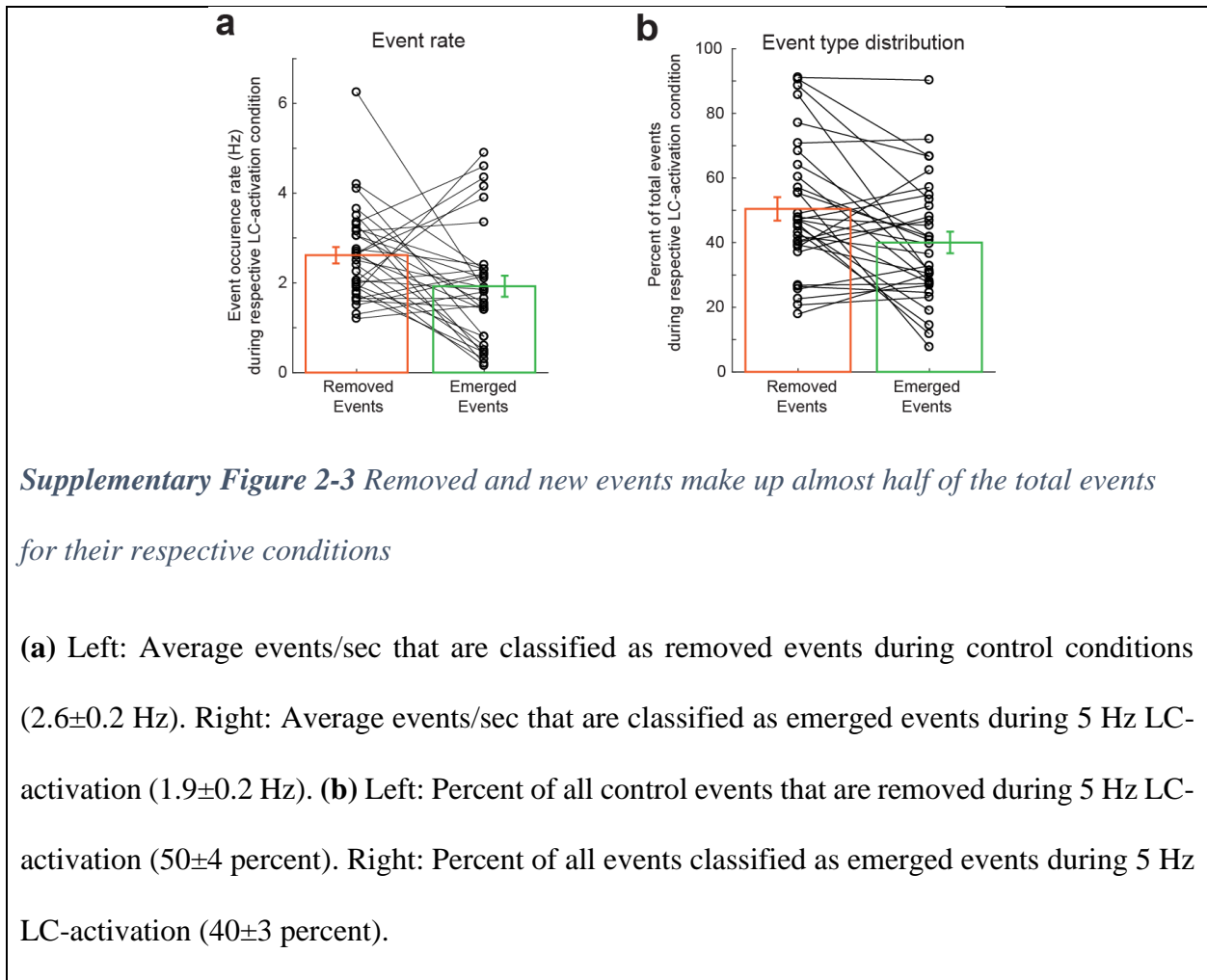
Here we investigate this question further by comparing the temporal structure of events each VPM neurons used to encode the frozen WGN stimulus with and without LC stimulation.

When we overlay the perievent raster and SDF of the VPm response with 5 Hz LC stimulation over that of the VPm response without LC stimulation, we can see that LC-activation clearly alters the temporal event structure (**Fig. 2-2a**). Some events are conserved across both control and LC-activation conditions (**Fig. 2-2a**, conserved events labeled with purple boxes). However, we interestingly see that LC-activation results in the removal of some events that were present under controlled conditions (**Fig. 2-2a**, removed events labeled with red boxes). Further, LC-activation results in the addition of some new events that were not present under control conditions (**Fig. 2-2a**, emerged events labeled with green boxes). This suggest that LC-activation may optimize the temporal structure each VPm neuron uses to encode a specific stimulus by removing less-optimal events and adding more-optimal events.



To allow us to further analyze the change in temporal event structure, we classified the event types as follows. Any 5 Hz LC stimulation event that overlapped with a 0 Hz LC stimulation event was considered a “conserved event”. VPM events during 0 Hz LC stimulation which did not overlap with any events during 5 Hz LC stimulation were considered “removed events” while VPM events during 5 Hz LC stimulation which did not overlap with any events during 0 Hz LC

stimulation were considered “emerged events” (**Fig. 2-2a**). Here we find that approximately half of the events found during control conditions were removed with LC stimulation; while approximately 40 percent of the events found during 5 Hz LC-activation were newly emerged and not present during control conditions (**Supplementary Fig. 2-2**, 32 neurons across 19 rats).



LC-activation resulted in a replacement of removed events with relatively more informative emerged events

Next, we determined if there was any difference between the feature selectivity of the spikes that fell in the different event types. To this end, we selected four different groups of spikes: spikes without LC stimulation that occurred during removed events, spikes without LC stimulation

that occurred during conserved events, spikes during 5 Hz LC-activation that occurred during conserved events, and spikes during 5 Hz LC-activation that occurred during emerged events. Interestingly, we find that when we recover the feature selectivity for each subtype of event, the feature selectivity of spikes during LC-activation that fell within newly emerged events had an improved feature selectivity as compared to spikes during control conditions that fell within removed events (**Fig. 2-3a,b**). This improved feature selectivity of emerged vs removed events confirms the LC-mediated removal and introduction of events favors optimal feature selectivity. The amplitude of the recovered features for removed and emerged event spikes was then compared with that of the amplitude of the feature selectivity recovered using all control condition spikes by calculating the feature modulation factor (**see methods**). The feature modulation factor increases to values greater than 1 when the recovered feature amplitude is greater than that of the feature selectivity recovered during the control periods. Here, we find that indeed spikes during emerged events had a significantly greater feature modulation factor than spikes during removed events (**Fig. 2-3c**, 1.0 ± 0.1 for spikes within removed events vs 1.7 ± 0.1 for spikes within emerged events, 59 features across 32 neurons across 19 rats, $p = 6.2e-5$, paired t-test). We then employed an information theoretic approach to quantify the information transmitted by these spikes about the absence/presence of the feature they selectively encode for in the stimulus. The results showed that spikes within emerged events carried significantly more information than spikes within removed events (**Fig. 2-3d**, 0.20 ± 0.02 bits/spike within removed events vs 0.67 ± 0.10 bits/spike within emerged events, 59 features across 32 neurons across 19 rats, $p = 3.9e-9$, Wilcoxon signed-rank test).

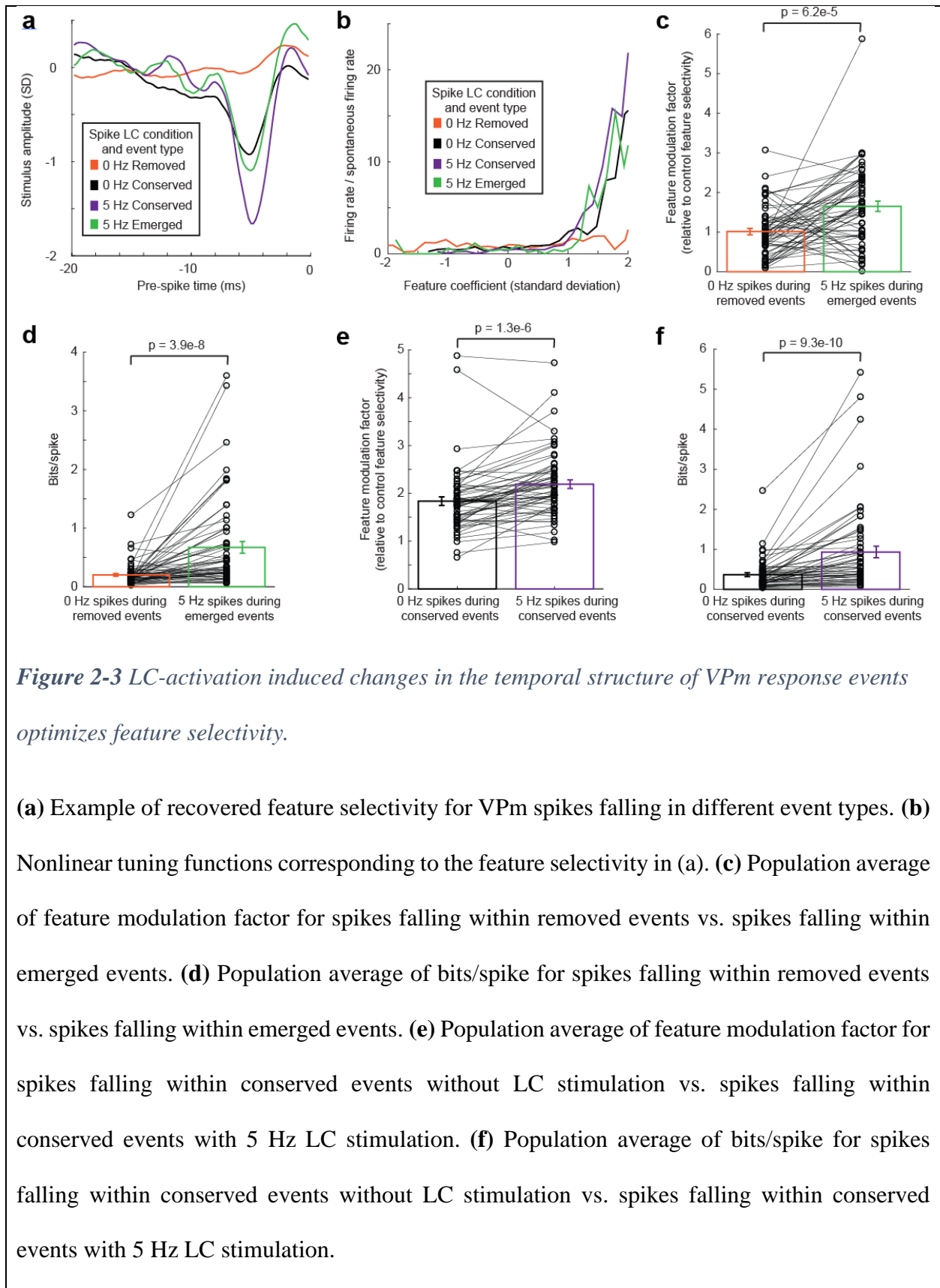


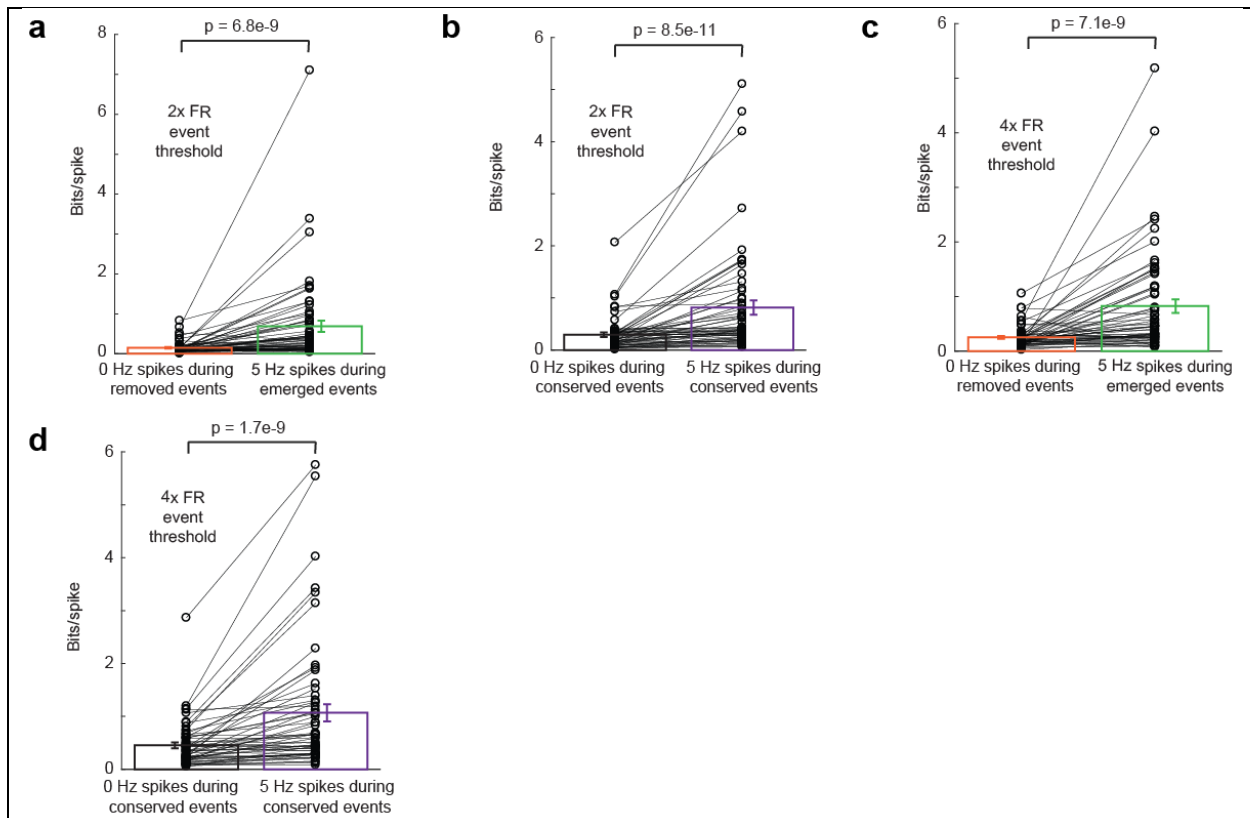
Figure 2-3 LC-activation induced changes in the temporal structure of VPM response events optimizes feature selectivity.

(a) Example of recovered feature selectivity for VPM spikes falling in different event types. **(b)** Nonlinear tuning functions corresponding to the feature selectivity in (a). **(c)** Population average of feature modulation factor for spikes falling within removed events vs. spikes falling within emerged events. **(d)** Population average of bits/spike for spikes falling within removed events vs. spikes falling within emerged events. **(e)** Population average of feature modulation factor for spikes falling within conserved events without LC stimulation vs. spikes falling within conserved events with 5 Hz LC stimulation. **(f)** Population average of bits/spike for spikes falling within conserved events without LC stimulation vs. spikes falling within conserved events with 5 Hz LC stimulation.

Interestingly, when we compared spikes that occurred during conserved event times without LC stimulation with spikes that occurred during conserved event times with LC stimulation, we find that the feature selectivity of these spikes are improved by LC-activation as well (**Fig. 2-3a,b**). This suggests that even within conserved events, LC-activation causes a shift of the distribution of spikes into the more informative conserved events and away from the less informative conserved events. Indeed we find a significantly greater feature modulation factor for spikes that occurred during conserved event times with LC stimulation than spikes that occurred during conserved event times without LC stimulation (**Fig. 2-3e**, 1.8 ± 0.1 for spikes within conserved events without LC stimulation vs 2.2 ± 0.1 for spikes within conserved events with 5 Hz LC stimulation, 59 features across 32 neurons across 19 rats, $p = 1.3e-6$, paired t-test). Further, spikes that occurred during conserved event times with LC stimulation carried significantly more information than spikes that occurred during conserved event times without LC stimulation (**Fig. 2-3f**, 0.37 ± 0.05 bits/spike within conserved events without LC stimulation vs 0.93 ± 0.14 bits/spike within conserved events with 5 Hz LC stimulation, 59 features across 32 neurons across 19 rats, $p = 9.3e-10$, paired t-test).

Importantly, we wanted to verify that the change in event structure and observed differences in the information encoded by spikes within the different event types was not an artifact of the threshold chosen to identify event times from the SDF. To this end, we performed the above analysis again, but used different event thresholds (i.e. 2x and 4x mean firing rate). Using either of the alternative event thresholds we still observed the same increase in bits/spike for emerged vs removed events (**Supplementary Fig. 2-4a**, 2x mean firing rate event threshold, 0.15 ± 0.02 bits/spike within removed events without LC stimulation vs 0.69 ± 0.14 bits/spike within emerged

events with 5 Hz LC stimulation, 59 features across 32 neurons across 19 rats, $p = 6.8e-9$, Wilcoxon signed-rank test, **Supplementary Fig. 2-4b**, 4x mean firing rate event threshold, 0.29 ± 0.04 bits/spike within removed events without LC stimulation vs 0.81 ± 0.14 bits/spike within emerged events with 5 Hz LC stimulation, 59 features across 32 neurons across 19 rats, $p = 8.5e-11$, Wilcoxon signed-rank test). Further with both event thresholds we still see the same increase in bits/spike between spikes in conserved events occurring with LC stimulation vs spikes in conserved events occurring without LC stimulation (**Supplementary Fig. 2-4c**, 2x mean firing rate event threshold, 0.25 ± 0.03 bits/spike within conserved events without LC stimulation vs 0.82 ± 0.12 bits/spike within conserved events with 5 Hz LC stimulation, 59 features across 32 neurons across 19 rats, $p = 7.1e-9$, Wilcoxon signed-rank test, **Supplementary Fig. 2-4d**, 4x mean firing rate event threshold, 0.45 ± 0.06 bits/spike within conserved events without LC stimulation vs 1.07 ± 0.16 bits/spike within conserved events with 5 Hz LC stimulation, 59 features across 32 neurons across 19 rats, $p = 1.7e-9$, Wilcoxon signed-rank test).



Supplementary Figure 2-4 LC-activation-induced changes in the temporal structure of VPM response were not artifacts of event threshold.

(a) Population average of bits/spike for spikes falling within removed events vs. spikes falling within emerged events. Event threshold of 2x mean SDF firing rate was used. **(b)** Population average of bits/spike for spikes falling within conserved events without LC stimulation vs. spikes falling within conserved events with 5 Hz LC stimulation. Event threshold of 2x mean SDF firing rate was used. **(c)** Population average of bits/spike for spikes falling within removed events vs. spikes falling within emerged events. Event threshold of 4x mean SDF firing rate was used. **(d)** Population average of bits/spike for spikes falling within conserved events without LC stimulation vs. spikes falling within conserved events with 5 Hz LC stimulation. Event threshold of 4x mean SDF firing rate was used.

The reorganization of the temporal response events of VPm neurons during LC activation favors ideal event placement for feature selectivity

Having found that LC-activation resulted in a restructuring of the temporal positions of the reliable response events used by the same VPm neuron to encode the same stimulus, we wanted to investigate how ideal the encoding pattern of each VPm neuron was with and without LC stimulation. To answer this question, we first had to define exactly what an ideal encoding of the stimulus into a corresponding response events would look like for a neuron with a specific feature selectivity. Here, we constrain our search for each neuron's ideal response by using the same exact number of events in our ideal response as were present in each neuron's actual SDF. To find ideal the timepoints to place these events, we first calculated the feature coefficient value (i.e. the dot product between the 20 ms of preceding stimulus and feature selectivity) for each timepoint of the WGN stimulus (**Fig. 2-4a,b**). A very informative neuron would only respond at timepoints corresponding to large magnitude feature coefficient, e.g. the peaks in the resulting feature coefficient vector. However, whether a neuron's response is directionally sensitive to the sign of the feature coefficient (i.e. sensitive to only large positive feature coefficient values vs both large negative and positive feature coefficient values) varies across neurons. A neuron selectively responding to a specific feature in a directional fashion would ideally fire at large magnitude feature coefficients only if they are positive value (**Fig. 2-4a**). While, a neuron selectively responding to a specific feature in a non-directional fashion would ideally fire at large magnitudes of feature coefficients regardless of whether they were negative (the inverse of the feature) or positive (**Fig. 2-4b**).

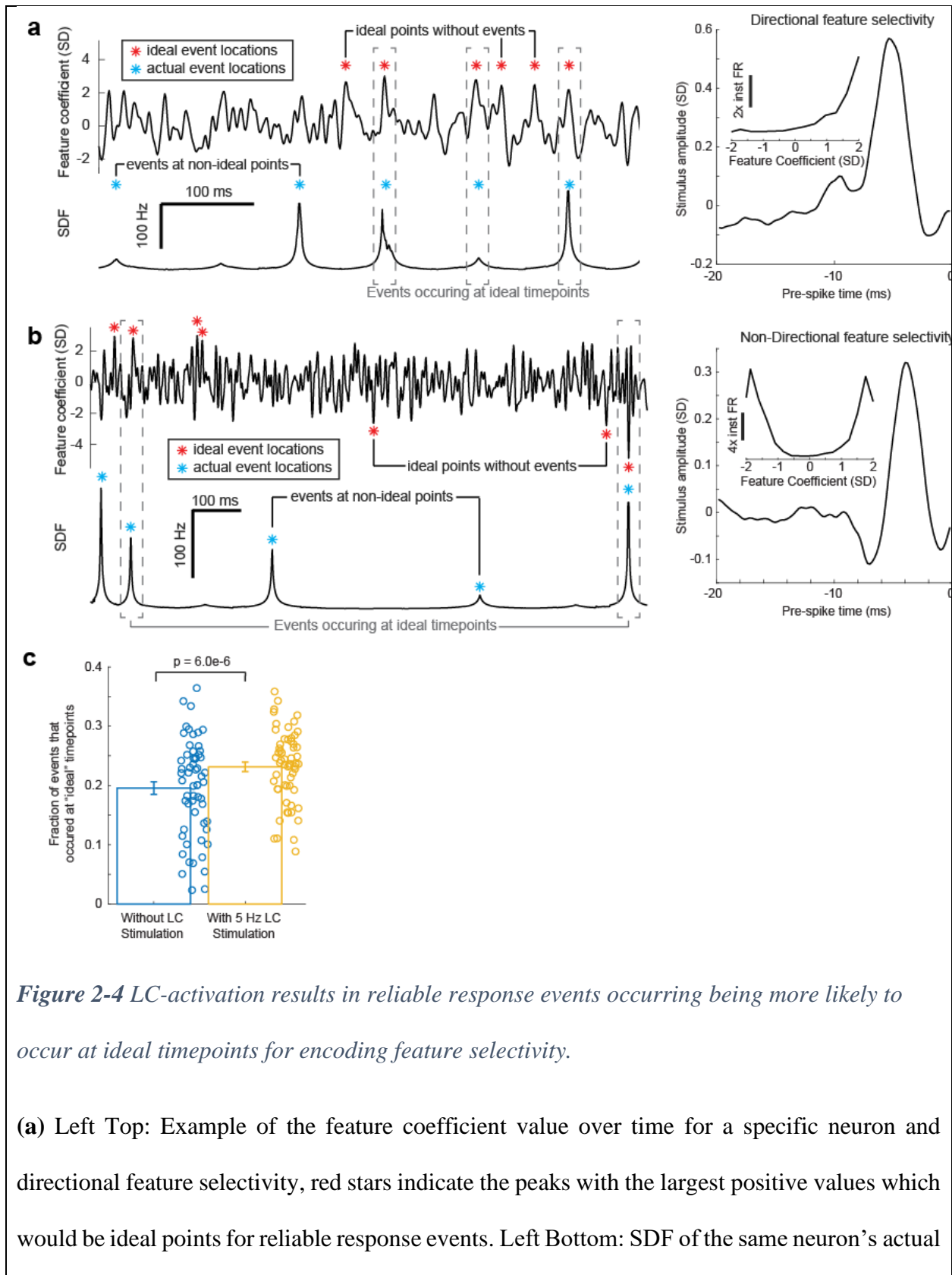


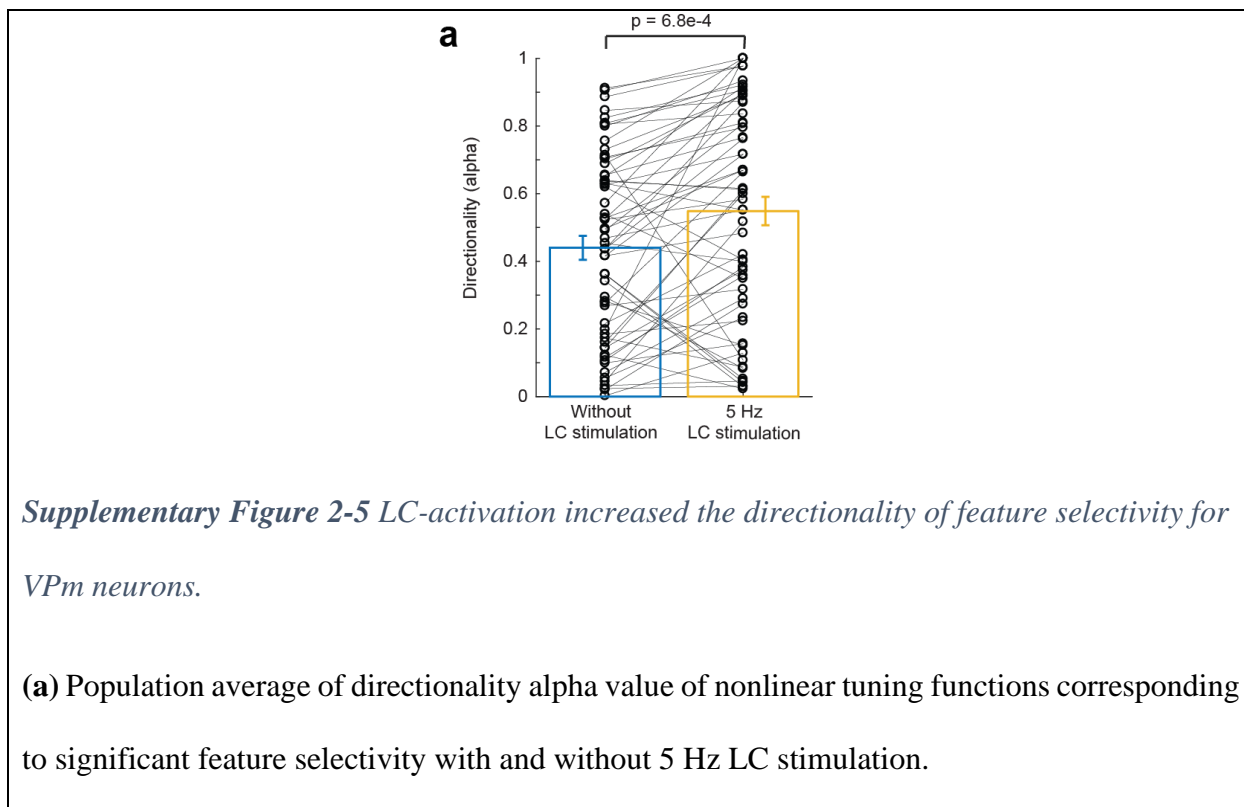
Figure 2-4 LC-activation results in reliable response events occurring being more likely to occur at ideal timepoints for encoding feature selectivity.

(a) Left Top: Example of the feature coefficient value over time for a specific neuron and directional feature selectivity, red stars indicate the peaks with the largest positive values which would be ideal points for reliable response events. Left Bottom: SDF of the same neuron's actual

response to the whisker stimulus, blue stars indicate observed events. Right: The directionally selective feature selectivity corresponding to the panels on the left. **(b)** Left Top: Example of the feature coefficient value over time for a specific neuron and non-directional feature selectivity, red stars indicate the peaks with the largest absolute value which would be ideal points for reliable response events. Left Bottom: SDF of the same neuron's actual response to the whisker stimulus, blue stars indicate observed events. Right: The non-directionally selective feature selectivity corresponding to the panels on the left. **(c)** LC stimulation increases the fraction of events occurring at ideal timepoints.

To determine whether a neuron's feature selectivity was directional or non-directional, for each feature we quantified the directionality of the corresponding nonlinear tuning index using an directionality alpha value ³⁵ (**see methods**). A feature selectivity which is directionally selective will exhibit an asymmetric nonlinear tuning function (**Fig. 2-4a**, right panel), and will have an alpha value close to 1. A feature selectivity which is not directionally selective will have a corresponding nonlinear tuning function that appears symmetric across the y axis (**Fig. 2-4b**, right panel), and an alpha value close to 0. Interestingly, we found that LC stimulation slightly increased the directionality of VPM feature selectivity as measured by alpha (**Supplementary Fig. 2-5a**, $\alpha = 0.44 \pm 0.04$ without LC stimulation vs 0.55 ± 0.04 with 5 Hz LC stimulation, 59 features across 32 neurons across 19 rats, $p = 6.8e-4$, paired t-test). Therefore, when deciding if each feature a neuron selectively responded to was encoded in a directional manner or not, we used the average directionality alpha values between the feature selectivity with and without LC-activation. Any resulting average directionality alpha value which fell beneath a threshold ($\alpha=0.3$) was

considered to be non-directionally selective while any average that fell above was considered to be directionally selective.



After that the directionality of each feature selectivity was calculated we could then identify the peaks in the corresponding feature coefficient vector which would be most ideal to position our events. Here, when locating ideal event points we conserved the same number of events as observed in the original response but moved these event times to be located at the peaks in the feature coefficient vector with the largest positive values for directionally selective features (**Fig. 2-4a**, red stars) or largest absolute values for non-directionally selective features (**Fig. 2-4b**, red stars). We were then able to compare these ideal event timepoints with the actual event timepoints observed with and without LC stimulation (**Fig. 2-4a,b**, blue stars). Here we found that LC stimulation increased the fraction of events that occurred at an ideal event timepoint (**Fig. 2-4c**,

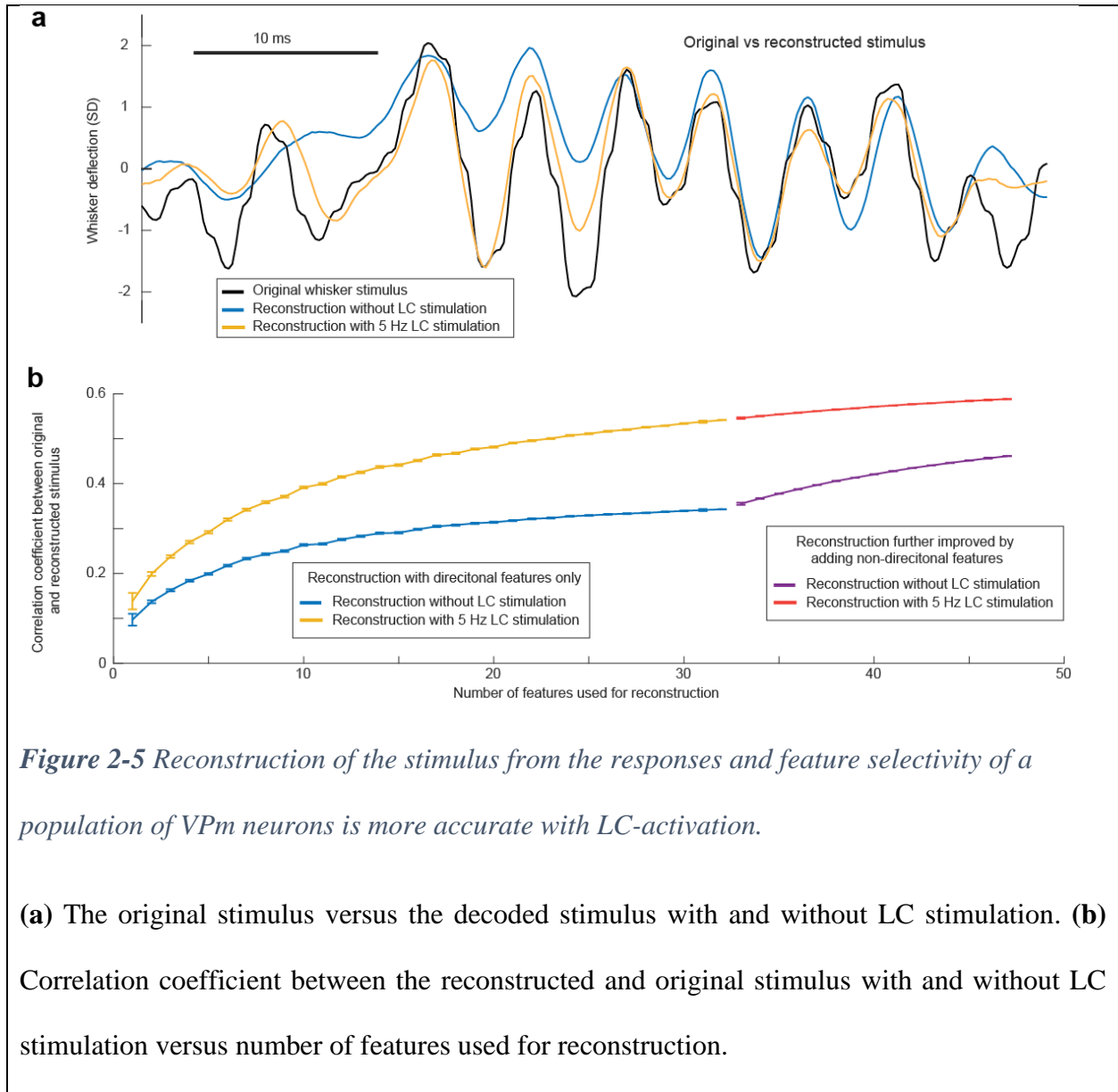
0.20±0.01 without LC stimulation vs 0.23±0.01 with 5 Hz LC stimulation, 59 features across 32 neurons across 19 rats, $p = 6.0e-6$, paired t-test). Taken together with the previous results, this shows that LC-activation results in a changing of the temporal event structure in such a way that favors a more ideal encoding.

LC activation improves the accuracy of stimulus reconstruction decoded from the response and feature selectivity of a population of VPm neurons

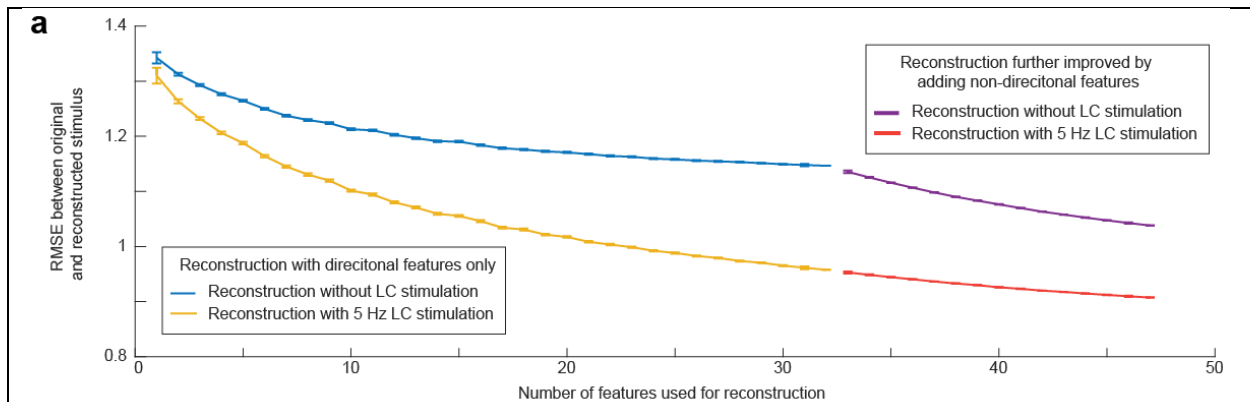
Next, we wanted to investigate how the changes in the stimulus encoding properties of individual thalamic cortical neurons impacted the ability of a population of VPm neurons to accurately encode a spatiotemporal whisker stimulus. To this end, we selected a subset of VPm recordings for which all the responses were driven by the same frozen WGN stimulus. We then analyzed from an ideal observer standpoint of view, how accurately we could decode and reconstruct the original stimulus knowing only the VPm neurons' responses and feature selectivity (see **Methods**). To reconstruct the original stimulus, we assumed the preceding strength of the feature in the stimulus was relative to the average spiking response of the neuron at that timepoint. Initially, only directional feature selectivity was used to reconstruct an approximation as non-directional feature selectivity needed to be orientated first to be used. We were then able to improve the reconstruction by adding non-directional feature selectivity by assuming the direction of the non-directional feature selectivity at any timepoint is that which most closely matches the approximation reconstructed using only directional feature selectivity.

Interestingly, we find that the final reconstruction is more accurate when using the spiking response and feature selectivity of the neurons during 5 Hz LC stimulation as compared to the reconstruction generated using the spiking response and feature selectivity of the neurons without LC stimulation (**Fig. 2-5a**). This shows that LC stimulation optimizes the encoding of

sensory-related information in the thalamus in a manner which allows for a more accurate recovery of the original stimuli from the thalamocortical spike trains, suggesting the accuracy of the perception of stimuli would be more accurate as well. Indeed, in our previous work, we found that LC-stimulation enhanced the perceptual sensitivity of rats discriminating between two different frequencies of whisker stimulation ¹⁰⁵.



We then wanted to quantify how LC stimulation affects how closely the reconstruction matches the original stimulus. Further, we were interested in how LC stimulation affected the ratio of decoded stimulus accuracy to the number of features used to decode it. To this end, we performed the above method of decoding the stimulus from directional PSTH-feature pairs multiple times for each possible number of features used (minimum of max unique pairs or 1000 unique pairs). For each directional reconstruction, the correlation coefficient between that reconstruction and the original stimulus was saved. When looking at a plot of average correlation coefficient versus number of features used for directional reconstruction, as expected we find that the accuracy of the reconstruction increases with increasing number of features used (**Fig. 2-5b**). We also find that the more features used, the less additional accuracy adding another feature provided, indicating there is some redundancy in the information carried by each feature selectivity. Importantly, we find that no matter how many features are used for reconstruction, LC stimulation resulted in a more accurate reconstruction as measured by either correlation coefficient (**Fig. 2-5b**) or RMSE between the reconstruction and original stimulus (**Supplementary Fig. 2-6**). Interestingly we observed that the difference between the accuracy of reconstruction with and without LC stimulation increased as the number of features decoded from increased, suggesting that perhaps LC activation decreases the redundancy of information carried by VPM neurons. We then performed a similar analysis investigating how the accuracy of the directional reconstruction is improved by adding in different amounts of non-directional features (**Fig. 2-5b**). The results of this analysis also showed that LC stimulation results in a more accurate reconstruction when decoded from both directional and non-directional features (**Fig. 2-5b, Supplementary Fig. 2-6**).



Supplementary Figure 2-6 Stimulus reconstruction using the responses and feature selectivity of a population of VPM neurons is more accurate with LC-activation.

(a) RMSE between the reconstructed and original stimulus versus number of features used for reconstruction.

Discussion

Further supporting our argument that LC enhances sensory processing not primarily through modulation of gain or SNR, we unexpectedly found that LC activation changed the temporally precise firing pattern the VPM used to encode the same stimulus. This was initially puzzling, as it is counterintuitive that this change in encoding pattern would occur without a change in the kinetic features the neuron is encoding for. However, we found the new encoded pattern is optimized as it increases the efficiency and rate of stimulus-related information transmitted by VPM neurons. Previously, LC-induced enhancement of sensory processing was shown to result in an enhancement of the feature selectivity as well as an improvement of information transmission efficiency and rate of VPM neurons¹⁰⁵. Here, we show that LC stimulation allows for a more accurate reconstruction of the original stimulus when decoding it from the response of a population

of VPM neurons as an ideal observer, suggesting that LC stimulation may enhance the accuracy of the perception of whisker stimuli.

When investigating whether event timepoints occur at ideal locations, it must be considered that a VPM neuron may selectively encode for multiple features. Therefore, event timepoints which may be non-ideal for one of the neuron's feature may be ideal for another. Interestingly here we find an increase in the fraction of events occurring at ideal times for the feature selectivity of neurons selective for one feature as well as neurons selective for multiple. If the change in the temporal structure of reliable events used to encode a whisker stimulus resulted in an improved feature selectivity for one feature at the cost of a degraded feature selectivity for another feature we would expect to see a mixed result of LC activation on the fraction of events at ideal times for each feature. Instead, we observed an improvement across the vast majority of feature selectivity, suggesting that removed events were not ideal events for any of the features the neuron encoded for. In this way LC-mediated changes in temporal response structure do not shift the feature selectivity towards one feature at the expense of another, but rather improve the feature selectivity for all features the neuron selectively responds to.

As we have shown previously, the mechanism underlying this optimization of thalamic state for sensory processing is the action of LC-induced increased NE concentration in the thalamus. We found that increased NE resulted in a reduction in calcium t-channel activity in both the VPM and TRN, which we hypothesized decreased the subthreshold membrane potential fluctuations of VPM neurons. Removal of these underlying noisy fluctuations may allow the response of VPM neurons to be more solely related to stimulus-relevant input from the PrV, resulting in the change in temporal structure of VPM response events observed with LC activation.

Chapter 3: Rapid and transient enhancement of thalamic information transmission induced by vagus nerve stimulation

Abstract

Vagus nerve stimulation (VNS) has been FDA-approved as a long-term, therapeutic treatment for multiple disorders, including pharmacoresistant epilepsy and depression. Here we elucidate the previously uninvestigated short-term effects of VNS on sensory processing through employing an information theoretic approach to examine the effects of VNS on thalamocortical transmission of sensory-related information along the somatosensory pathway. We found that VNS enhanced the selectivity of the response of thalamic neurons to specific kinetic features in the stimuli, resulting in a significant increase in the efficiency and rate of stimulus-related information conveyed by thalamic spikes. VNS-induced improvements in thalamic sensory processing coincided with a decrease in thalamic burst firing, suggesting the underlying mechanism may involve the noradrenergic system which was found to also enhance thalamic sensory processing through burst suppression. Importantly, we found VNS-induced enhancement of sensory processing had a rapid onset and offset, completely disappearing one minute after cessation of VNS. The timescales of these effects indicate against an underlying mechanism involving long-term neuroplasticity. We found several patterns of VNS (tonic, standard duty cycle, and fast duty cycle) all induced similar improvements in sensory processing. Under closer inspection we noticed that due to the fast timescale of VNS effects on sensory processing, standard duty-cycle VNS induced a fluctuating sensory processing state which would be sub-optimal for perceptual behavior. Fast duty-cycle VNS and continuous, tonic VNS induced quantitatively similar improvement in thalamic information transmission as standard duty-cycle VNS without

inducing fluctuations. Further, we found the strength of VNS-induced improvements in sensory processing increased monotonically with amplitude and frequency of VNS. These results demonstrate, for the first time, the feasibility of utilizing specific patterns of VNS to rapidly improve sensory processing and confirm fast duty-cycle and tonic patterns as optimal for this purpose, while showing standard duty-cycle VNS causes non-optimal fluctuations in thalamic state.

Introduction

The vagus nerve, the longest cranial nerve and part of the parasympathetic nervous system, originates from the medulla and innervates organs in the thorax and abdomen. The majority of vagus nerve afferent fibers project to the brain through the nucleus tractus solitarius (NTS) ^{176, 177}. However, in addition to this pathway the vagus nerve also has ipsilateral projections to the area postrema, dorsal motor nucleus of the vagus, nucleus ambiguus, medullary reticular formation, and the spinal trigeminal nucleus ¹⁷⁸. Vagus nerve stimulation (VNS) has long been known to have profound effects on the neural dynamics of the central nervous system. Due to the ease at which the vagus nerve can be accessed, VNS has attracted tremendous interest from the clinical community, and has been FDA-approved for many different treatments including therapies for intractable epilepsy and pharmaco-resistant depression ¹⁷⁹⁻¹⁸¹. In the last decade, numerous efforts have been made to test the efficacy of VNS in treating a wide variety of other neurological and psychiatric disorders, including autism, stroke-induced damage, PTSD, pain, inflammation, addiction, and obesity ¹⁸²⁻¹⁹². More recently transdermal VNS was proven as an effective method to non-invasively activate the vagus nerve ¹⁹³⁻¹⁹⁶, as evidenced by the FDA approving multiple commercial transdermal VNS systems for use in clinical applications.

The vagus nerve presumably modulates brain circuit dynamics through influence on several neuromodulatory systems, including the locus coeruleus – norepinephrine (LC-NE) system¹⁹⁷. Elevated firing rate of LC neurons in response to VNS has been confirmed by several previous studies^{198, 199}. Indeed, previous work has suggested that the LC is one of the main brain structures mediating the beneficial therapeutic effects of VNS on abnormal brain activity. For example, the ability of VNS to abort seizures was significantly reduced after lesioning of the LC²⁰⁰. The LC is the primary source of NE to the forebrain and as such plays a pivotal role in many brain functions. Our recent work demonstrated that LC activation dramatically improved information transmission in the somatosensory thalamus, a critical stage for sensory processing and perceptual performance. Moreover, we found the mechanism underlying this improvement was LC-NE mediated suppression of burst firing in the intra-thalamic circuitry via direct action of NE on thalamic noradrenergic receptors. Reduction of calcium t-channel activity, the membrane channels responsible for burst firing, led to an increased ability of thalamic relay neurons to respond selectively to the specific kinetic features each neuron encodes¹⁰⁵. We therefore reasoned it would be possible to utilize VNS as a method for enhancement of sensory processing. However, the extent to which VNS affects thalamic information transmission had not been examined.

In this study, we sought to investigate the effects of VNS on the feature selectivity and information transmission of neurons of the ventroposterior medial nucleus of thalamus (VPM), the thalamic relay stage of the rat vibrissa system. We recorded single-unit VPM responses to white Gaussian noise (WGN) whisker stimulation while systematically varying VNS patterns. We found VNS significantly enhanced the feature selectivity of VPM neurons, resulting in improved transmission of sensory-related information. Interestingly, this improvement was similar to that induced by direct LC stimulation as both VNS and direct LC stimulation suppressed VPM burst

firing. Previous VNS techniques have focused on facilitating long-term, neuroplastic change of brain circuits^{201, 202}. In contrast, here we found VNS was also able to produce rapid and short-lasting effects on thalamic feature selectivity and information transmission, evidenced by the fact that thalamic sensory processing returned to baseline conditions approximately 60 s after VNS cessation.

In clinical applications, VNS is commonly delivered in a duty-cycle fashion, with a standard pattern consisting of on periods consisting of 30 s of continuous VNS delivered at 30 Hz interleaved with off periods of 60 s or longer²⁰³⁻²⁰⁶. Having found that VNS-induced enhancement of sensory processing rapidly dissipated following cessation of VNS, we wondered how duty-cycle VNS with standard off periods would affect the sensory processing state of the thalamus. As expected, we found that improvement in information transmission was significantly stronger during the 30 s VNS on period when compared to the second 30 s of the VNS off period of standard duty-cycle VNS. This indicates that standard duty-cycle VNS creates a fluctuating thalamic sensory processing state. Such a state would be detrimental for discrimination of stimuli, as the same stimulus would evoke different VPM responses depending on if it was received during the on or off period of the standard duty-cycle VNS.

To find a VNS pattern that could be safely used to enhance sensory processing without inducing a fluctuating state we also examined VNS with a fast duty-cycle (i.e. 3 s on 7 s off) and 10 Hz tonic VNS. We found these patterns both induced quantitatively similar improvement in thalamic information transmission when compared to standard duty-cycle VNS. Importantly we found that fast duty-cycle VNS did not produce fluctuations in sensory processing as evidenced by equal rates of burst suppression and information improvement found to occur during the on period versus the second half of the off period. Further, both fast duty-cycle and tonic VNS-

induced improvements increased monotonically with increased VNS amplitude and tonic VNS-induced improvements increase monotonically with increased VNS frequency. Taken together, our results have demonstrated, for the first time, that VNS is able to rapidly enhance information processing in the sensory system. Moreover, our data suggested that specific patterns of VNS without long off periods, such as fast duty-cycle and tonic VNS, should be used for VNS-enhancement of information transmission as the relatively long off periods used by standard duty-cycle VNS create a non-optimal fluctuating sensory processing state.

Methods

All animal work was approved by the Columbia University Institutional Animal Care and Use Committee and the procedures were conducted in compliance with NIH guidelines. 16 adult albino rats (Sprague-Dawley, Charles River Laboratories, Wilmington, MA; ~225-275 g at time of implantation) were used in this study. Animals were housed 1-2 per cage in a dedicated housing facility, which maintained a twelve-hour light and dark cycle.

Surgery

Rats were sedated with 5% vaporized isoflurane in their home cages before being transported to the surgery suite at 2% vaporized isoflurane. Rats were then mounted on a stereotaxic frame, and the anesthetic was switched to ketamine/xylazine (80/8 mg/kg)¹⁹⁸. Body temperature was kept at 37 °C by a servo-controlled heating pad (FHC Inc, Bowdoin, ME). Blood-oxygen saturation level and heart rate were continuously monitored using a non-invasive monitor (Nonin Medical Inc, Plymouth, MN).

To allow for implantation of the VNS cuff, an incision was made on the left ventral side of the rats. A magnetic fixator retraction system (Fine Scientific Tools, Foster City, CA) was used to separate the sternohyoid and sternomastoid muscles longitudinally, providing clear access to the

vagus nerve running next to the carotid artery within the carotid sheath. Glass tools were used to separate the vagus nerve from the carotid sheath to minimize any potential damage to the nerve. A platinum–iridium bipolar cuff electrode²⁰⁷ was then placed around the vagus nerve to allow for delivery of VNS. An insulated lead connected to the VNS cuff was then ran out of the incision, which was closed with sutures.

Following VNS implantation, the animal was carefully mounted on a custom-modified stereotaxic frame (RWD Life Science, China) on top of a floating air table so that a craniotomy could be created above the VPm to allow for insertion of a recording electrode. On a subset of animals which did not have a VNS cuff implanted, a second craniotomy was also opened above the LC to allow for direct LC stimulation (3 rats). Retaining wells were created around the craniotomies to allow for any exposed brain surface to be covered in warm saline.

Electrophysiology

Single, sharp, tungsten microelectrodes (75 μm in diameter, impedance of $\sim 3\text{-}5\text{ M}\Omega$, FHC Inc, Bowdoin, ME) were used to record extracellular single-unit activity. A hydraulic micropositioner (David Kopf, Tujunga, CA) allowed for slow, controlled electrode positioning with micrometer resolution, and thus allowed for close proximity placement to recorded neurons. Extracellular neural signals were referenced to a ground screw in contact with the surface of the dura, contralateral to the recording site, then band-pass filtered (300-8k Hz) and digitized at 40 kHz using a Plexon recording system (OmniPlex, Plexon Inc., Dallas, TX). Spike sorting of single units was performed using commercially available software (Offline Sorter, Plexon).

The VPm was targeted using stereotaxic coordinates from the rat brain atlas¹⁴⁶. VPm neuron identity was confirmed by a strong response to the mechanical stimulation of the neuron's principal whisker^{33, 208, 209}. Only large, easily isolatable VPm units with a minimum refractory

period greater than 1 ms and a stable waveform throughout the entire recording were used. Burst spiking was defined as any two or more spikes occurring with an ISIs of 4 ms or less and following at least 100 ms of quiescence ¹³².

To estimate the effect of direct LC stimulation on thalamic sensory processing, in some experiments, a tungsten microelectrode with a lower impedance ($\sim 2\text{ M}\Omega$, FHC Inc, Bowdoin, ME) was used to first electrophysiologically locate and subsequently microstimulate the LC. LC neuron identity was confirmed by a wide spike waveform and biphasic response to a paw pinch ^{105, 145}.

Vagus nerve stimulation

The vagus nerve cuff lead was connected to a calibrated electrical microstimulator (Multi Channel Systems, Reutlingen, Germany), which was then triggered by an xPC target real-time system (MathWorks, MA) running at 1 kHz. During periods of VNS, cathode-leading biphasic current pulses (250 μs per phase) were delivered at either 10 or 30 Hz with amplitudes of either 0.4, 1, or 1.6 mA with duty-cycles of either continuous, fast (3 s on / 7 s off), or standard (30 s on / 60 s off). For each recording, multiple repetitions of each VNS condition were delivered in a random order. Each VNS condition delivery lasted 180 s with 75-90 seconds of rest time inserted following to allow for the system to reset to baseline conditions before beginning the next condition. As currently practiced in humans, only the left vagus nerve was stimulated as stimulation of the right vagus nerve has been shown to cause cardiac irregularities due to right vagus nerve efferents innervating the sinoatrial node ²¹⁰. Further, the polarity of VNS was fixed, with the (negative electrode cranial) as a reversal of this polarity has been shown to induce bradycardia ²¹¹.

Locus coeruleus microstimulation

Microstimulation of the LC was described in detail previously^{105, 145}. Briefly, after the LC was electrophysiologically confirmed, the recording microelectrode was disconnected from the recording system and connected to a calibrated electrical microstimulator (Multi Channel Systems, Reutlingen, Germany), which was then triggered by an xPC target real-time system running at 1 kHz. During periods of microstimulation of the LC, cathode-leading biphasic current pulses (200 μ s/phase, 60 μ A) were continuously delivered at either 2 or 5 Hz. Each LC activation condition was delivered, in a random order, beginning 5 s before whisker stimulation and lasting throughout the entire period of whisker stimulation for a total length of 165 s. Ninety-five seconds of dead time was inserted between each stimulation period to allow for the system to return to baseline conditions.

Whisker stimulation

A custom modified galvo motor (galvanometer optical scanner model 6210H, Cambridge Technologies) controlled by a closed-loop system (micromax 67145 board, Cambridge Technology) as described in¹⁷⁵ was used to deliver precise, high-frequency mechanical whisker stimulations (12.5 mm shaft). The galvo motor's position was controlled via the same xPC target real-time system controlling VNS/LC activation. Accuracy of whisker stimulation was verified by using the Plexon recording system to also record the galvo motor's output analog position signal. Whiskers were cut to a length of ~10 mm and inserted into the deflecting arm, which was positioned ~5 mm from whiskerpad. The WGN was low pass filtered (butterworth, 10th order) at 250 Hz¹⁰⁵. The galvo motor was used to continuously deliver whisker deflection following a signal consisting of continuous repetitions of a 15 second clip of frozen white Gaussian noise (WGN).

As we aimed to determine if neurons had similar or altered responses to identical stimuli under varying conditions of VNS, the plane of whisker deflection was fixed throughout the recording.

Data analysis

Here, we assume VPM neurons encode for stimulus-related information via the linear-nonlinear-Poisson model (LNP) as previously detailed by^{35,47,105}. Through analyzing the neuron's spiking response to a repeated delivery of a frozen WGN whisker deflection pattern, we can recover the neurons' feature selectivity, which can be represented by a linear filter set and the corresponding set of nonlinear tuning functions. Specifically, each neuron's first significant feature was recovered as the spike triggered average (STA) whisker displacement during the 20 ms window preceding each spike. Spike triggered covariance (STC) analysis was then used to recover the remaining set of significant features for any neurons which selectively responded to more than one kinetic feature⁴⁷.

$$STA = \frac{1}{N} \sum_{n=1}^N \vec{S}(t_n)$$

$$STC = \frac{1}{N-1} \sum_{n=1}^N [\vec{S}(t_n) - STA][\vec{S}(t_n) - STA]^T$$

Where t_n is the time of the n^{th} spike, $\vec{S}(t_n)$ is a vector representing the stimulus during the temporal window preceding a spike, and N is the total number of spikes.

Statistical significance of STAs was determined using a bootstrap procedure with 1000 bootstrap trials. Recovered STAs were considered insignificant if their amplitude fell within the 99.9 percentile of the bootstrap displacement range. The significance of STC recovered filters was determined using nested bootstrapping of the eigenvalues corresponding to the STC recovered filters. A recovered eigenvalue that exceeded the 99.9 percentile of its corresponding bootstrap

range of its filter was considered significant. Neurons without significant feature selectivity were excluded from further analysis.

To quantify the modulation of the recovered features by LC activation, we defined a feature modulation factor as ¹⁰⁵:

$$\text{feature modulation factor} = \frac{\text{control feature} \cdot \text{conditional feature}}{\text{control feature} \cdot \text{control feature}}$$

To estimate each nonlinear tuning function corresponding to each significant recovered feature, we first calculated the feature coefficient for each spike, i.e. the dot product between a neuron's linear filter and the stimulus preceding each spike. The probability distribution of feature coefficient values k given a spike (i.e. $\text{Prob}(k|\text{spike})$) could then be determined. To calculate all possible feature coefficients for the stimulus used, a 20 ms window was slid through the 15 s WGN stimulus, from which a probability distribution of all feature coefficient values (i.e. $\text{Prob}(k)$) was generated. By dividing $\text{Prob}(k|\text{spike})$ by $\text{Prob}(k)$, we produced the nonlinear tuning functions that map firing rate to feature coefficient value.

To quantify the information the spike train conveys about the absence/presence of a feature under varying VNS or LC stimulation conditions, we calculated mutual information between the presence/absence of a feature and the observation of a spike for each condition as ¹⁵²

$$\text{Info}(k; \text{spike}) = \int dk * \text{Prob}(k|\text{spike}) * \log_2\left(\frac{\text{Prob}(k|\text{spike})}{\text{Prob}(k)}\right)$$

Where k is the feature. Information transmission rate (i.e. bits/second) was calculated by multiplying bits/spike by the average firing rate of the neuron in response to WGN stimulus.

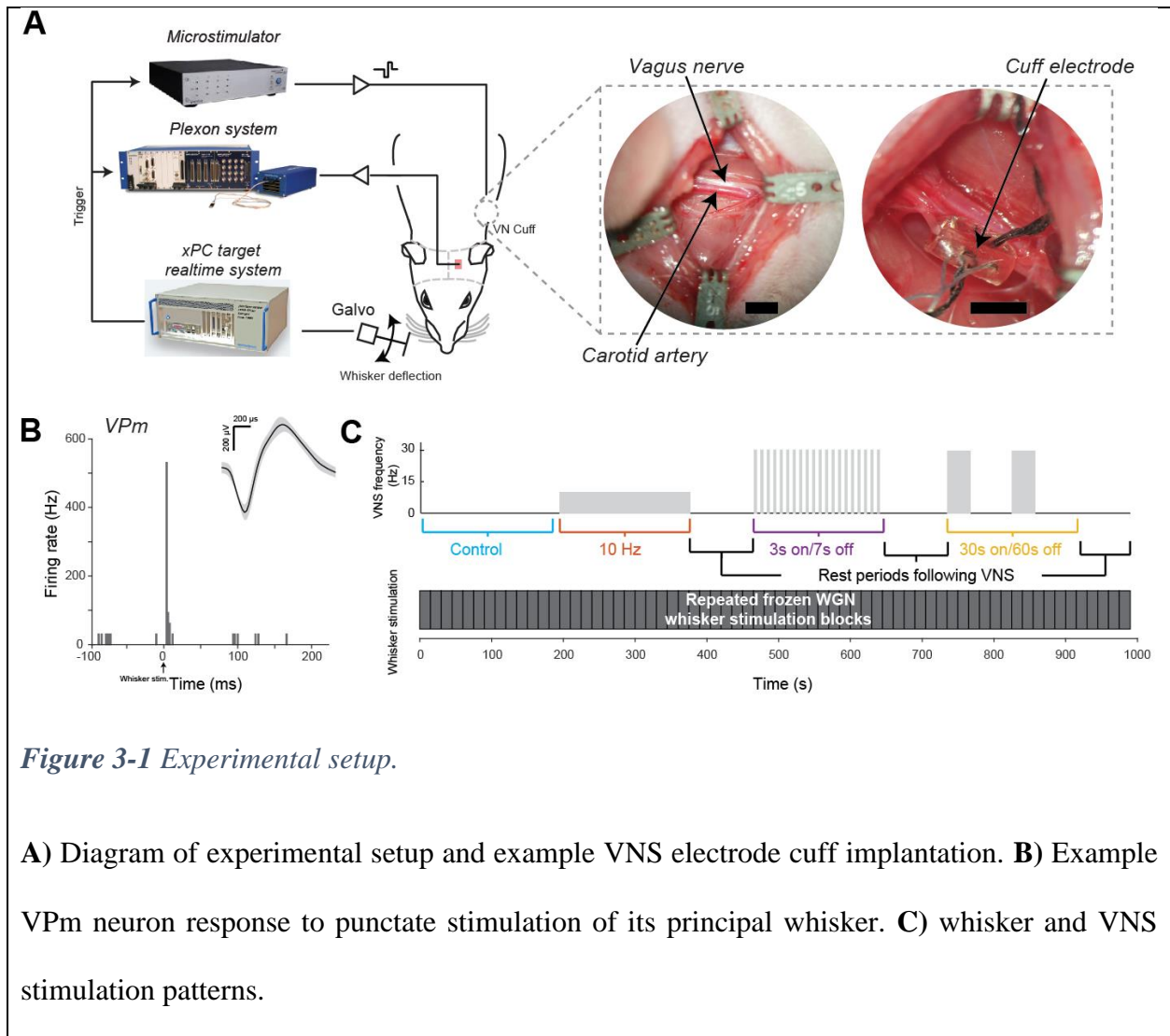
Statistics

A one-sample Kolmogorov-Smirnov test was used to assess the normality of data before performing statistical tests. If the samples were normally distributed, a paired or unpaired t-test

was used. Otherwise, the Mann-Whitney U-test was used for unpaired samples or the Wilcoxon signed-rank test for paired samples. Multiple comparisons were corrected with Bonferroni correction.

Results

To understand the extent to which VNS modulates thalamic sensory processing, we recorded single-unit activity from the VPm of the rat vibrissa pathway in response to repeated WGN whisker deflection while systematically varying VNS stimulation patterns (**Fig. 3-1a**). The VPm is a relay nucleus in the thalamus that gates somatosensory information to the cortex^{41, 209}. VPm neurons reliably respond to stimulation of the neuron's corresponding principle whisker^{33, 208} (**Fig. 3-1b**). Four different VNS patterns were tested: no stimulation (as a control), standard duty-cycle (30 Hz, 30 s on / 60 s off duty-cycle), continuous tonic (10 Hz), and fast duty-cycle (30 Hz, 3 s on / 7 s off duty-cycle) (**Fig. 3-1c**). Each VNS pattern lasted 180 s, during which 15 repetitions of the frozen 15 s WGN whisker stimulation were delivered, with at least 75 s of rest period between them.



Standard duty-cycle VNS improved thalamic feature selectivity and information transmission

To estimate the feature selectivity of VPM neurons and the effects of VNS on thalamic sensory processing, for each VPM neuron we compared its response to the same frozen white Gaussian noise (WGN) whisker stimulation with and without VNS. The striations clearly visible in the raster plots of recorded VPM spiking activity in response to repeated presentations of the same WGN stimulation indicated that the neurons were sensitive to certain kinetic features in the stimulus, as the cells reliably fired at certain time points during each presentation (**Fig. 3-2a**).

Standard duty-cycle VNS (i.e. 30 Hz, 30 s on / 60 s off) did not change the firing rate of the thalamic relay neurons (**Fig. 3-2b**; 11.0 ± 0.6 Hz during control periods vs 11.5 ± 0.7 Hz during standard duty-cycle VNS, 25 neurons, 6 rats, $p = 0.20$, paired t-test; Mean \pm SEM reported for all results unless otherwise stated). However, through using spike triggered covariance analysis to assess the selectivity of the response of the VPM neurons to specific kinetic features^{35, 105} (**Fig. 3-2c**), we found that VNS improved the feature selectivity of VPM neurons, indicated by an increase in the amplitude of the recovered features which the neurons selectively responded to and the tilting up of nonlinear tuning function at high feature coefficient values¹⁰⁵ (**Fig. 3-2d**). As the magnitude of the feature coefficient at any given time point represents the similarity between the stimulus and a feature, this alteration in the shape of the nonlinear tuning function indicates an increased selectivity of the neuron to only spike following stimuli that closely match the neuron's encoded feature. To quantitatively measure the change in the amplitude of the recovered features, we used a feature modulation factor as previously defined¹⁰⁵ (**see Methods**). A feature modulation factor of 1 suggests that there was no significant change in encoded kinetic features, whereas a value greater than 1 suggests an increase in amplitude without a change in shape. Standard duty-cycle VNS was found to result in feature modulation factors significantly larger than 1 (**Fig. 3-2e**; 1 without VNS vs 1.21 ± 0.05 during standard duty-cycle VNS, 36 features, 25 neurons, 6 rats, $p = 1.8e-2$, paired t-test).

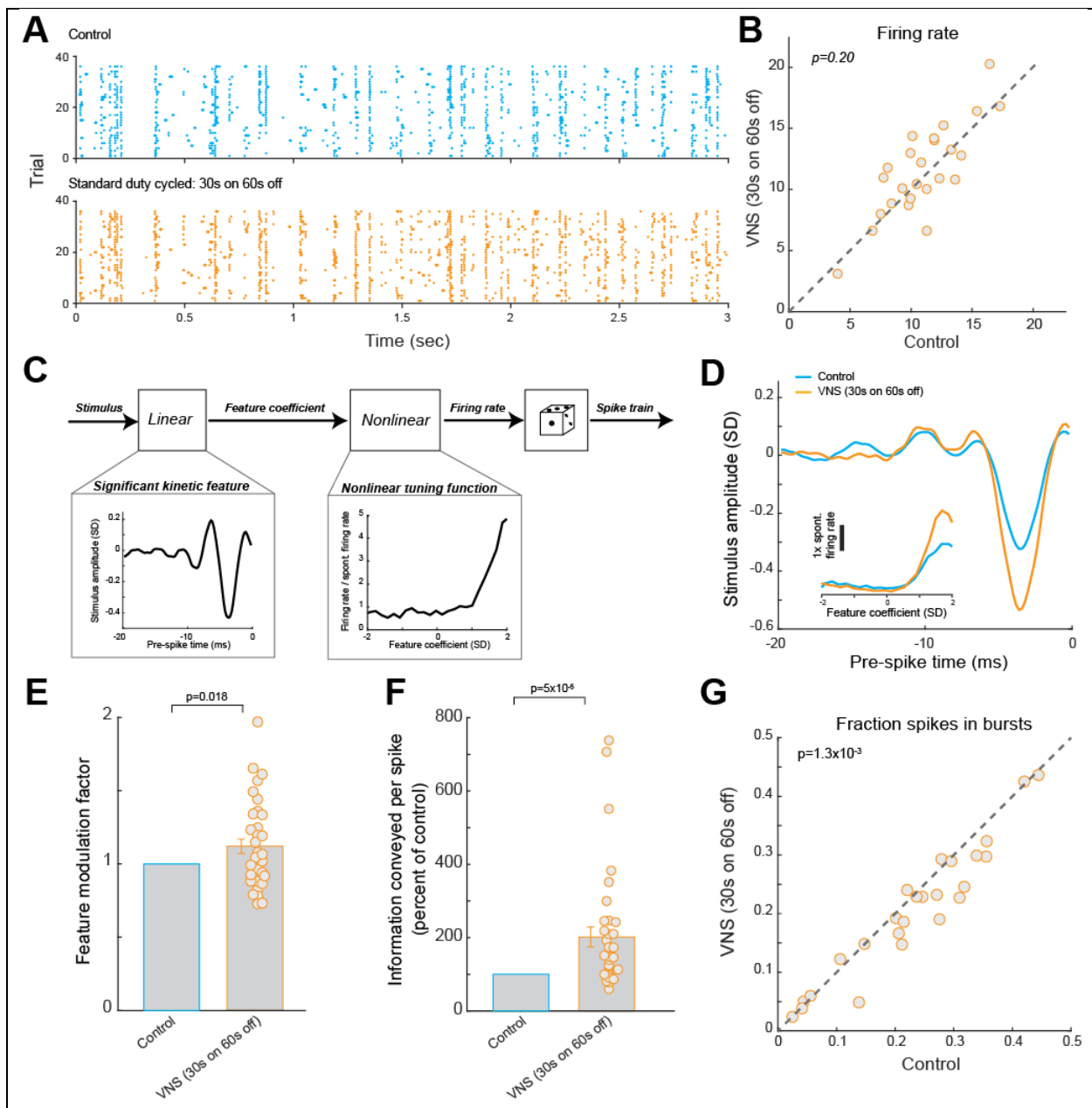
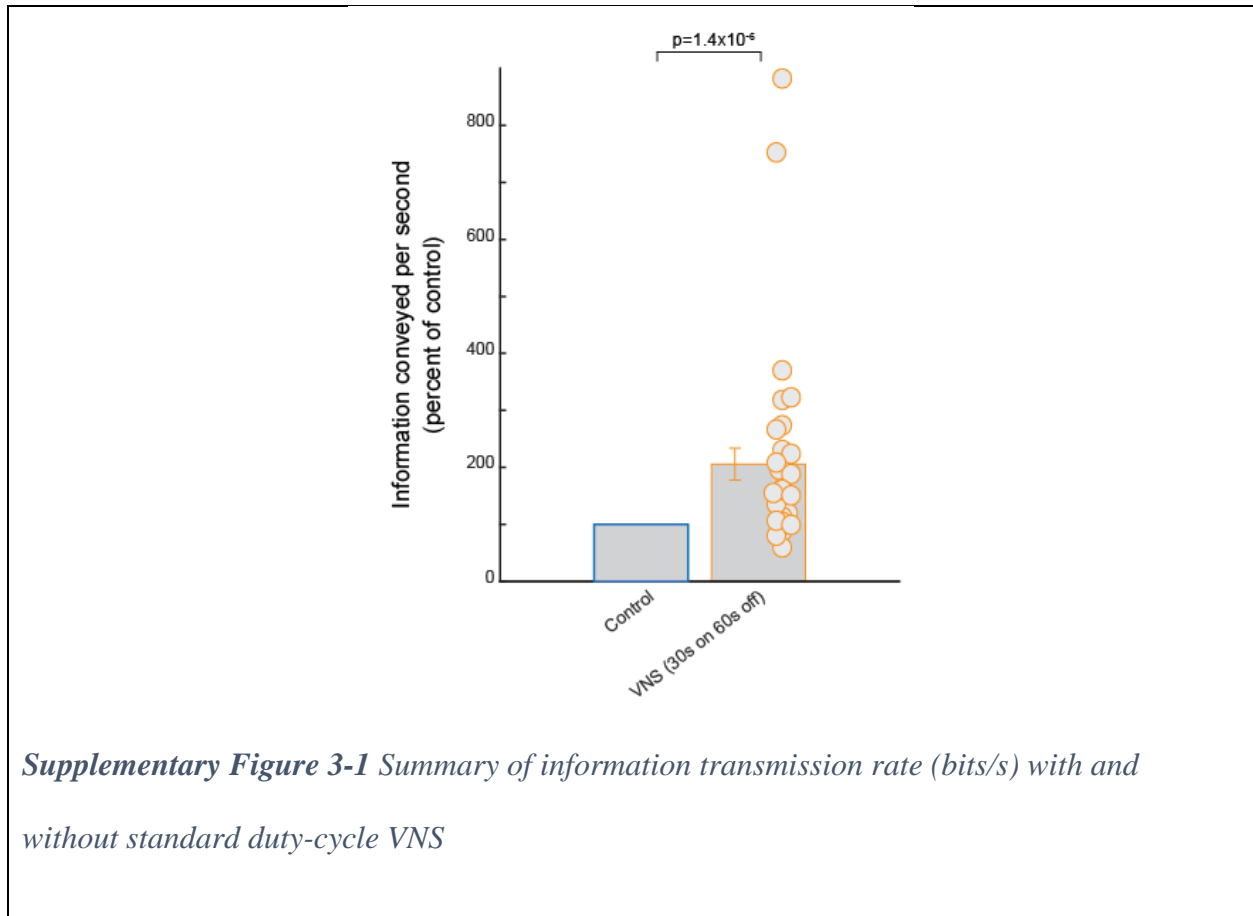


Figure 3-2 Standard duty cycle VNS improved thalamic feature selectivity and information transmission while suppressing burst firing.

A) Spike raster plot of an example VPM response to repeated presentation of the same white Gaussian noise (WGN) whisker stimulation. **B)** Firing rate of VPM neurons to the same WGN whisker stimulation with and without VNS. **C)** Linear-Nonlinear-Poisson model used for white

noise reverse correlation analysis. **D)** The kinetic feature encoded by an example VPm neuron recovered with and without VNS, inset: corresponding nonlinear tuning functions. **E)** Summary of feature modulation factor with and without VNS. **F)** Summary of improvement in information transmission efficiency by VNS. **G)** Summary of percent of thalamic spikes in bursts with and without VNS.

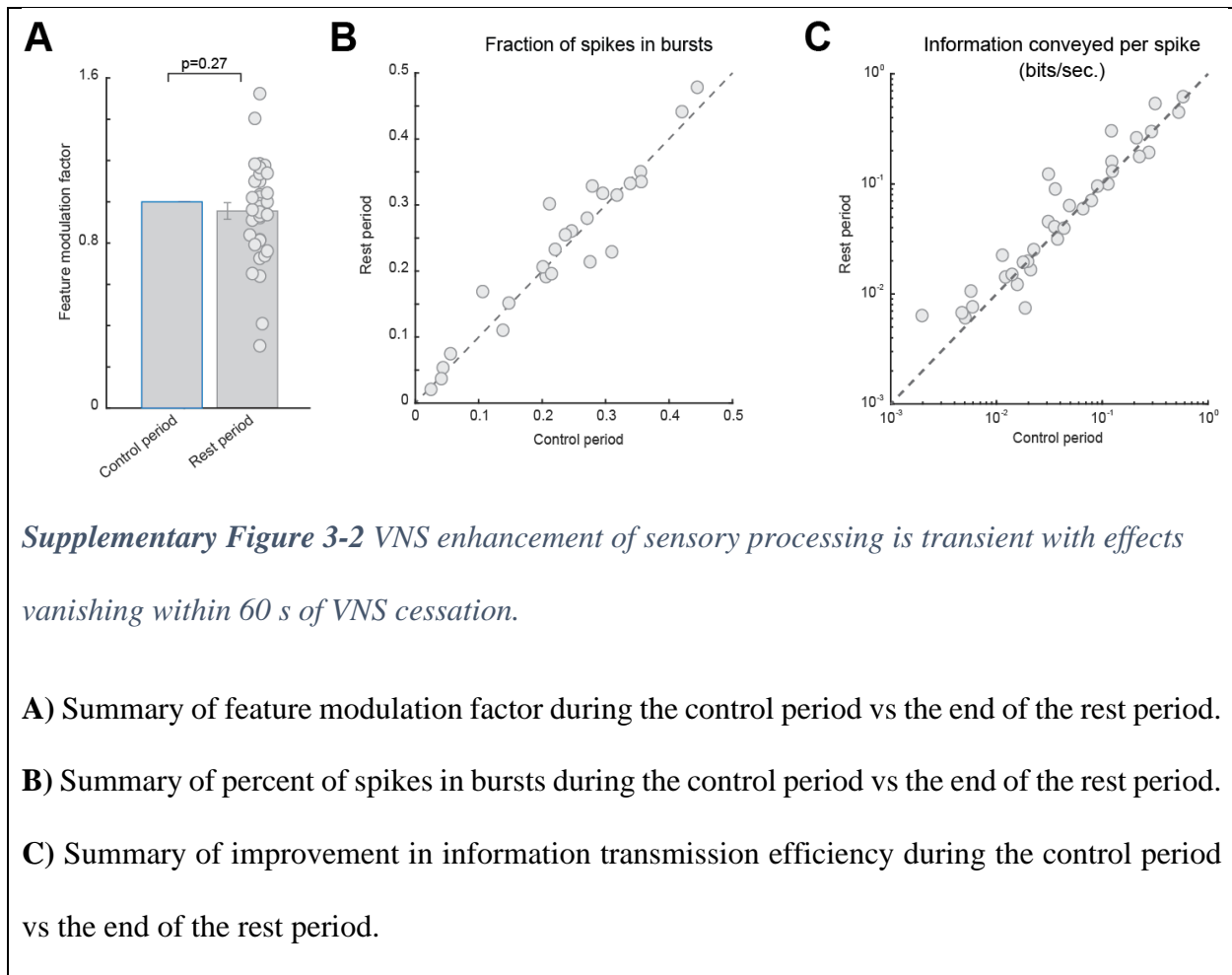
To quantify the effects of VNS on both the encoded kinetic features and nonlinear tuning functions for each neuron, we employed an information theoretic approach to estimate the information transmitted by each VPm spike about the presence/absence of the encoded feature¹⁰⁵. Consistent with observations of improved feature selectivity, we found standard duty-cycle VNS dramatically increased both information transmission efficiency (**Fig. 3-2f**; $202 \pm 27\%$ of control bits/spike with standard duty-cycle VNS, 36 features, 25 neurons, 6 rats, $p = 5.0e-5$, Wilcoxon signed-rank test) and information transmission rate (**Supplementary Fig. 3-1**; $206 \pm 28\%$ of control bits/second with standard duty-cycle VNS, 36 features, 25 neurons, 6 rats, $p = 1.4e-6$, Wilcoxon signed-rank test).



Consistent with previous work, we also observed thalamic relay neurons exhibited burst firing under control conditions^{99, 105}. Since thalamic bursts have been linked to deterioration of transmission of information about detailed stimulus features^{132, 168}, we hypothesized that VNS-induced enhancement of sensory processing might also coincide with suppressed burst firing of VPM neurons. As we expected, VNS decreased the fraction of VPM spikes in bursts (**Fig. 3-2g**; $23 \pm 2\%$ without VNS vs $21 \pm 2\%$ during standard duty-cycle VNS, 25 neurons, 6 rats, $p = 1.3 \times 10^{-3}$, paired t-test).

To ensure the system had ample time to reset to baseline conditions during the rest periods interleaved between VNS conditions, we compared each VPM neuron's response during the

control time period without VNS stimulation to the same neurons response occurring during the second half of all of the rest periods (45 - 75 s after the cessation of the preceding VNS condition). Confirming our correct experimental design, we found the effects of VNS on sensory processing were transient and dissipated within 60 seconds of cessation of VNS. This was quantitatively confirmed as we found no significant difference in feature modulation (**Supplementary Fig. 3-2a**; 1 during control period vs 0.96 ± 0.04 during second half of rest periods, 36 features, 25 neurons, 6 rats, $p = 0.27$, paired t-test), the percent of spikes in bursts (**Supplementary Fig. 3-2b**; $23 \pm 2\%$ during control period vs $24 \pm 2\%$ during second half of rest periods, 25 neurons, 6 rats, $p = 0.48$, paired t-test), and information transmission (**Supplementary Fig. 3-2c**; 0.13 ± 0.03 bits/spike during control period vs 0.14 ± 0.04 bits/spike during second half of rest periods, 36 features, 25 neurons, 6 rats, $p = 0.21$, Wilcoxon signed-rank test). These results suggest that, unlike previously reported VNS-induced effects which are neuroplasticity-based and last over long timescales, VNS enhancement of sensory processing rapidly dissipates following cessation of VNS. Further, this confirms that the periods of rest time we inserted between VNS conditions were long enough to allow for the system to return to baseline conditions.

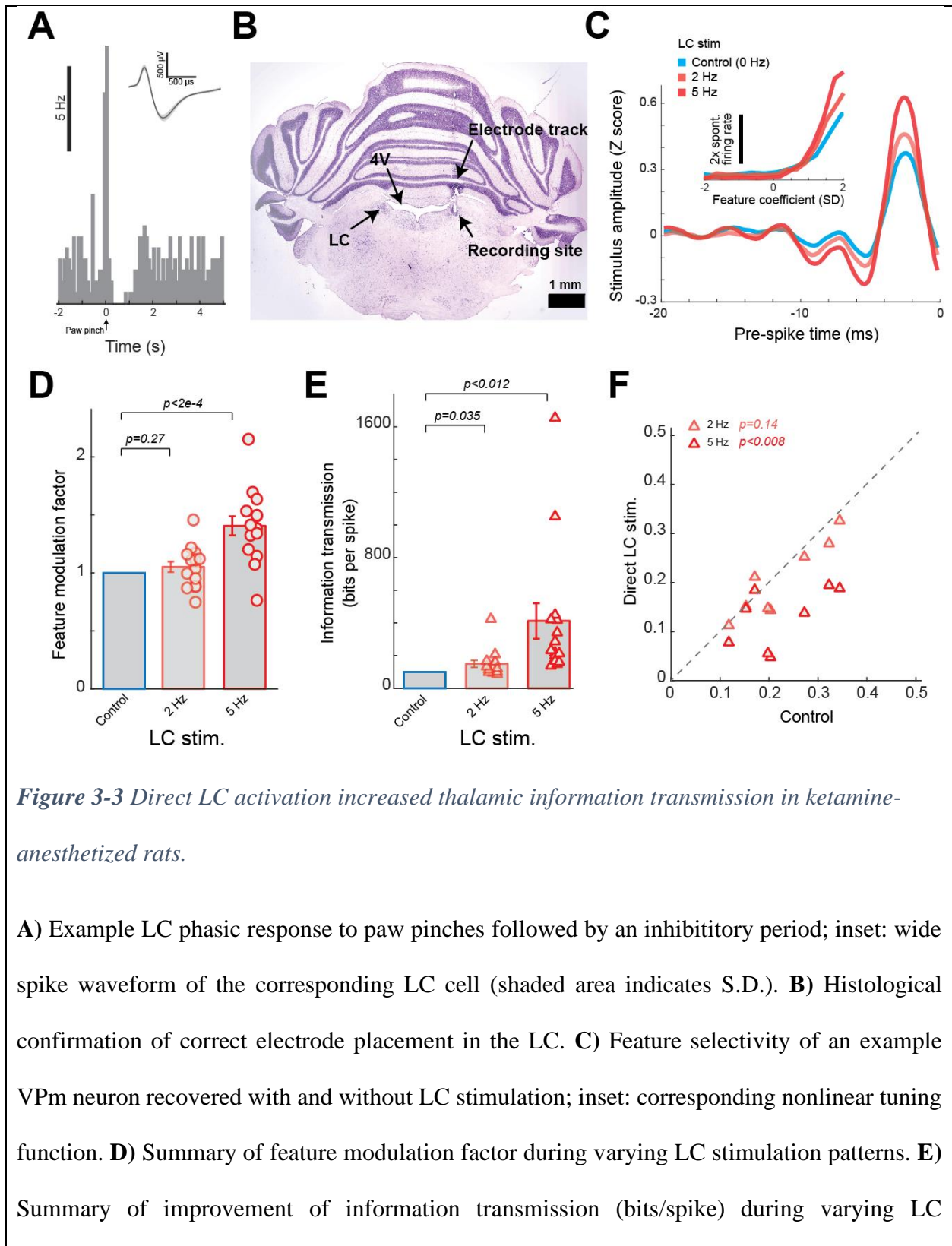


VNS-induced improvement of thalamic information transmission is similar to that induced by direct LC activation

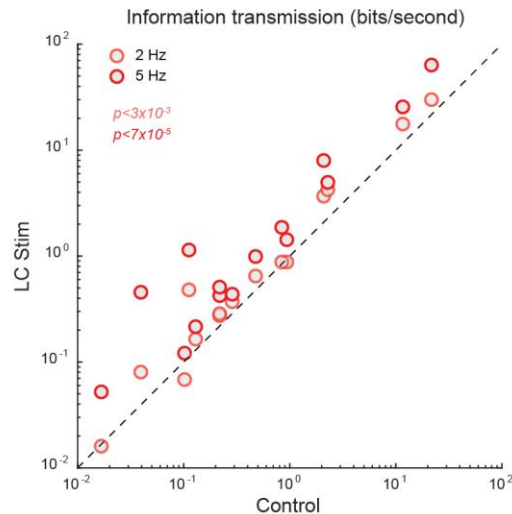
Our recent work demonstrated that direct LC activation improved thalamic feature selectivity and information transmission through regulating thalamoreticulo-thalamic circuit dynamics in pentobarbital-anesthetized rats. Here we observed that VNS produced similar effects as those we observed in result to direct LC stimulation, specifically VNS both improved thalamic feature selectivity and information transmission while decreasing thalamic burst firing. As a recent study demonstrated the causal link between VNS and LC activity¹⁹⁸, we wanted to confirm that direct LC stimulation in ketamine-anesthetized rats would produce similar effects as we observed

with VNS. To this end, we measured thalamic feature selectivity and information transmission with and without direct LC activation in rats under ketamine anesthesia. LC neurons were identified based on their wide spike waveform, phasic response to paw pinch followed by inhibition¹⁴⁵, and electrode placement in the LC which was histologically verified on a subset of recordings (**Fig. 3-3a&b**). After electrophysiologically confirming the position of the electrode within the LC, we disconnected the recording system and connected an electrical microstimulator to the electrode. Similar to our previous work, we found both direct 2 Hz and 5 Hz LC stimulation significantly improved the feature selectivity as shown qualitatively by the change in the recovered feature and nonlinear tuning function (**Fig. 3-3c**) and measured quantitatively by the feature modulation factor (**Fig. 3-3d**; 1 without LC stimulation vs 1.05 ± 0.05 during 2 Hz LC stimulation or 1.41 ± 0.08 during 5 Hz LC stimulation, 15 features across 8 neurons across 3 rats, $p = 0.27$ and $= 1.9 \times 10^{-4}$ respectively, paired t-test). Consequently this improvement in feature selectivity translated to an improvement in information transmission efficiency (**Fig. 3-3e**; $150 \pm 21\%$ of control bits/spike during 2 Hz LC stimulation or $412 \pm 109\%$ of control bits/spike during 5 Hz LC stimulation, 15 features across 8 neurons across 3 rats, $p = 3.5 \times 10^{-2}$ and $= 1.2 \times 10^{-2}$ respectively, paired t-test) and rate (**Supplementary Fig. 3-3**; $153 \pm 22\%$ of control bits/sec during 2 Hz LC stimulation or $337 \pm 81\%$ of control bits/sec during 5 Hz LC stimulation, 15 features across 8 neurons across 3 rats, $p = 2.9 \times 10^{-2}$ and $= 1.1 \times 10^{-2}$ respectively, paired t-test). Importantly, direct LC stimulation in ketamine anesthetized rats also significantly suppressed burst firing, as indicated by a significant reduction in the fraction of spikes in bursts (**Fig. 3-3f**; $22 \pm 3\%$ without LC stimulation vs $20 \pm 3\%$ during 2 Hz LC stimulation or $13 \pm 2\%$ during 5 Hz LC stimulation, 8 neurons across 3 rats, $p = 0.14$ and $= 7.4 \times 10^{-3}$ respectively, paired t-test). Taken together, these results suggest that VNS

modulates thalamic sensory processing at least partially through the LC-NE system (see **Discussion**).



stimulation patterns. **F)** Summary of thalamic burst firing under varying patterns of LC stimulation.

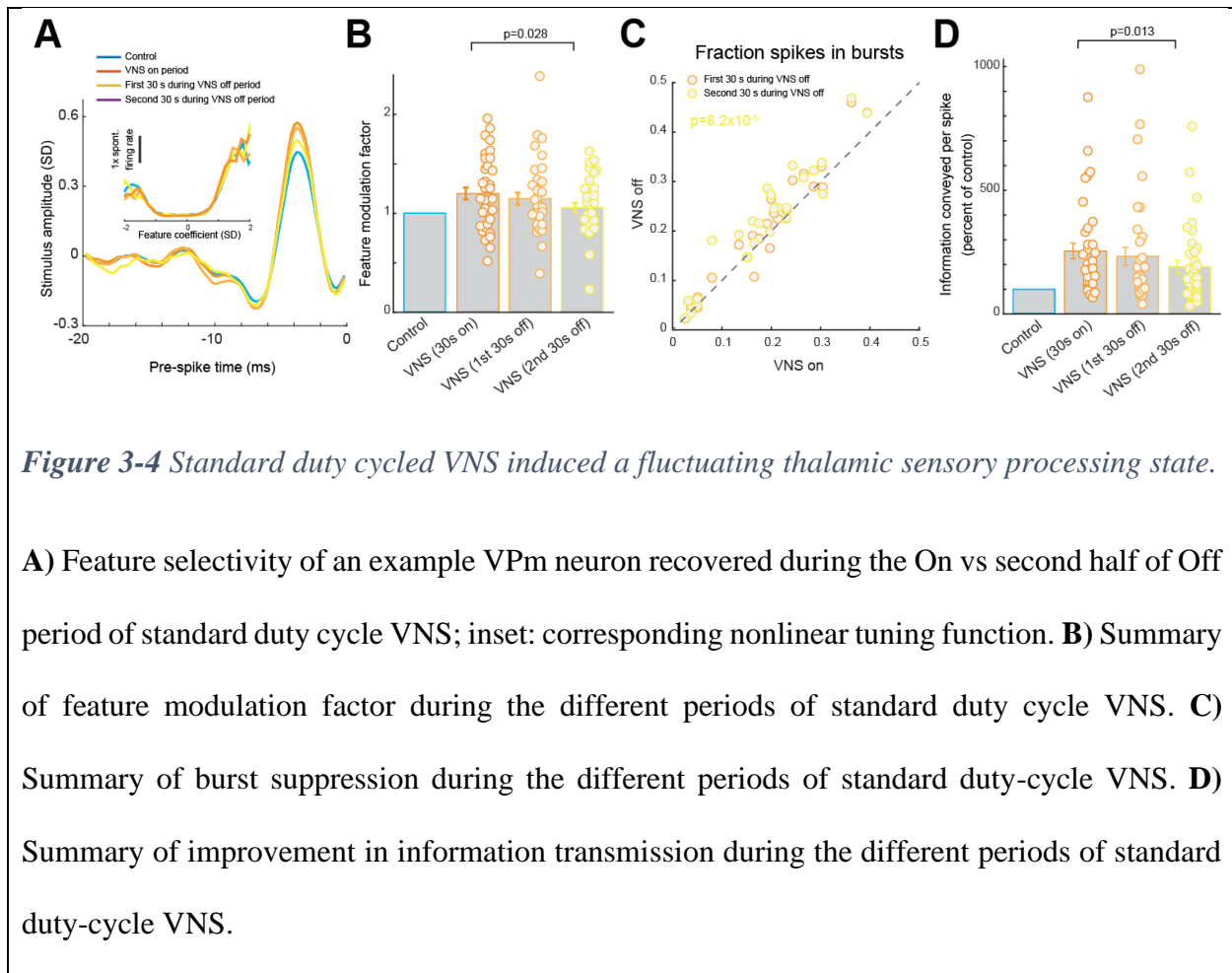


Supplementary Figure 3-3 Summary of information transmission rate (bits/s) with and without direct LC stimulation.

The short timescale of VNS effects on thalamic sensory processing caused standard duty-cycle patterns of VNS to induce a fluctuating thalamic sensory processing state

A typical therapeutically employed VNS stimulation pattern traditionally uses a relatively slow duty-cycle (e.g. 30 s on / 60 s off). Importantly, the off period of the standard VNS pattern used in this paper (60 s) is longer than the period we found it takes for the effects of VNS on sensory processing to dissipate (~45 s). Although relatively slow duty-cycled patterns have proved to efficiently mitigate symptoms in neurological disorders, it was unclear how switching VNS on and off would modulate thalamic state given that the effects of VNS on VPM sensory processing occur and dissipate on such short timescales. To test this, we compared the responses of VPM

neurons during the on period of VNS to the same neurons' responses during the first 30 s and second 30 s of the off period. Interestingly, we found that the effect of VNS on thalamic feature selectivity and information transmission rapidly diminished during the off period. The amplitude of the recovered encoded features was significantly smaller during the second 30 s of the VNS off period than during the VNS on period (**Fig. 3-4a**). Quantifying this difference in recovered feature amplitude using the feature modulation factor, we found that the factor was larger during the on sections than the off sections of the standard duty-cycle VNS (**Fig. 3-4b**; 1.20 ± 0.06 during on period vs 1.06 ± 0.05 during second half of off period, 36 features, 25 neurons, 6 rats, $p = 2.8e-2$, paired t-test). The fluctuations in thalamic processing state induced by standard duty-cycle VNS were further evidenced by the observation that there was a significant change in percent of spikes in bursts in the second 30 s of the VNS off period as compared to the VNS on period (**Fig. 3-4c**; $19 \pm 2\%$ during on period vs $22 \pm 2\%$ during second half of off period, 25 neurons, 6 rats, $p = 8.2e-5$, paired t-test). Accordingly, the information transmitted per spike was significantly less during the second half of the off period than the on period of the standard duty-cycle VNS (**Fig. 3-4d**; $254 \pm 31\%$ of control bits/spike during on period vs $190 \pm 26\%$ of control bits/spike during second half of off period, 36 features, 25 neurons, 6 rats, $p = 1.3e-2$, paired t-test). Taken together these results indicate that standard duty-cycle VNS created a fluctuating state of sensory processing in the thalamus. Here we predict that this fluctuating state would be sub-optimal for perceptual sensitivity, as the same stimulus occurring during the on period of the VNS cycle would evoke a different thalamic response than if it occurred during the off period of the VNS cycle and therefore may be incorrectly perceived as a different stimulus.



Fast duty-cycle VNS enhanced thalamic information transmission without inducing fluctuations

Our data have shown that as VNS rapidly induced improvement in thalamic sensory processing, and that this improvement quickly faded away once VNS is turned off, standard duty-cycle VNS patterns result in a fluctuating thalamic sensory processing state. A possible way to achieve the benefits of VNS on thalamic sensory processing without inducing a fluctuating state would be to use fast duty-cycle VNS (e.g. 3 s on / 7 s off) or continuous tonic VNS which do not have long off periods. To assess whether these stimulation patterns could be used for optimal, fluctuation-free enhancement of sensory processing, we performed standard duty-cycle (30 s on

60 s off), fast duty-cycle (3 s on 7 s off), and continuous (10 Hz) VNS in the same recording session, and compared the effects of the various VNS patterns on thalamic feature selectivity.

None of the three VNS patterns resulted in a significantly different VPM firing rate as compared to control conditions (**Fig. 3-5a**; 11.0 ± 0.6 Hz without VNS vs 10.9 ± 0.7 Hz during 10 Hz tonic VNS, 11.2 ± 0.7 Hz during fast duty-cycle VNS, and 11.6 ± 0.7 Hz during standard duty-cycle VNS, 25 neurons, 6 rats, $p = 0.79, 0.53$ and 0.21 respectively, paired t-test). Further, we found that all 3 conditions produced similar improvements in thalamic feature selectivity as quantified by the feature modulation factor (**Fig. 3-5b**; 1.12 ± 0.05 during standard duty-cycle VNS vs 1.14 ± 0.04 during 10 Hz tonic VNS or 1.15 ± 0.05 during fast duty-cycle VNS, 36 features, 25 neurons, 6 rats, $p = 0.61$ and 0.33 , respectively, paired t-test) and information transmission efficiency (**Fig. 3-5c**; $202 \pm 27\%$ of control bits/spike during standard duty-cycle VNS vs $197 \pm 19\%$ of control bits/spike during 10 Hz tonic VNS or $223 \pm 29\%$ of control bits/spike during fast duty-cycle VNS, 36 features, 25 neurons, 6 rats, $p = 0.84$ and 0.19 , respectively, paired t-test). Further, all VNS patterns produced a VPM response with a similar percent of spikes in bursts (**Fig. 3-5d**; $21 \pm 2\%$ during standard duty-cycle VNS vs $20 \pm 2\%$ during 10 Hz tonic VNS or $21 \pm 2\%$ during fast duty-cycle VNS, 25 neurons, 6 rats, $p = 0.04$ and 0.56 , respectively, paired t-test), with all VNS patterns resulting in a decrease in the percent of spikes in bursts when compared to control conditions.

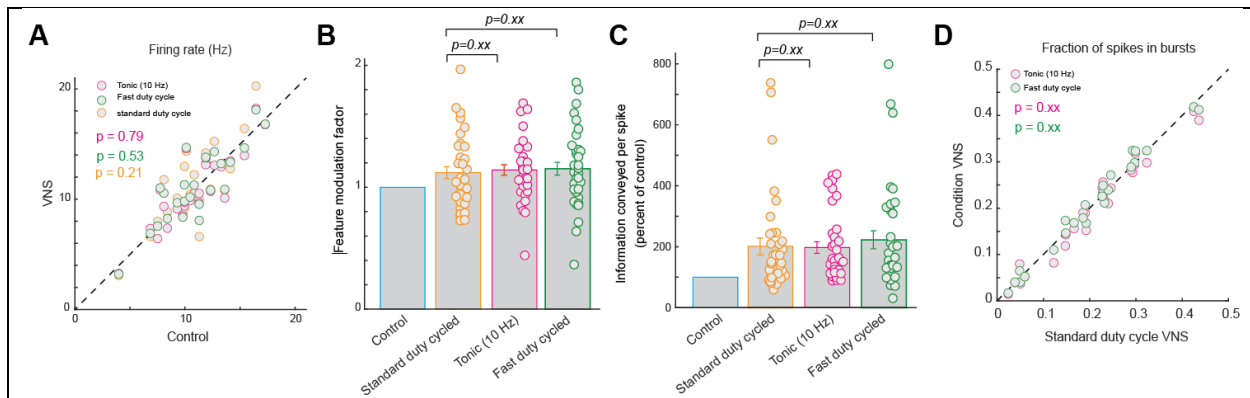
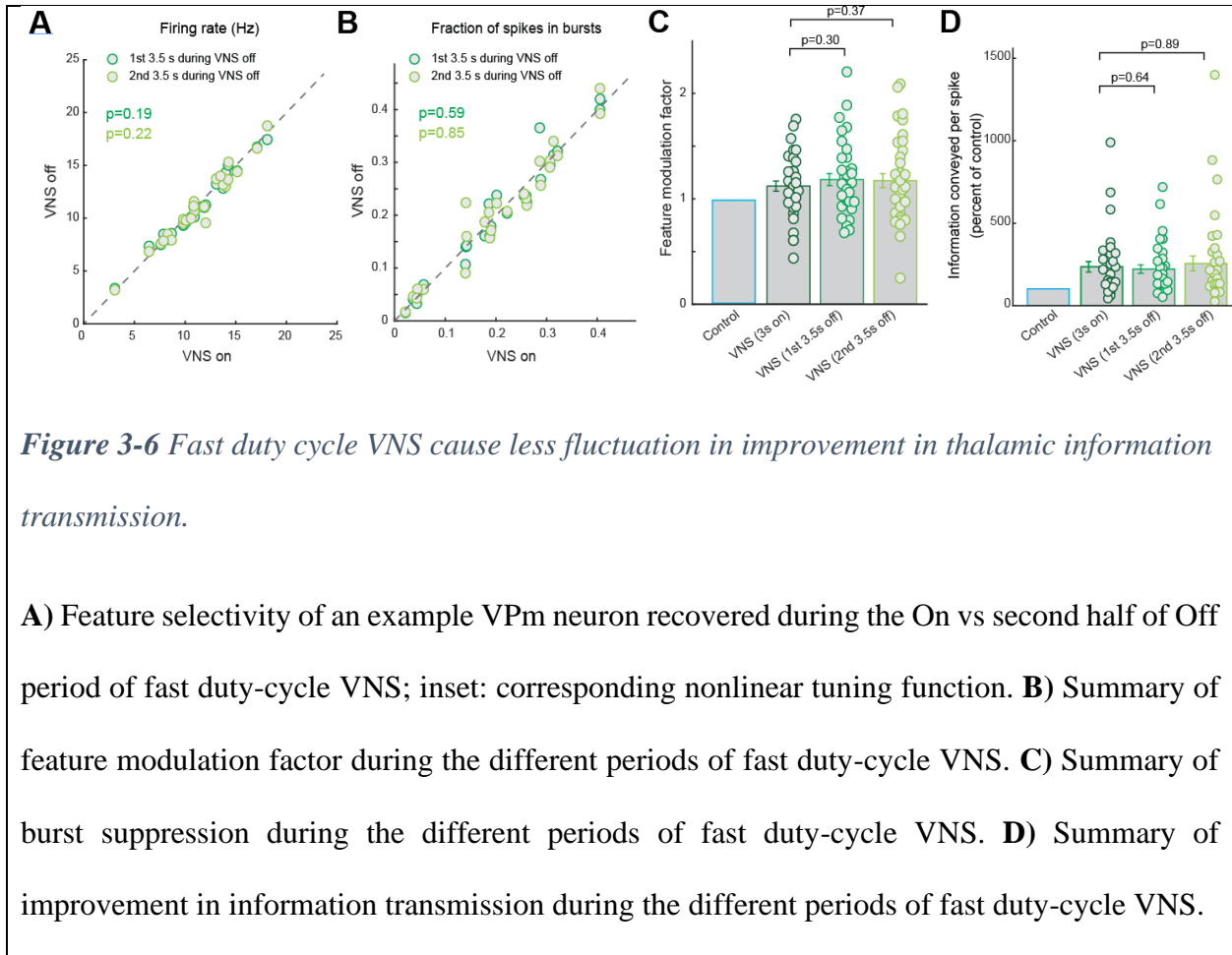


Figure 3-5 Fast duty cycle and tonic VNS induce similar improvement in thalamic information transmission as observed with standard duty-cycle VNS.

A) Summary of VPM firing rate in response to the same whisker stimulation during the varying patterns. **B)** Summary of feature modulation factor during the different VNS patterns. **C)** Summary of improvement in information transmission efficiency during the different VNS patterns. **D)** Summary of fraction of spikes in bursts during the different VNS patterns.

We next investigated whether fast duty-cycle VNS introduced any fluctuations in VPM sensory processing state similar to those observed to be induced by standard duty-cycle VNS. In a similar fashion as to our analysis of the different stages of the standard duty-cycle, we separated the response of the VPM neurons during the on periods of the fast duty-cycle stimulus and compared it with the same neuron's response during the first or second half of the off period. Here we found no significant difference in firing rate (**Fig. 3-6a**; 11.3 ± 0.7 Hz during on period vs 11.2 ± 0.7 Hz during first half of off period or 11.1 ± 0.7 Hz during second half of off period, 25 neurons, 6 rats, $p = 0.19$ and $= 0.22$ respectively, paired t-test) and percent of spikes in bursts (**Fig. 3-6b**; $21 \pm 2\%$ during on period vs $21 \pm 2\%$ during first half of off period or $21 \pm 2\%$ during second

half of off period, 25 neurons, 6 rats, $p = 0.59$ and $= 0.85$ respectively, paired t-test) between on the on period of fast duty-cycle VNS and the first half or second half of the off cycle.



More importantly, both the improvement in feature selectivity and change in nonlinear tuning function did not fluctuate between the on period and first half and second half of the off periods of fast duty-cycle VNS. This lack of fluctuation in feature selectivity during fast duty-cycle VNS translated to no difference in the feature modulation factor between the on period and either half of the off period (**Fig. 3-6c**; 1.12 ± 0.05 during on period vs 1.18 ± 0.06 during first half of off period or 1.17 ± 0.07 during second half of off period, 36 features, 25 neurons, 6 rats, $p = 0.30$ and $= 0.37$ respectively, paired t-test). Further, we find no difference in the strength of

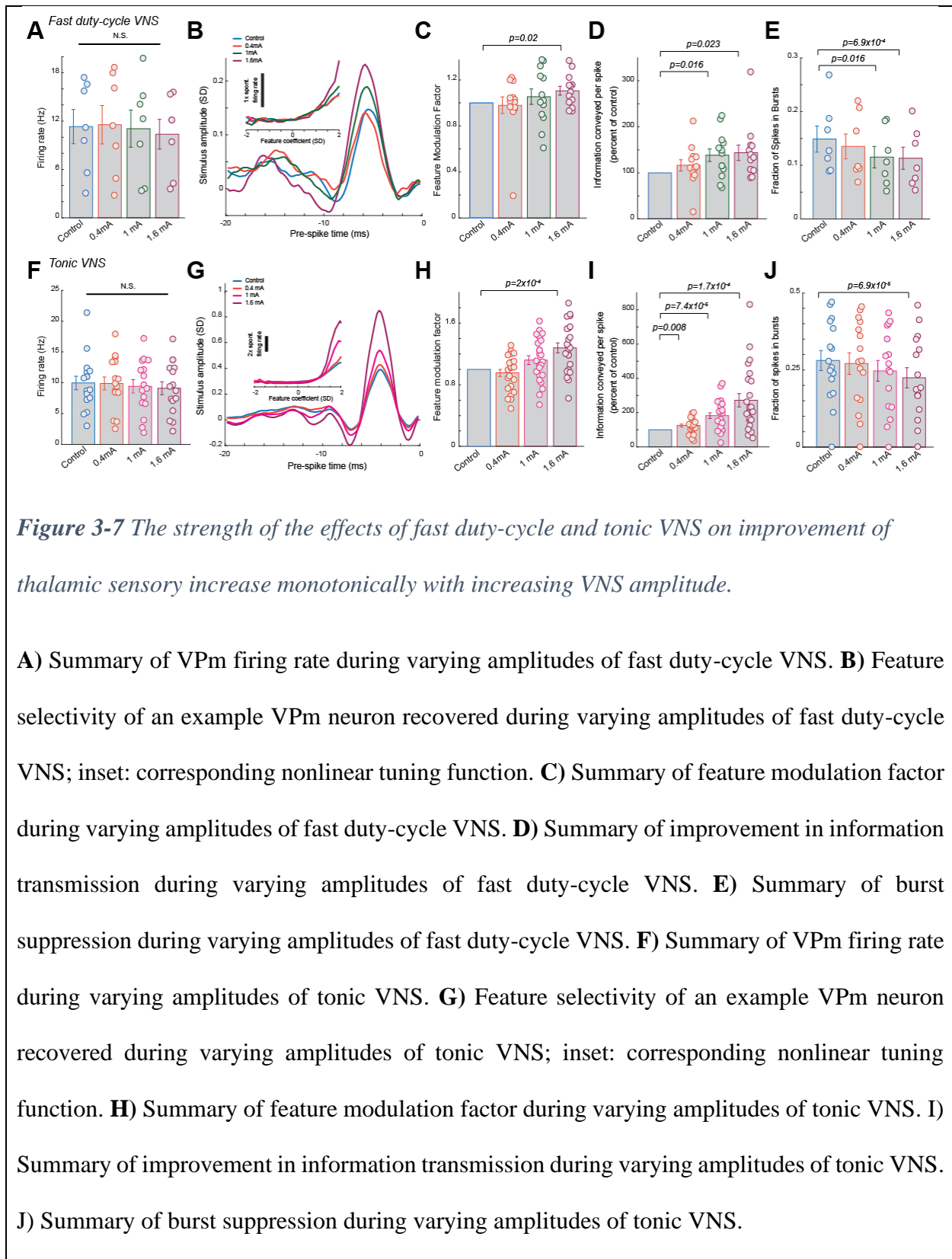
improvement of information transmission efficiency between the on period and either half of the off periods of fast duty-cycle VNS (**Fig. 3-6d**; $236 \pm 32\%$ of control bits/spike during on period vs $223 \pm 25\%$ of control bits/spike during first half of off period or $256 \pm 45\%$ of control bits/spike during second half of off period, 36 features, 25 neurons, 6 rats, $p = 0.64$ and $= 0.89$ respectively, paired t-test and Wilcoxon signed-rank test respectively). Together, these results indicate that both fast duty-cycle VNS and tonic VNS result in the same level of improvement in thalamic sensory processing as standard duty-cycle VNS, without inducing a fluctuating thalamic sensory processing state that would be suboptimal for perceptual performance, and that was induced by standard duty-cycle VNS. This is important as during a fluctuating thalamic sensory processing state, the same stimulus would evoke a different thalamic response if received at different time points in the fluctuation which may degrade the ability to discriminate between similar stimuli.

The effects of fast duty-cycle and tonic VNS on thalamic sensory processing were amplitude dependent

Our results have suggested that both fast duty-cycle and tonic VNS could be used to optimally enhance thalamic sensory processing whereas standard duty-cycle VNS is suboptimal for this purpose as it induces fluctuations in thalamic processing state. During the experiments which compared the effects of these stimulation patterns, all VNS pulses were delivered at a fixed current amplitude of 1 mA. However, The amplitude of VNS being currently used in clinical situations can vary from patient to patient and exists within a wide range of values^{203, 204, 206}. More importantly, it's been found that some effects of VNS have an inverted U shape relationship with VNS amplitude²¹²⁻²¹⁶. Therefore, we wanted to determine the effects of different amplitudes of VNS on sensory processing. To this end, we carried out new experiments to examine the sensitivity

of VNS effects on thalamic information transmission to VNS amplitude. We compared four different VNS amplitudes: 0 (as a control), 0.4 mA, 1 mA, and 1.6 mA.

When analyzing fast duty-cycle VNS at different amplitudes, we found none of the three amplitudes induced changes in VPM firing rate in response to WGN whisker stimulation as compared to the control period (**Fig. 3-7a**, 11.3 ± 2.1 Hz during control without VNS vs. 11.6 ± 2.4 Hz during 0.4 mA fast duty-cycle VNS, 11.1 ± 2.3 Hz during 1 mA fast duty-cycle VNS, and 10.36 ± 1.8 Hz during 1.6 mA fast duty-cycle VNS, 7 neurons, 2 rats, $p = 0.65, 0.80,$ and 0.21 respectively, paired t-test). However, we found that the strength of fast duty-cycle VNS-induced improvements in feature selectivity and information transmission monotonically increased with fast duty-cycle amplitude (**Fig. 3-7b**) as quantitatively measured by the feature modulation factor (**Fig. 3-7c**; 1 during control without VNS vs. 0.98 ± 0.07 during 0.4 mA fast duty-cycle VNS, 1.05 ± 0.07 during 1 mA fast duty-cycle VNS, or 1.11 ± 0.04 during 1.6 mA fast duty-cycle VNS, 13 features, 7 neurons, 2 rats, $p = 0.78, 0.44,$ and 0.02 respectively, paired t-test) and information transmission efficiency (**Fig. 3-7d**, $116 \pm 12\%$ of control bits/spike during 0.4 mA fast duty-cycle VNS, $138 \pm 14\%$ of control bits/spike during 1 mA fast duty-cycle VNS, or $144 \pm 17\%$ of control bits/spike during 1.6 mA fast duty-cycle VNS, 13 features, 7 neurons, 2 rats, $p = 0.20, 1.6e-2,$ and $2.3e-2$ respectively, paired t-test). As expected, burst firing also decreased monotonically with the increase in fast duty-cycle VNS amplitude as evidenced by a decrease in the percent of spikes in bursts (**Fig. 3-7e**, $14.9 \pm 2.4\%$ during control without VNS vs. $13.5 \pm 2.3\%$ during 0.4 mA fast duty-cycle VNS, $11.5 \pm 2.0\%$ during 1 mA fast duty-cycle VNS, or $11.3 \pm 2.0\%$ during 1.6 mA fast duty-cycle VNS, 7 neurons, 2 rats, $p = 0.17, 1.6e-2,$ and $6.9e-4$ respectively, paired t-test).



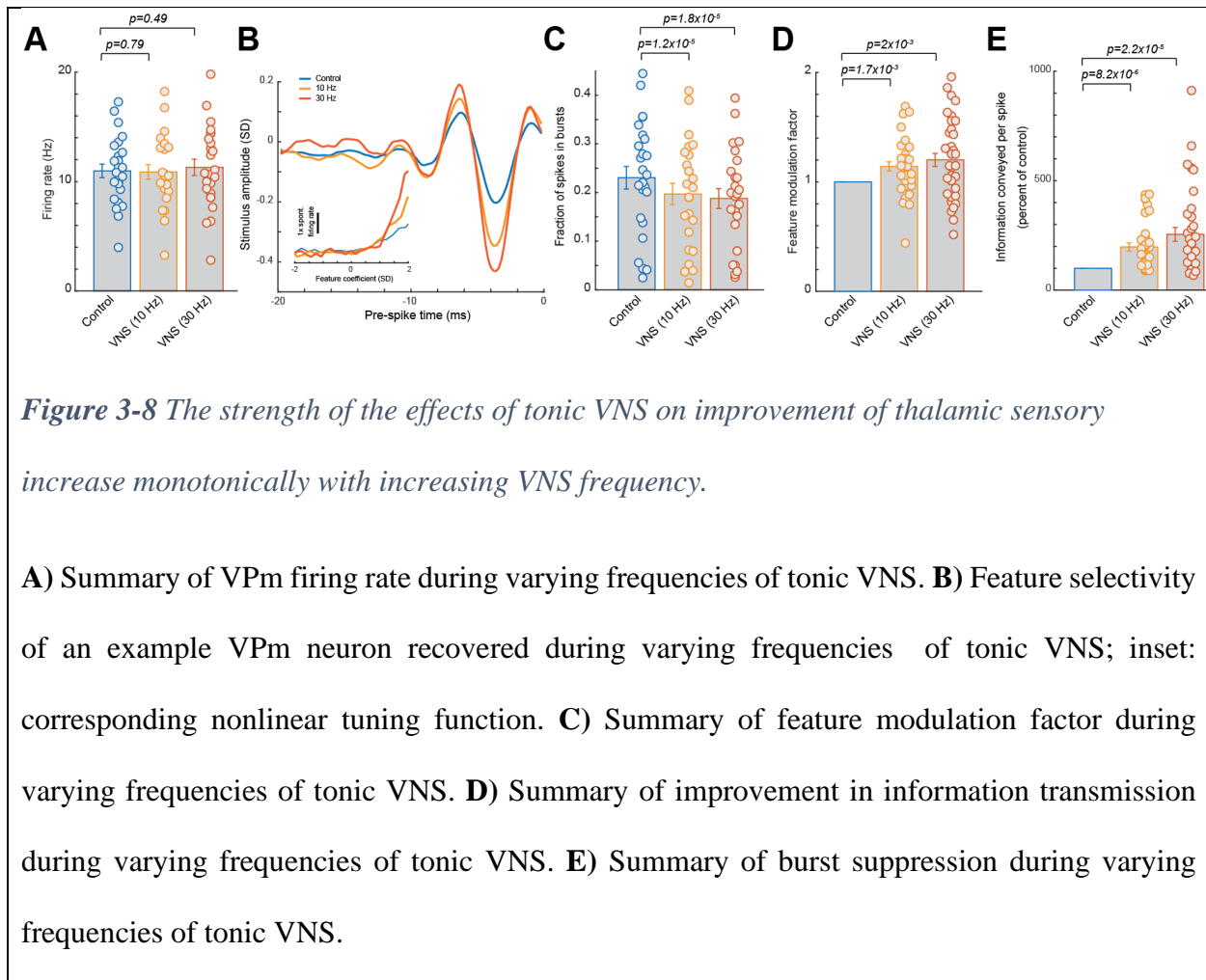
Similarly, when analyzing 10 Hz tonic VNS at different amplitudes, we found none of the three amplitudes induced changes in VPM firing rate in response to WGN whisker stimulation as compared to the control period (**Fig. 3-7f**, 10.0 ± 1.1 Hz during control without VNS vs. 9.9 ± 1.1 Hz during 0.4 mA 10 Hz VNS, 9.4 ± 1.1 Hz during 1 mA 10 Hz VNS, and 9.1 ± 1.1 Hz during 1.6 mA 10 Hz VNS, 16 neurons, 5 rats, $p = 0.84, 0.46,$ and 0.08 respectively, paired t-test). We also found that the strength of tonic VNS-induced improvements in feature selectivity and information transmission efficiency monotonically increased with tonic VNS amplitude (**Fig. 3-7g**) as quantitatively measured by the feature modulation factor (**Fig. 3-7h**; 1 during control without VNS vs. 0.95 ± 0.05 during 0.4 mA 10 Hz VNS, 1.12 ± 0.06 during 1 mA 10 Hz VNS, or 1.28 ± 0.06 during 1.6 mA 10 Hz VNS, 24 features, 16 neurons, 5 rats, $p = 0.33, 0.048,$ and 2.0×10^{-4} respectively, paired t-test) and information transmission efficiency (**Fig. 3-7i**, $125 \pm 8\%$ of control bits/spike during 0.4 mA 10 Hz VNS, $182 \pm 17\%$ of control bits/spike during 1 mA 10 Hz VNS, or $272 \pm 38\%$ of control bits/spike during 1.6 mA 10 Hz VNS, 24 features, 16 neurons, 5 rats, $p = 7.5 \times 10^{-3}, 7.4 \times 10^{-5},$ and 1.7×10^{-4} respectively, paired t-test). As expected, burst firing also decreased monotonically with increasing tonic VNS amplitude as evidenced by a decrease in the percent of spikes in bursts (**Fig. 3-7j**, $28.1 \pm 3.3\%$ during control without VNS vs. $27.1 \pm 3.5\%$ during 0.4 mA 10 Hz VNS, $24.7 \pm 3.4\%$ during 1 mA 10 Hz VNS, or $22.5 \pm 3.3\%$ during 1.6 mA 10 Hz VNS, 16 neurons, 5 rats, $p = 0.36, 5.6 \times 10^{-2},$ and 6.9×10^{-5} respectively, paired t-test). Taken together, these characterization results suggest that VNS rapidly improves thalamic sensory processing in an amplitude dependent fashion.

The effects of VNS on thalamic sensory processing were frequency dependent

VNS with different frequencies can have distinguishable effects in clinical applications^{203,}
^{204, 206}. Therefore, we wanted to evaluate how different frequencies of VNS affect thalamic sensory

processing. To this end we compared the responses of VPM neurons during 10 Hz, 1 mA continuous tonic VNS to the same neurons' responses during 30 Hz, 1 mA continuous tonic VNS (taken from the on periods of the standard duty-cycle VNS).

Again, we found that both frequencies of tonic VNS resulted in firing rates that were not significantly different than during the control period (**Fig. 3-8a**, 11.0 ± 0.6 Hz during control without VNS vs 10.9 ± 0.7 Hz with 10 Hz VNS or 11.3 ± 0.7 Hz during 30 Hz VNS, 25 neurons, 6 rats, $p = 0.79$ and 0.49 respectively, paired t-test). However, the percent of spikes in bursts decreased monotonically with increasing tonic VNS frequency (**Fig. 3-8b**, $23.0 \pm 2.3\%$ during control without VNS vs $19.4 \pm 2.2\%$ with 10 Hz VNS or $18.8 \pm 2.0\%$ during 30 Hz VNS, 25 neurons, 6 rats, $p = 1.2e-5$ and $1.8e-5$ respectively, paired t-test). Moreover, we found that 30 Hz VNS produced a stronger increase in recovered feature amplitude and tilting up of the nonlinear tuning function. When we quantified the effects of 10 Hz and 30 Hz tonic VNS on the recovered features, we observed that both produced a significantly larger feature modulation factor than 1, which increased monotonically with increasing tonic VNS frequency (**Fig. 3-8c**, 1 during control without VNS vs 1.14 ± 0.04 during 10 Hz VNS or 1.20 ± 0.06 during 30 Hz VNS, 36 features, 25 neurons, 6 rats, $p = 1.7e-3$ and $1.9e-3$ respectively, paired t-test). Consequently, due to VNS effects on sensory processing increasing monotonically with tonic VNS frequency, we found the information transmission efficiency also monotonically increased with tonic VNS frequency (**Fig. 3-8d**, $198 \pm 19\%$ of control bits/spike during 10 Hz VNS vs. $255 \pm 32\%$ of control bits/spike during 30 Hz VNS, 36 features, 25 neurons, 6 rats, $p = 8.2e-6$ and $2.2e-5$, respectively, paired t-test). Further we found information transmission efficiency was significantly more strongly improved with 30 Hz VNS than with 10 Hz ($p = 6.8e-3$, paired t-test).



Discussion

Previous work has focused on using VNS to facilitate the neuroplasticity of brain circuits, likely through activation of neuromodulatory systems which are known to induce neuroplasticity²⁰². These changes require pairing stimuli or tasks with VNS activation and take place over weeks to months²⁰¹. In contrast, we found that VNS was also able to drastically affect the sensory processing within the thalamus at a short timescale, requiring no prior pairing. Further, we found the effects of VNS on sensory processing to be transient as they dissipated quickly following cessation of VNS. This new application of VNS therefore does not depend on long-term changes

induced by neuroplasticity, instead we hypothesize that VNS activation results in rapid, transient regulation of sensory processing in the thalamus most likely through activation of neuromodulation centers that can rapidly change thalamic neurochemical state, such as the LC. We found that VNS-induced improvements of thalamic sensory processing occurred through enhancement of feature selectivity that resulted in an increased efficiency and rate of sensory information transmitted by VPM neurons. Previous studies have shown a causal link between enhanced thalamic sensory processing and improved perceptual performance^{105, 217}. Therefore, as our data shows that VNS improves thalamic sensory processing, we predict that certain patterns of VNS could potentially be used to improve behavioral performance in perceptual tasks. Future work is warranted to probe the relationship between different VNS patterns and the enhancement of perceptual performance.

We found that VNS improved thalamic feature selectivity and information transmission in similar fashion as direct LC stimulation. As our previous work demonstrated a causal relationship between LC-stimulation induced suppression of thalamic bursts and improvement in information transmission¹⁰⁵, it is important to note that VNS also suppressed burst firing in the thalamus. This is not unexpected as it has been shown that the vagus nerve exerts influence on LC activity through the projection of the NTS and that VNS increases LC activity^{198, 199}. However, the NTS also projects to other neuromodulatory nuclei in addition to the LC, including the basal forebrain²¹⁸ which also projects to the sensory thalamus. Activation of either the LC or the basal forebrain has been shown to modulate sensory processing^{105, 164, 165}. Therefore, the improved thalamic sensory processing that we observed here may involve the collective action of multiple neuromodulatory systems activated by VNS. Future work utilizing pharmacological manipulation would be able to

tease apart the contribution of the different neuromodulatory systems to the observed VNS-induced improvement in thalamic sensory processing.

In current clinical treatments, VNS is most commonly given in a duty-cycle fashion, such as 30 s on / 60 s off ²⁰³⁻²⁰⁶, which is based on the assumption that duty-cycled stimulation poses less of a risk of damaging a nerve ²¹⁹. Here we found VNS improvement of thalamic sensory processing is transient and rapidly dissipates following cessation of VNS, which resulted in the effects of VNS dissipating during the off periods of the standard duty-cycle VNS. This fluctuating thalamic processing state resulted in VPM neurons exhibiting a difference in feature modulation, sensory information transmission efficiency, and burst firing rate during the on versus the off period of standard duty-cycle VNS. This fluctuating sensory processing state would presumably induce a fluctuating bias in perception that was not related to the stimulus and therefore would act as noise, which may be detrimental to the precise information processing needed during perceptual discrimination tasks. For example, the same stimulus would produce different neural responses if received during the on period versus the off period of the standard duty-cycle, which may cause the same stimuli to be perceived as two different stimuli. Interestingly we found that, VNS with a fast duty-cycle of 3 s on / 7 s off did not induce fluctuations in thalamic sensory processing state, presumably due to the fact that the time constants of VNS modulation of sensory processing in the thalamus are faster than those of standard duty-cycle VNS patterns but not those of a fast duty-cycle VNS pattern.

Compromised or abnormal sensory processing, caused by many underlying disorders such as Parkinson's disease, depression, migraine, central pain syndrome, and ADHD, can strongly impact daily life ²²⁰⁻²²³. Relevant to our results here, abnormal thalamic bursting activity has been implicated in the aforementioned disorders ²²⁴⁻²³¹. Our results have shown that VNS decreased

thalamic bursting suggesting that VNS-induced decrease of thalamic bursting may be one of the mechanisms underlying current VNS-based treatments. Here we found that increasing the frequency of VNS as well as the amplitude of fast duty-cycle VNS and tonic VNS resulted in stronger improvements in sensory processing as evidenced by increased feature selectivity and improved stimulus-related information transmission. Therefore, our results suggest that an optimal state for perceptual processing is best achieved using high frequency and high amplitude VNS delivered either continuously or with a high frequency duty-cycle.

As we have found that high current and frequency patterns of VNS provided the best enhancement of thalamic sensory processing, a pertinent question is how to deliver these aggressive VNS patterns while minimizing risk of vagus nerve damage or patient discomfort. One method would be to use a closed-loop system which engages high amplitude and frequency tonic VNS only during specific time periods, such as when the user expects to receive sensory stimuli or is identified to be in a non-optimal sensory processing state using non-invasive indexes of brain state such as pupil dilation ¹⁴⁵. This type of on-demand VNS-enhancement of sensory processing would be facilitated by the fact that VNS-induced improvements in perception rapidly onset once VNS is initiated. In addition, our previous work suggested that the activation of the LC-NE system is more beneficial during more difficult perceptual tasks ¹⁰⁵, indicating task-dependent VNS may be an optimal configuration for enhancing behavioral performance.

Newly developed sensory neuroprotheses use patterned microstimulation of different regions along sensory pathways to recover senses lost due to disease, degeneration, or injury ²³²⁻²³⁷. The accuracy of the perception induced by these neuroprotheses may be dependent on sensory processing state, as it has been shown that brain-state affects the manner in which information is encoded and processed in these pathways ^{105, 171, 238}. Further research exploring the ability of VNS

to modulate sensory processing state in such a manner that optimizes it for the writing of patterned microstimulation may improve the ability of brain-machine-interfaces to correctly encode information along sensory pathways.

Conclusion

Here, we find that the activation of the LC-NE system alters intrathalamic dynamics in a manner which optimizes VPM neurons' feature selectivity therefore increasing the sensory-related information encoded by their response. As it is well known that the LC is a major neuromodulator of arousal, these findings indicate that the LC-NE system is able to modulate both brain state and sensory processing, likely allowing for brain-state dependent optimization of perception. LC activation was found to not affect the response of VPM neurons via altering the feedforward input from the PrV or modulating corticothalamic interactions. Instead we determined the mechanism behind LC-activation-improved thalamic sensory processing was the release of NE in the thalamus affecting both VPM and TRN neurons via action on thalamic noradrenergic receptors resulting in a decrease in the activity of thalamic calcium channels responsible for burst spiking. The observed LC-activation-induced improvement in VPM feature selectivity was not due to simply removing bursting spikes, as tonic spikes carried more information with LC activation than without. Rather we find that the LC-activation-induced changes in intrathalamic dynamics resulted in VPM neurons using a different temporal structure of reliable response events to encode the same stimuli. This change in the temporal pattern of encoding favored sensory information transmission as newly emerged events during LC stimulation carried more information than events that were removed by LC stimulation. Further, we found that LC stimulation resulted in VPM responses from which the original stimulus could be more accurately decoded, suggesting LC activation enhances accuracy of perception. Finally, we investigated methods to translate these findings using peripheral nerve stimulation and determined that minimally invasive VNS could be used to rapidly and transiently enhance thalamic feature selectivity. This is an exciting finding as it provides a potential method of

enhancement of perceptual acuity for individuals with both healthy and compromised sensory perception. We then determined an optimal pattern of VNS for sensory enhancement which was non-trivial as we found certain duty-cycle patterns induced fluctuating thalamic processing states.

Here we conclusively showed the mechanism underlying LC-induced optimization of thalamic state for sensory processing is increased NE concentration acting on thalamic noradrenergic receptors resulting in a reduction of calcium t-channel activity in both the VPM and TRN. Further, our results suggest this decrease in calcium t-channel activity results in a decrease in the subthreshold membrane potential fluctuations of VPM neurons. Removal of these underlying noisy fluctuations may change the response of VPM neurons to allow for the relay of stimulus-relevant input from the PrV with high-fidelity. Still, further research is needed to understand exactly how the LC-NE system alters intrathalamic dynamics in such a way that alters the temporal structure of response events a VPM neuron uses to encode the same whisker stimuli. We propose that further research into the effects of LC activation on TRN feature selectivity may help elucidate this question. The TRN receives topographically aligned input from sensory thalamus regions, and in return provides topographically aligned inhibitory input to thalamic relay cells^{78, 79}, thus whether the TRN is responding in a non-selective or selective fashion heavily impacts thalamocortical transmission of sensory information. If TRN neurons project to, and therefore inhibit, VPM neurons with relatively different feature selectivity, then increases in the selectivity of the TRN neurons should sharpen the innervated VPM neurons' feature selectivity. For example, if a VPM neuron receives inhibitory TRN input when features in the stimulus occur which do not match its feature selectivity, then that VPM neuron's ability to selectively respond to only features which do match its feature selectivity should be enhanced. An LC-activation-induced shift from

general to feature selective TRN inhibition of VPM neurons may then explain why LC-activation changes the temporal response structure of a VPM neuron to the same whisker stimulus.

We believe this study provides direct evidence of the hypothesized behavioral state linked shift in thalamocortical processing²³⁹. An LC-mediated shift from bursting to tonic firing is conserved across thalamic sensory regions, indicating the same LC modulated mechanism of sensory processing improvement may be present in other thalamic sensory modalities as well. For example, the LGN has also been shown to have both tonic and firing mode, with bursting evoked by prolonged inhibitory stimulation¹⁵⁵ and naturalistic visual stimuli²⁴⁰. The reticular nucleus has also been implicated in feature selective processing of the visual pathway²⁴¹. Attention has been shown to change signal-to-noise ratio in the LGN⁹ with bursting shown to be less prevalent when the animal is attended to a stimulus²⁴². A similar reduction of bursting in response to LC activation²⁴³ and during awake states^{244,245} has been shown in the LGN, and an inhibition-driven increase in feature selectivity related to a shift from bursting to tonic firing has been proposed²⁴⁶⁻²⁴⁸ supported by evidence showing visual TRN activity increases with attention⁶² and LC activation. Further, the LC has also been shown to enhance sensory responses²⁹ and increase signal to noise ratio²⁴⁹ and discrimination²⁵⁰ in the olfactory bulb, argued to be analogous to an olfactory thalamus²⁵¹. Finally, LC-NE modulation of sensory processing has also been shown to induce selective plasticity in the auditory thalamus²⁵². Taken together this research indicates the LC-NE system as a major modulator of thalamic sensory processing across multiple sensory modalities, underlying the importance of understanding exactly how the LC activity affects sensory processing.

In this work we find that VNS can be used to rapidly enhance sensory processing in naïve subjects. This technique could potentially be translated to technology that would give individuals

with compromised sensory processing the ability to restore and enhance their sensory perception on-demand during time periods when perceptual performance is critical. The loss of perceptual ability can be highly disruptive to daily life, for example, individuals with compromised senses of touch often struggle with tasks such as buttoning their shirt or grasping objects ²⁵³.

Compromised or abnormal sensory processing can result from many underlying disorders including Parkinson's disease, depression, migraine, central pain syndrome, ADHD, as well as others. Further, many types of injuries, such as traumatic brain injuries or strokes, can also lead to compromised perceptual ability. As many necessary daily activities require perceptual ability, the loss of this skill limits the ability of individuals suffering from compromised sensory perception to live independently. A non-invasive VNS system could be designed in such a way that the user could activate it in task-dependent fashion. This would allow for the delivery of high frequency, high amplitude, continuous tonic or fast duty-cycle VNS with minimal risk of nerve damage as stimulation length would be limited to the length of the task. This type of on-demand perception enhancement device may be possible due to the rapid onset of sensory processing enhancement by VNS shown here, and would potentially not require long-term periods of stimulation to see effects such as the neuroplasticity-based methods used to treat epilepsy and depression.

Research detailing the effects of brain state on sensory encoding are critical to neural interface development, as optimal brain-machine interface design should consider how the state of the neural pathways they are writing to affects the ability to accurately write information ^{171, 238}. Newly developed sensory neuroprotheses have attempted to use patterned microstimulation of different regions along the sensory pathway, such as the sensory cortex and thalamus, to recover senses lost due to disease, degeneration, or injury ²³²⁻²³⁷. Changes in brain state may

cause the same microstimulation pattern to produce different results of neuron activation in these regions or may change the decoding of the resulting neural activation patterns by higher-order brain regions. Our study suggests VNS or LC activation shifts intrathalamic dynamics in such a manner that reduces membrane potential fluctuations of sensory thalamic relay neurons ¹⁰⁵.

Membrane potential fluctuations are non-optimal for sensory processing as they introduce a non-stimulus-related bias. For this same reason it is likely that membrane potential fluctuations would be non-optimal for the writing of information to sensory regions necessitated by sensory neuroprotheses. Therefore, coupling the ability to modulate sensory processing state through patterned VNS with current sensory neuroprosthetic writing techniques, may allow for improvements in the accuracy and reliability of neuroprosthetic sensations. In sensory neuroprotheses using patterned microstimulation, a major goal is for patients to better discriminate between sensations evoked by microstimulation from neighboring electrodes in the implanted array. For example, the ability of individuals with cochlear implants to discriminate between stimulation from neighboring electrodes in their cochlear implant varies widely across patients ²⁵⁴ and improved discriminability is associated with better speech recognition. Therefore, it would be worthwhile to investigate the effects of non-invasive-VNS-induced modulation on the minimal distance between discriminable microstimulation electrodes in sensory systems.

References

1. Aston-Jones, G. & Cohen, J.D. An integrative theory of locus coeruleus-norepinephrine function: adaptive gain and optimal performance. *Annual Review of Neuroscience* **28**, 403-450 (2005).
2. Aston-Jones, G. & Cohen, J.D. Adaptive gain and the role of the locus coeruleus-norepinephrine system in optimal performance. *Journal of Comparative Neurology* **493**, 99-110 (2005).
3. Sara, S.J. The locus coeruleus and noradrenergic modulation of cognition. *Nature reviews. Neuroscience* **10**, 211-223 (2009).
4. Schwarz, L.A. & Luo, L. Organization of the Locus Coeruleus-Norepinephrine System. *Current biology : CB* **25**, R1051-1056 (2015).
5. Usher, M., Cohen, J.D., Servan-Schreiber, D., Rajkowski, J. & Aston-Jones, G. The Role of Locus Coeruleus in the Regulation of Cognitive Performance. *Science* **283**, 549-554 (1999).
6. Cano, M., Bezdudnaya, T., Swadlow, H.A. & Alonso, J.-M. Brain state and contrast sensitivity in the awake visual thalamus. *Nature Neuroscience* **9**, 1240-1242 (2006).
7. Niell, C.M. & Stryker, M.P. Modulation of visual responses by behavioral state in mouse visual cortex. *Neuron* **65**, 472-479 (2010).
8. Reimer, J., *et al.* Pupil Fluctuations Track Fast Switching of Cortical States during Quiet Wakefulness. *Neuron* **84**, 355-362 (2014).
9. Briggs, F., Mangun, G.R. & Usrey, W.M. Attention enhances synaptic efficacy and the signal-to-noise ratio in neural circuits. *Nature* **499**, 476-480 (2013).
10. Fanselow, E.E., Sameshima, K., Baccala, L.A. & Nicolelis, M.A. Thalamic bursting in rats during different awake behavioral states. *Proceedings of the National Academy of Sciences of the United States of America* **98**, 15330-15335 (2001).
11. Keil, A., *et al.* Electrocortical and electrodermal responses covary as a function of emotional arousal: A single-trial analysis. *Psychophysiology* **45**, 516-523 (2008).
12. Lee, S.-H., *et al.* Activation of specific interneurons improves V1 feature selectivity and visual perception. *Nature* **488**, 379-383 (2012).
13. McGinley, Matthew J., *et al.* Waking State: Rapid Variations Modulate Neural and Behavioral Responses. *Neuron* **87**, 1143-1161 (2015).
14. Sara, Susan J. & Bouret, S. Orienting and Reorienting: The Locus Coeruleus Mediates Cognition through Arousal. *Neuron* **76**, 130-141 (2012).
15. Vinck, M., Batista-Brito, R., Knoblich, U. & Cardin, Jessica A. Arousal and Locomotion Make Distinct Contributions to Cortical Activity Patterns and Visual Encoding. *Neuron* **86**, 740-754 (2015).
16. Lee, S.-H. & Dan, Y. Neuromodulation of Brain States. *Neuron* **76**, 209-222 (2012).

17. McGinley, Matthew J., David, Stephen V. & McCormick, David A. Cortical Membrane Potential Signature of Optimal States for Sensory Signal Detection. *Neuron* **87**, 179-192 (2015).
18. Poulet, J.F.A., Fernandez, L.M.J., Crochet, S. & Petersen, C.C.H. Thalamic control of cortical states. *Nature Neuroscience* **15**, 370-372 (2012).
19. Scholvinck, M.L., Saleem, A.B., Benucci, A., Harris, K.D. & Carandini, M. Cortical state determines global variability and correlations in visual cortex. *Journal of neuroscience* **35**, 170-178 (2015).
20. Song, A.H., *et al.* Pharmacological Modulation of Noradrenergic Arousal Circuitry Disrupts Functional Connectivity of the Locus Coeruleus in Humans. *The Journal of Neuroscience* **37**, 6938-6945 (2017).
21. Lindvall, O., Bjorklund, A., Nobin, A. & Stenevi, U. The adrenergic innervation of the rat thalamus as revealed by the glyoxylic acid fluorescence method. *Journal of Comparative Neurology* **154**, 317-347 (1974).
22. Simpson, K.L., *et al.* Lateralization and functional organization of the locus coeruleus projection to the trigeminal somatosensory pathway in rat. *Journal of Comparative Neurology* **385**, 135-147 (1997).
23. Devilbiss, D.M., Page, M.E. & Waterhouse, B.D. Locus Coeruleus Regulates Sensory Encoding by Neurons and Networks in Waking Animals. *The Journal of Neuroscience* **26**, 9860-9872 (2006).
24. Devore, S. & Linster, C. Noradrenergic and cholinergic modulation of olfactory bulb sensory processing. *Frontiers in Behavioral Neuroscience* **6**, 1-12 (2012).
25. Aston-Jones, G. & Waterhouse, B. Locus coeruleus: From global projection system to adaptive regulation of behavior. *Brain research* **1645**, 75-78 (2016).
26. Vankov, A., Hervé-Minvielle, A. & Sara, S.J. Response to Novelty and its Rapid Habituation in Locus Coeruleus Neurons of the Freely Exploring Rat. *European Journal of Neuroscience* **7**, 1180-1187 (1995).
27. Lecas, J.-C. Locus coeruleus activation shortens synaptic drive while decreasing spike latency and jitter in sensorimotor cortex. Implications for neuronal integration. *The European journal of neuroscience* **19**, 2519-2530 (2004).
28. Hirata, A., Aguilar, J. & Castro-Alamancos, M.A. Noradrenergic activation amplifies bottom-up and top-down signal-to-noise ratios in sensory thalamus. *Journal of neuroscience* **26**, 4426-4436 (2006).
29. Manella, L.C., Petersen, N. & Linster, C. Stimulation of the locus coeruleus modulates signal-to-noise ratio in the olfactory bulb. *The Journal of Neuroscience* **37**, 2026-2017 (2017).
30. Devilbiss, D.M. & Waterhouse, B.D. The Effects of Tonic Locus Coeruleus Output on Sensory-Evoked Responses of Ventral Posterior Medial Thalamic and Barrel Field Cortical Neurons in the Awake Rat. *The Journal of Neuroscience* **24**, 10773-10785 (2004).
31. Steriade, M., McCormick, D.A. & Sejnowski, T.J. Thalamocortical oscillations in the sleeping and aroused brain. *Science* **262**, 679-685 (1993).

32. Wang, H.-P., Spencer, D., Fellous, J.-M. & Sejnowski, T.J. Synchrony of Thalamocortical Inputs Maximizes Cortical Reliability. *Science* **328**, 106-109 (2010).
33. Wang, Q., Webber, R. & Stanley, G.B. Thalamic Synchrony and the Adaptive Gating of Information Flow to Cortex. *Nature Neuroscience* **13**, 1534-1541 (2010).
34. Jadhav, S.P., Wolfe, J. & Feldman, D.E. Sparse temporal coding of elementary tactile features during active whisker sensation. *Nature Neuroscience* **12**, 792-800 (2009).
35. Petersen, R.S., *et al.* Diverse and Temporally Precise Kinetic Feature Selectivity in the VPM Thalamic Nucleus. *Neuron* **60**, 890-903 (2008).
36. Vaingankar, V., Soto-Sanchez, C., Wang, X., Sommer, F.T. & Hirsch, J.A. Neurons in the thalamic reticular nucleus are selective for diverse and complex visual features. *Frontiers in integrative neuroscience* **6**, 118 (2012).
37. Bale, M.R. & Maravall, M. Organization of sensory feature selectivity in the whisker system. *Neuroscience*, 1-11 (2017).
38. Bialek, W. & Rieke, F. Reliability and information transmission in spiking neurons. *Trends in Neurosciences* **15**, 428-434 (1992).
39. Jones, L.M., Depireux, D.A., Simons, D.J. & Keller, A. Robust Temporal Coding in the Trigeminal System. *Changes* (2006).
40. Bale, M.R., Davies, K., Freeman, O.J., Ince, R.A.A. & Petersen, R.S. Low-Dimensional Sensory Feature Representation by Trigeminal Primary Afferents. *The Journal of Neuroscience* **33**, 12003-12012 (2013).
41. Diamond, M.E., von Heimendahl, M., Knutsen, P.M., Kleinfeld, D. & Ahissar, E. 'Where' and 'what' in the whisker sensorimotor system. *Nature reviews. Neuroscience* **9**, 601-612 (2008).
42. Minnery, B.S. & Simons, D.J. Response properties of whisker-associated trigeminothalamic neurons in rat nucleus principalis. *Journal of neurophysiology* **89**, 40-56 (2003).
43. Ito, M. Response properties and topography of vibrissa-sensitive VPM neurons in the rat. *Journal of neurophysiology* **60**, 1181-1197 (1988).
44. Agüera y Arcas, B. & Fairhall, A.L. What causes a neuron to spike? *Neural computation* **15**, 1789-1807 (2003).
45. Arabzadeh, E., Zorzin, E. & Diamond, M.E. Neuronal encoding of texture in the whisker sensory pathway. *PLoS Biology* **3** (2005).
46. Montemurro, M.A., *et al.* Role of Precise Spike Timing in Coding of Dynamic Vibrissa Stimuli in Somatosensory Thalamus. *Journal of neurophysiology* **98**, 1871-1882 (2007).
47. Schwartz, O., Pillow, J.W., Rust, N.C. & Simoncelli, E.P. Spike-triggered neural characterization. *Journal of Vision* **6**, 484-507 (2006).

48. Ahlssar, E., Sosnik, R. & Haldarilu, S. Transformation from temporal to rate coding in a somatosensory thalamocortical pathway. *Nature* **406**, 302-306 (2000).
49. Liu, R.C., Tzonev, S., Rebrik, S. & Miller, K.D. Variability and information in a neural code of the cat lateral geniculate nucleus. *Journal of neurophysiology* **86**, 2789-2806 (2001).
50. Reich, D.S., Victor, J.D., Knight, B.W., Ozaki, T. & Kaplan, E. Response variability and timing precision of neuronal spike trains in vivo. *Journal of neurophysiology* **77**, 2836-2841 (1997).
51. Shannon, C.E. & Weaver, W. The mathematical theory of communication. (1963).
52. Aljadeff, J., Lansdell, B.J., Fairhall, A.L. & Kleinfeld, D. Analysis of Neuronal Spike Trains, Deconstructed. *Neuron* **91**, 221-259 (2016).
53. Mitchell, A.S., *et al.* Advances in Understanding Mechanisms of Thalamic Relays in Cognition and Behavior. *Journal of neuroscience* **34**, 15340-15346 (2014).
54. Gabernet, L., Jadhav, S.P., Feldman, D.E., Carandini, M. & Scanziani, M. Somatosensory integration controlled by dynamic thalamocortical feed-forward inhibition. *Neuron* **48**, 315-327 (2005).
55. Wimmer, R.D., *et al.* Thalamic control of sensory selection in divided attention. *Nature* **526**, 705-709 (2015).
56. Varela, C. Thalamic neuromodulation and its implications for executive networks. *Frontiers in Neural Circuits* **8**, 1-22 (2014).
57. Crick, F. Function of the thalamic reticular complex: the searchlight hypothesis. *Proceedings of the National Academy of Sciences* **81**, 4586-4590 (1984).
58. McAlonan, K. & Brown, V.J. The Thalamic Reticular Nucleus: More Than a Sensory Nucleus? *The Neuroscientist* **8**, 302-305 (2002).
59. Guillery, R.W. & Harting, J.K. Structure and connections of the thalamic reticular nucleus: Advancing views over half a century. *Journal of Comparative Neurology* **463**, 360-371 (2003).
60. Hartings, J.A., Temereanca, S. & Simons, D.J. State-Dependent Processing of Sensory Stimuli by Thalamic Reticular Neurons. *Journal of neuroscience* **23**, 5264-5271 (2003).
61. Pinault, D. The thalamic reticular nucleus: structure, function and concept. *Brain research. Brain research reviews* **46**, 1-31 (2004).
62. McAlonan, K. Attentional Modulation of Thalamic Reticular Neurons. *Journal of neuroscience* **26**, 4444-4450 (2006).
63. Destexhe, A., Contreras, D., Sejnowski, T. & Steriade, M. Modeling the control of reticular thalamic oscillations by neuromodulators. *Neuroreport* **5**, 2217-2220 (1994).
64. Halassa, M.M., *et al.* Selective optical drive of thalamic reticular nucleus generates thalamic bursts and cortical spindles. *Nat Neurosci* **14**, 1118-1120 (2011).

65. Huguenard, J.R. & Prince, D.A. A novel T-type current underlies prolonged Ca²⁺-dependent burst firing in GABAergic neurons of rat thalamic reticular nucleus. *The Journal of Neuroscience* **12**, 3804-3817 (1992).
66. Bal, T. & McCormick, D.A. Mechanisms of oscillatory activity in guinea-pig nucleus reticularis thalami in vitro: a mammalian pacemaker. *The Journal of physiology* **468**, 669-691 (1993).
67. Huguenard, J.R. & Prince, D.a. Intrathalamic rhythmicity studied in vitro: nominal T-current modulation causes robust antioscillatory effects. *The Journal of neuroscience : the official journal of the Society for Neuroscience* **14**, 5485-5502 (1994).
68. Coulter, B.Y.D.a., Huguenard, J.R. & Prince, D.a. CALCIUM CURRENTS IN RAT THALAMOCORTICAL RELAY NEURONES: KINETIC PROPERTIES OF THE TRANSIENT, LOW-THRESHOLD CURRENT. *Journal of Physiology*, 587-604 (1989).
69. McCormick, D.A. & Pape, H.C. Properties of a hyperpolarization-activated cation current and its role in rhythmic oscillation in thalamic relay neurones. *The Journal of Physiology* **431**, 291-318 (1990).
70. Crunelli, V. & Leresche, N. A role for GABAB receptors in excitation and inhibition of thalamocortical cells. *Trends in neurosciences* **14**, 16-21 (1991).
71. Kim, U. Functional Dynamics of GABAergic Inhibition in the Thalamus. *Science* **278**, 130-134 (1997).
72. Perez-reyes, E. & Perez-reyes, E. Molecular Physiology of Low-Voltage-Activated T-type Calcium Channels. 117-161 (2003).
73. Herd, M.B., Brown, A.R., Lambert, J.J. & Belelli, D. Extrasynaptic GABAA Receptors Couple Presynaptic Activity to Postsynaptic Inhibition in the Somatosensory Thalamus. *Journal of neuroscience* **33**, 14850-14868 (2013).
74. Jahnsen, H. & Llinas, R. Electrophysiological Properties Of Guinea-Pig Thalamic Neurons - An Invitro Study. *Journal of Physiology-London* **349**, 205-& (1984).
75. Sumitomo, I. & Iwama, K. Neuronal organization of rat thalamus for processing information of vibrissal movements. *Brain research* **415**, 389-392 (1987).
76. Avanzini, G., de Curtis, M., Panzica, F. & Spreafico, R. Intrinsic properties of nucleus reticularis thalami neurones of the rat studied in vitro. *J Physiol* **416**, 111-122 (1989).
77. Cox, C.L. & Sherman, S.M. Glutamate inhibits thalamic reticular neurons. *The Journal of neuroscience : the official journal of the Society for Neuroscience* **19**, 6694-6699 (1999).
78. Guillery, R.W., Feig, S.L. & Lozsádi, D.A. Paying attention to the thalamic reticular nucleus. *Trends in Neurosciences* **21**, 28-32 (1998).
79. Ohara, P.T. & Lieberman, a.R. The thalamic reticular nucleus of the adult rat: experimental anatomical studies. *Journal of neurocytology* **14**, 365-411 (1985).

80. Cox, C.L., Huguenard, J.R. & Prince, D.A. Nucleus reticularis neurons mediate diverse inhibitory effects in thalamus. *Proceedings of the National Academy of Sciences* **94**, 8854-8859 (1997).
81. Halassa, M.M. & Acsady, L. Thalamic Inhibition: Diverse Sources, Diverse Scales. *Trends in Neurosciences* **39**, 680-693 (2016).
82. Hartings, J.E.D.A., *et al.* High Responsiveness and Direction Sensitivity of Neurons in the Rat Thalamic Reticular Nucleus to Vibrissa Deflections. 2791-2801 (2000).
83. Cox, C.L., Huguenard, J.R. & Prince, D.A. Heterogeneous axonal arborizations of rat thalamic reticular neurons in the ventrobasal nucleus. *Journal of Comparative Neurology* **366**, 416-430 (1996).
84. Hartings, J.a., Temereanca, S. & Simons, D.J. Processing of periodic whisker deflections by neurons in the ventroposterior medial and thalamic reticular nuclei. *Journal of neurophysiology* **90**, 3087-3094 (2003).
85. McCormick, D.A. & Wang, Z. Serotonin and noradrenaline excite GABAergic neurones of the guinea-pig and cat nucleus reticularis thalami. *The Journal of physiology* **442**, 235-255 (1991).
86. Destexhe, A., Contreras, D., Steriade, M., Sejnowski, T.J. & Huguenard, J.R. In vivo, in vitro, and computational analysis of dendritic calcium currents in thalamic reticular neurons. *The Journal of neuroscience : the official journal of the Society for Neuroscience* **16**, 169-185 (1996).
87. McCormick, D.a. Cellular mechanisms underlying cholinergic and noradrenergic modulation of neuronal firing mode in the cat and guinea pig dorsal lateral geniculate nucleus. *The Journal of neuroscience : the official journal of the Society for Neuroscience* **12**, 278-289 (1992).
88. McCormick, D.a. & Prince, D.a. Noradrenergic modulation of firing pattern in guinea pig and cat thalamic neurons, in vitro. *Journal of neurophysiology* **59**, 978-996 (1988).
89. Shosaku, A., Kayama, Y., Sumitomo, I., Sugitani, M. & Iwama, K. Analysis of recurrent inhibitory circuit in rat thalamus: Neurophysiology of the thalamic reticular nucleus. *Progress in neurobiology* **32**, 77-102 (1989).
90. Llinas, R. & Jahnsen, H. Electrophysiology of mammalian thalamic neurones in vitro. *Nature* **297**, 406-408 (1982).
91. Kimura, A., Imbe, H., Donishi, T. & Tamai, Y. Axonal projections of single auditory neurons in the thalamic reticular nucleus: Implications for tonotopy-related gating function and cross-modal modulation. *European Journal of Neuroscience* **26**, 3524-3535 (2007).
92. Kimura, A. Robust interactions between the effects of auditory and cutaneous electrical stimulations on cell activities in the thalamic reticular nucleus. *Brain research* **1661**, 49-66 (2017).
93. Kimura, A. Diverse subthreshold cross-modal sensory interactions in the thalamic reticular nucleus: Implications for new pathways of cross-modal attentional gating function. *European Journal of Neuroscience* **39**, 1405-1418 (2014).

94. Kimura, A., Yokoi, I., Imbe, H., Donishi, T. & Kaneoke, Y. Auditory thalamic reticular nucleus of the rat: Anatomical nodes for modulation of auditory and cross-modal sensory processing in the loop connectivity between the cortex and thalamus. *Journal of Comparative Neurology* **520**, 1457-1480 (2012).
95. Lam, Y.-W. & Sherman, S.M. Functional Organization of the Thalamic Input to the Thalamic Reticular Nucleus. *Journal of neuroscience* **31**, 6791-6799 (2011).
96. Llinas, R.R. & Steriade, M. Bursting of thalamic neurons and states of vigilance. *Journal of neurophysiology* **95**, 3297-3308 (2006).
97. Saalmann, Y.B. & Kastner, S. Cognitive and Perceptual Functions of the Visual Thalamus. *Neuron* **71**, 209-223 (2011).
98. Sherman, S.M. Thalamic relays and cortical functioning. *Progress in Brain Research* **149**, 107-126 (2005).
99. Sherman, S.M. Dual response modes in lateral geniculate neurons: Mechanisms and functions. *Visual neuroscience* **13**, 205-213 (1996).
100. Sherman, S.M. & Guillery, R.W. Functional organization of thalamocortical relays. *Journal of neurophysiology* **76**, 1367-1395 (1996).
101. Steriade, M. & Llinas, R. The Functional States of the Thalamus and the Associated Neuronal Interplay. *The American Physiological Society* **68**, 649-724 (1998).
102. Usrey, W.M. & Alitto, H.J. Visual Functions of the Thalamus. *Annual Review of Vision Science* **1**, 351-371 (2015).
103. Weyand, T.G. The multifunctional lateral geniculate nucleus. *Reviews in the Neurosciences* **27**, 135-157 (2016).
104. Alitto, H.J., Moore, B.D., Rathbun, D.L. & Martin Usrey, W. A comparison of visual responses in the lateral geniculate nucleus of alert and anaesthetized macaque monkeys. *The Journal of Physiology* **589**, 87-99 (2011).
105. Rodenkirch, C., Liu, Y., Schriver, B.J. & Wang, Q. Locus coeruleus activation enhances thalamic feature selectivity via norepinephrine regulation of intrathalamic circuit dynamics. *Nature Neuroscience* **22**, 120-133 (2019).
106. Guido, W. & Weyand, T. Burst responses in thalamic relay cells of the awake behaving cat. *Journal of neurophysiology* **74**, 1782-1786 (1995).
107. Ramcharan, E.J., Cox, C.L., Zhan, X.J., Sherman, S.M. & Gnadt, J.W. Cellular Mechanisms Underlying Activity Patterns in the Monkey Thalamus During Visual Behavior Cellular Mechanisms Underlying Activity Patterns in the Monkey Thalamus During Visual Behavior. **2000**, 1982-1987 (2012).
108. Ramcharan, E.J., Gnadt, J.W. & Sherman, S.M. Burst and tonic firing in thalamic cells of unanesthetized, behaving monkeys. *Visual neuroscience* **17**, 55-62 (2000).

109. Sherman, S.M. A wake-up call from the thalamus. *Nat Neurosci* **4**, 344-346 (2001).
110. Zhan, X.J., Cox, C.L., Rinzel, J. & Sherman, S.M. Current clamp and modeling studies of low-threshold calcium spikes in cells of the cat's lateral geniculate nucleus. *Journal of neurophysiology* **81**, 2360-2373 (1999).
111. Guido, W., Lu, S.M. & Sherman, S.M. Relative contributions of burst and tonic responses to the receptive field properties of lateral geniculate neurons in the cat. *Journal of neurophysiology* **68**, 2199-2211 (1992).
112. Kepecs, A. & Lisman, J. Information encoding and computation with spikes and bursts. *Network: Computation in Neural Systems* **14**, 103-118 (2003).
113. Reinagel, P. The Inner Life of Bursts. *Neuron* **55**, 339-341 (2007).
114. Wang, X., *et al.* Feedforward excitation and inhibition evoke dual modes of firing in the cat's visual thalamus during naturalistic viewing. *Neuron* **55**, 465-478 (2007).
115. Alitto, H.J., Weyand, T.G. & Usrey, W.M. Distinct Properties of Stimulus-Evoked Bursts in the Lateral Geniculate Nucleus. *Journal of neuroscience* **25**, 514-523 (2005).
116. Ortuño, T., Grieve, K.L., Cao, R., Cudeiro, J. & Rivadulla, C. Bursting thalamic responses in awake monkey contribute to visual detection and are modulated by corticofugal feedback. *Frontiers in behavioral neuroscience* **8**, 198 (2014).
117. Martinez-Conde, S., Macknik, S.L. & Hubel, D.H. The function of bursts of spikes during visual fixation in the awake primate lateral geniculate nucleus and primary visual cortex. *Proceedings of the National Academy of Sciences* **99**, 13920-13925 (2002).
118. Denning, K.S. Visual Control of Burst Priming in the Anesthetized Lateral Geniculate Nucleus. *Journal of neuroscience* **25**, 3531-3538 (2005).
119. Gaudry, K.S. & Reinagel, P. Information measure for analyzing specific spiking patterns and applications to LGN bursts. *Network: Computation in Neural Systems* **19**, 69-94 (2008).
120. Elijah, D., Samengo, I. & Montemurro, M. Thalamic neuron models encode stimulus information by burst-size modulation. *Frontiers in Computational Neuroscience* **9**, 113 (2015).
121. Kepecs, A., Wang, X.-J. & Lisman, J. Bursting neurons signal input slope. *The Structure of Large-Scale Synchronized Firing in Primate Retina* **22**, 9053-9062 (2002).
122. Mease, R.A., Kuner, T., Fairhall, A.L. & Groh, A. Multiplexed Spike Coding and Adaptation in the Thalamus. *Cell Reports* **19**, 1130-1140 (2017).
123. Samengo, I., Mato, G., Elijah, D.H., Schreiber, S. & Montemurro, M.A. Linking dynamical and functional properties of intrinsically bursting neurons. *Journal of Computational Neuroscience* **35**, 213-230 (2013).

124. McCormick, D. & Feeseer, H. Functional properties of burst firing and single spike activity in thalamic relay neurons. *Neuroscience* **39**, 103-113 (1990).
125. Castro-Alamancos, M.a. Properties of primary sensory (lemniscal) synapses in the ventrobasal thalamus and the relay of high-frequency sensory inputs. *Journal of neurophysiology* **87**, 946-953 (2002).
126. Murray Sherman, S. Tonic and burst firing: Dual modes of thalamocortical relay. *Trends in Neurosciences* **24**, 122-126 (2001).
127. Laughlin, S.B., de Ruyter Van Steveninck, R.R. & Anderson, J.C. The metabolic cost of neural information. *Nature neuroscience* **1**, 36-41 (1998).
128. Bruno, R.M. Cortex Is Driven by Weak but Synchronously Active Thalamocortical Synapses. *Science* **312**, 1622-1627 (2006).
129. Bruno, R.M. Synchrony in sensation. *Current Opinion in Neurobiology* **21**, 701-708 (2011).
130. Dan, Y., Alonso, J.M., Usrey, W.M. & Reid, R.C. Coding of visual information by precisely correlated spikes in the lateral geniculate nucleus. *Nature neuroscience* **1**, 501-507 (1998).
131. Froudarakis, E., *et al.* Population code in mouse V1 facilitates readout of natural scenes through increased sparseness. *Nature Neuroscience* **17**, 851-857 (2014).
132. Sherman, S.M. Tonic and burst firing: dual modes of thalamocortical relay. *Trends in Neurosciences* **24**, 122-126 (2001).
133. Swadlow, H.A. & Gusev, A.G. The impact of 'bursting' thalamic impulses at a neocortical synapse. *Nat Neurosci* **4**, 402-408 (2001).
134. Guido, W. & Sherman, S.M. Response latencies of cells in the cat's lateral geniculate nucleus are less variable during burst than tonic firing. *Visual neuroscience* **15**, 231-237 (1998).
135. Lisman, J.E. Bursts as a unit of neural information: Making unreliable synapses reliable. *Trends in Neurosciences* **20**, 38-43 (1997).
136. Usrey, W.M., Alonso, J.M. & Reid, R.C. Synaptic interactions between thalamic inputs to simple cells in cat visual cortex. *The Journal of neuroscience : the official journal of the Society for Neuroscience* **20**, 5461-5467 (2000).
137. Guido, W., Lu, S.-M., Vaughan, J.W., Godwin, D.W. & Sherman, S.M. Receiver operating characteristic (ROC) analysis of neurons in the cat's lateral geniculate nucleus during tonic and burst response mode. *Visual neuroscience* **12**, 723-741 (1995).
138. Lu, S.M., Guido, W. & Sherman, S.M. Effects of membrane voltage on receptive field properties of lateral geniculate neurons in the cat: contributions of the low-threshold Ca²⁺ conductance. *Journal of neurophysiology* **68**, 2185-2198 (1992).
139. Rivadulla, C., Martinez, L., Grieve, K.L. & Cudeiro, J. Receptive field structure of burst and tonic firing in feline lateral geniculate nucleus. *The Journal of Physiology* **553**, 601-610 (2003).

140. McCormick, D.A. Neurotransmitter actions in the thalamus and cerebral cortex and their role in neuromodulation of thalamocortical activity. *Progress in neurobiology* **39**, 337-388 (1992).
141. Whitmire, C.J., Millard, D.C. & Stanley, G.B. Thalamic state control of cortical paired-pulse dynamics. *Journal of neurophysiology* **117**, 163-177 (2017).
142. Poulet, J.F.A. & Petersen, C.C.H. Internal brain state regulates membrane potential synchrony in barrel cortex of behaving mice. *Nature* **454**, 881-885 (2008).
143. Guo, Z.V., *et al.* Maintenance of persistent activity in a frontal thalamocortical loop. *Nature* **545**, 181-186 (2017).
144. Cardin, J.A., Palmer, L.A. & Contreras, D. Stimulus Feature Selectivity in Excitatory and Inhibitory Neurons in Primary Visual Cortex. *The Journal of Neuroscience* **27**, 10333 (2007).
145. Liu, Y., Rodenkirch, C., Moskowitz, N., Schriver, B. & Wang, Q. Dynamic Lateralization of Pupil Dilation Evoked by Locus Coeruleus Activation Results from Sympathetic, Not Parasympathetic, Contributions. *Cell Reports* **20**, 3099–3112 (2017).
146. Paxinos, G. & Watson, C. *The Rat Brain in Stereotaxic Coordinates* (Academic Press, 1998).
147. Aston-Jones, G., Rajkowski, J. & Kubiak, P. Conditioned responses of monkey locus coeruleus neurons anticipate acquisition of discriminative behavior in a vigilance task. *Neuroscience* **80**, 697-715 (1997).
148. Ghazanfar, A.A., Krupa, D.J. & Nicolelis, M.A. Role of cortical feedback in the receptive field structure and nonlinear response properties of somatosensory thalamic neurons. *Experimental brain research* **141**, 88-100 (2001).
149. Xiang, Z., *et al.* The Discovery and Characterization of ML218: A Novel, Centrally Active T-Type Calcium Channel Inhibitor with Robust Effects in STN Neurons and in a Rodent Model of Parkinson's Disease. *ACS chemical neuroscience* **2**, 730-742 (2011).
150. Deleuze, C., *et al.* T-type calcium channels consolidate tonic action potential output of thalamic neurons to neocortex. *Journal of neuroscience* **32**, 12228-12236 (2012).
151. Moore, J.D., *et al.* Hierarchy of orofacial rhythms revealed through whisking and breathing. *Nature* **497**, 205-210 (2013).
152. Adelman, T.L., Bialek, W. & Olberg, R.M. The information content of receptive fields. *Neuron* **40**, 823-833 (2003).
153. Mainen, Z.F. & Sejnowski, T.J. Reliability of spike timing in neocortical neurons. *Science* **268**, 1503-1506 (1995).
154. Moxon, K.A., Devilbiss, D.M., Chapin, J.K. & Waterhouse, B.D. Influence of norepinephrine on somatosensory neuronal responses in the rat thalamus: A combined modeling and in vivo multi-channel, multi-neuron recording study. *Brain research* **1147**, 105-123 (2007).

155. Lesica, N.A., *et al.* Dynamic Encoding of Natural Luminance Sequences by LGN Bursts. *PLoS Biol* **4**, e209 (2006).
156. Abbott, S.B.G., Stornetta, R.L., Socolovsky, C.S., West, G.H. & Guyenet, P.G. Photostimulation of channelrhodopsin-2 expressing ventrolateral medullary neurons increases sympathetic nerve activity and blood pressure in rats. *The Journal of Physiology* **587**, 5613-5631 (2009).
157. Crandall, S.R., Cruikshank, S.J. & Connors, B.W. A corticothalamic switch: controlling the thalamus with dynamic synapses. *Neuron* **86**, 768-782 (2015).
158. Berridge, C.W. & Waterhouse, B.D. The locus coeruleus–noradrenergic system: modulation of behavioral state and state-dependent cognitive processes. *Brain Research Reviews* **42**, 33-84 (2003).
159. Martins, A.R.O. & Froemke, R.C. Coordinated forms of noradrenergic plasticity in the locus coeruleus and primary auditory cortex. *Nat Neurosci* **18**, 1483-1492 (2015).
160. Reinagel, P., Godwin, D., Sherman, S.M. & Koch, C. Encoding of visual information by LGN bursts. *Journal of neurophysiology* **81**, 2558-2569 (1999).
161. Harris, K.D. & Thiele, A. Cortical state and attention. *Nature reviews. Neuroscience* **12**, 509-523 (2011).
162. Joshi, S., Li, Y., Kalwani, Rishi M. & Gold, Joshua I. Relationships between Pupil Diameter and Neuronal Activity in the Locus Coeruleus, Colliculi, and Cingulate Cortex. *Neuron* **89**, 221-234 (2016).
163. Polack, P.O., Friedman, J. & Golshani, P. Cellular mechanisms of brain state-dependent gain modulation in visual cortex. *Nature Neuroscience* **16**, 1331-1339 (2013).
164. Goard, M. & Dan, Y. Basal forebrain activation enhances cortical coding of natural scenes. *Nat Neurosci* **12**, 1444-1449 (2009).
165. Pinto, L., *et al.* Fast modulation of visual perception by basal forebrain cholinergic neurons. *Nat Neurosci* **16**, 1857-1863 (2013).
166. Fu, Y., *et al.* A cortical circuit for gain control by behavioral state. *Cell* **156**, 1139-1152 (2014).
167. Lee, A.M., *et al.* Identification of a brainstem circuit regulating visual cortical state in parallel with locomotion. *Neuron* **83**, 455-466 (2014).
168. Wolfart, J., Debay, D., Le Masson, G., Destexhe, A. & Bal, T. Synaptic background activity controls spike transfer from thalamus to cortex. *Nature Neuroscience* **8**, 1760 (2005).
169. Bennett, C., Arroyo, S. & Hestrin, S. Subthreshold mechanisms underlying state-dependent modulation of visual responses. *Neuron* **80**, 350-357 (2013).
170. Stern, E.A., Kincaid, A.E. & Wilson, C.J. Spontaneous subthreshold membrane potential fluctuations and action potential variability of rat corticostriatal and striatal neurons in vivo. *Journal of neurophysiology* **77**, 1697-1715 (1997).

171. Schriver, B., Bagdasarov, S. & Wang, Q. Pupil-linked arousal modulates behavior in rats performing a whisker deflection direction discrimination task. *Journal of Neurophysiology* **120**, 1655-1670 (2018).
172. Lambert, R.C., Bessaïh, T., Crunelli, V. & Leresche, N. The many faces of T-type calcium channels. *Pflugers Archiv European Journal of Physiology* **466**, 415-423 (2014).
173. Leresche, N. & Lambert, R.C. GABA receptors and T-type Ca²⁺ channels crosstalk in thalamic networks. *Neuropharmacology* (2017).
174. Leresche, N., Lightowler, S., Soltesz, I., Jassik-Gerschenfeld, D. & Crunelli, V. Low-frequency oscillatory activities intrinsic to rat and cat thalamocortical cells. *The Journal of physiology* **441**, 155-174 (1991).
175. Chagas, A.M., *et al.* Functional analysis of ultra high information rates conveyed by rat vibrissal primary afferents. *Front Neural Circuits* **7**, 190 (2013).
176. Groves, D.A. & Brown, V.J. Vagal nerve stimulation: a review of its applications and potential mechanisms that mediate its clinical effects. *Neuroscience & Biobehavioral Reviews* **29**, 493-500 (2005).
177. George, M.S., *et al.* Vagus nerve stimulation: a new tool for brain research and therapy. *Biological psychiatry* **47**, 287-295 (2000).
178. Krahl, S.E. & Clark, K.B. Vagus nerve stimulation for epilepsy: A review of central mechanisms. *Surg Neurol Int* **3**, S255-S259 (2012).
179. Pisapia, J. & Baltuch, G. Vagus nerve stimulation. in *Neuromodulation in Psychiatry* 325-334 (John Wiley & Sons, Ltd, 2015).
180. Yuan, H. & Silberstein, S.D. Vagus Nerve and Vagus Nerve Stimulation, a Comprehensive Review: Part II. *Headache* **56**, 259-266 (2016).
181. Gonzalez, H.F.J., Yengo-Kahn, A. & Englot, D.J. Vagus Nerve Stimulation for the Treatment of Epilepsy. *Neurosurg Clin N Am* **30**, 219-230 (2019).
182. Spindler, P., Bohlmann, K., Straub, H.B., Vajkoczy, P. & Schneider, U.C. Effects of vagus nerve stimulation on symptoms of depression in patients with difficult-to-treat epilepsy. *Seizure* **69**, 77-79 (2019).
183. van Hoorn, A., *et al.* Neuromodulation of autism spectrum disorders using vagal nerve stimulation. *Journal of clinical neuroscience : official journal of the Neurosurgical Society of Australasia* **63**, 8-12 (2019).
184. Lamb, D.G., Porges, E.C., Lewis, G.F. & Williamson, J.B. Non-invasive Vagal Nerve Stimulation Effects on Hyperarousal and Autonomic State in Patients with Posttraumatic Stress Disorder and History of Mild Traumatic Brain Injury: Preliminary Evidence. *Frontiers in medicine* **4**, 124 (2017).
185. Pelot, N.A. & Grill, W.M. Effects of vagal neuromodulation on feeding behavior. *Brain Res* **1693**, 180-187 (2018).

186. Huffman, W.J., *et al.* Modulation of neuroinflammation and memory dysfunction using percutaneous vagus nerve stimulation in mice. *Brain Stimul* **12**, 19-29 (2019).
187. Engineer, N.D., *et al.* Reversing pathological neural activity using targeted plasticity. *Nature* **470**, 101-104 (2011).
188. Conway, C.R., Udaiyar, A. & Schachter, S.C. Neurostimulation for depression in epilepsy. *Epilepsy & behavior : E&B* **88s**, 25-32 (2018).
189. Khodaparast, N., *et al.* Vagus nerve stimulation delivered during motor rehabilitation improves recovery in a rat model of stroke. *Neurorehabilitation and neural repair* **28**, 698-706 (2014).
190. Chakravarthy, K., Chaudhry, H., Williams, K. & Christo, P.J. Review of the Uses of Vagal Nerve Stimulation in Chronic Pain Management. *Curr Pain Headache Rep* **19**, 54 (2015).
191. Romero-Ugalde, H.M., *et al.* A novel controller based on state-transition models for closed-loop vagus nerve stimulation: Application to heart rate regulation. *PLoS One* **12**, e0186068 (2017).
192. Childs, J.E., DeLeon, J., Nickel, E. & Kroener, S. Vagus nerve stimulation reduces cocaine seeking and alters plasticity in the extinction network. *Learn Mem* **24**, 35-42 (2017).
193. Mwamburi, M., Liebler, E.J. & Tenaglia, A.T. Review of non-invasive vagus nerve stimulation (gammaCore): efficacy, safety, potential impact on comorbidities, and economic burden for episodic and chronic cluster headache. *The American journal of managed care* **23**, S317-s325 (2017).
194. Reuter, U., McClure, C., Liebler, E. & Pozo-Rosich, P. Non-invasive neuromodulation for migraine and cluster headache: a systematic review of clinical trials. *Journal of neurology, neurosurgery, and psychiatry* (2019).
195. Hamer, H.M. & Bauer, S. Lessons learned from transcutaneous vagus nerve stimulation (tvNS). *Epilepsy research* **153**, 83-84 (2019).
196. Mourdoukoutas, A.P., Truong, D.Q., Adair, D.K., Simon, B.J. & Bikson, M. High-Resolution Multi-Scale Computational Model for Non-Invasive Cervical Vagus Nerve Stimulation. *Neuromodulation : journal of the International Neuromodulation Society* **21**, 261-268 (2018).
197. Dorr, A.E. & Debonnel, G. Effect of Vagus Nerve Stimulation on Serotonergic and Noradrenergic Transmission. *Journal of Pharmacology and Experimental Therapeutics* **318**, 890 (2006).
198. Hulse, D.R., *et al.* Parametric characterization of neural activity in the locus coeruleus in response to vagus nerve stimulation. *Experimental neurology* **289**, 21-30 (2017).
199. Groves, D.A., Bowman, E.M. & Brown, V.J. Recordings from the rat locus coeruleus during acute vagal nerve stimulation in the anaesthetised rat. *Neuroscience letters* **379**, 174-179 (2005).
200. Krahl, S.E., Clark, K.B., Smith, D.C. & Browning, R.A. Locus coeruleus lesions suppress the seizure-attenuating effects of vagus nerve stimulation. *Epilepsia* **39**, 709-714 (1998).

201. Buell, E.P., *et al.* Vagus Nerve Stimulation Rate and Duration Determine whether Sensory Pairing Produces Neural Plasticity. *Neuroscience* **406**, 290-299 (2019).
202. Hays, S.A., Rennaker, R.L. & Kilgard, M.P. Targeting Plasticity with Vagus Nerve Stimulation to Treat Neurological Disease. *Progress in brain research* **207**, 275-299 (2013).
203. Yamamoto, T. Vagus nerve stimulation therapy: indications, programing, and outcomes. *Neurologia medico-chirurgica* **55**, 407-415 (2015).
204. Heck, C., Helmers, S.L. & DeGiorgio, C.M. Vagus nerve stimulation therapy, epilepsy, and device parameters: scientific basis and recommendations for use. *Neurology* **59**, S31-37 (2002).
205. DeGiorgio, C., *et al.* Vagus nerve stimulation for epilepsy: randomized comparison of three stimulation paradigms. *Neurology* **65**, 317-319 (2005).
206. Musselman, E.D., Pelot, N.A. & Grill, W.M. Empirically Based Guidelines for Selecting Vagus Nerve Stimulation Parameters in Epilepsy and Heart Failure. *Cold Spring Harbor perspectives in medicine* (2018).
207. Rios, M.U., *et al.* Protocol for Construction of Rat Nerve Stimulation Cuff Electrodes. *Methods and protocols* **2** (2019).
208. Wang, Q., Millard, D.C., Zheng, H.J.V. & Stanley, G.B. Voltage-sensitive dye imaging reveals improved topographic activation of cortex in response to manipulation of thalamic microstimulation parameters. *Journal of Neural Engineering* **9**, 026008 (2012).
209. Millard, D.C., Wang, Q., Gollnick, C.A. & Stanley, G.B. System identification of the nonlinear dynamics in the thalamocortical circuit in response to patterned thalamic microstimulation in vivo. *Journal of Neural Engineering* **10**, 066011 (2013).
210. Ben-Menachem, E. Vagus nerve stimulation, side effects, and long-term safety. *Journal of clinical neurophysiology : official publication of the American Electroencephalographic Society* **18**, 415-418 (2001).
211. Asconape, J.J., Moore, D.D., Zipes, D.P., Hartman, L.M. & Duffell, W.H., Jr. Bradycardia and asystole with the use of vagus nerve stimulation for the treatment of epilepsy: a rare complication of intraoperative device testing. *Epilepsia* **40**, 1452-1454 (1999).
212. Clark, K.B., Krahl, S.E., Smith, D.C. & Jensen, R.A. Post-training unilateral vagal stimulation enhances retention performance in the rat. *Neurobiology of learning and memory* **63**, 213-216 (1995).
213. Clark, K.B., *et al.* Posttraining electrical stimulation of vagal afferents with concomitant vagal efferent inactivation enhances memory storage processes in the rat. *Neurobiology of learning and memory* **70**, 364-373 (1998).
214. Clark, K.B., Naritoku, D.K., Smith, D.C., Browning, R.A. & Jensen, R.A. Enhanced recognition memory following vagus nerve stimulation in human subjects. *Nat Neurosci* **2**, 94-98 (1999).

215. Revesz, D., Tjernstrom, M., Ben-Menachem, E. & Thorlin, T. Effects of vagus nerve stimulation on rat hippocampal progenitor proliferation. *Experimental neurology* **214**, 259-265 (2008).
216. Zuo, Y., Smith, D.C. & Jensen, R.A. Vagus nerve stimulation potentiates hippocampal LTP in freely-moving rats. *Physiology & behavior* **90**, 583-589 (2007).
217. Ollerenshaw, Douglas R., Zheng, He J.V., Millard, Daniel C., Wang, Q. & Stanley, Garrett B. The Adaptive Trade-Off between Detection and Discrimination in Cortical Representations and Behavior. *Neuron* **81**, 1152-1164 (2014).
218. Lopes, L.T., *et al.* Anatomical and functional connections between the locus coeruleus and the nucleus tractus solitarius in neonatal rats. *Neuroscience* **324**, 446-468 (2016).
219. Agnew, W.F., McCreery, D.B., Yuen, T.G. & Bullara, L.A. Histologic and physiologic evaluation of electrically stimulated peripheral nerve: considerations for the selection of parameters. *Ann Biomed Eng* **17**, 39-60 (1989).
220. Goadsby, P.J., *et al.* Pathophysiology of Migraine: A Disorder of Sensory Processing. *Physiological reviews* **97**, 553-622 (2017).
221. Serafini, G., *et al.* Extreme sensory processing patterns show a complex association with depression, and impulsivity, alexithymia, and hopelessness. *Journal of affective disorders* **210**, 249-257 (2017).
222. Shimizu, V.T., Bueno, O.F. & Miranda, M.C. Sensory processing abilities of children with ADHD. *Brazilian journal of physical therapy* **18**, 343-352 (2014).
223. Carron, S.F., Alwis, D.S. & Rajan, R. Traumatic Brain Injury and Neuronal Functionality Changes in Sensory Cortex. *Frontiers in systems neuroscience* **10**, 47 (2016).
224. Lenz, F.A., Kwan, H.C., Dostrovsky, J.O. & Tasker, R.R. Characteristics of the bursting pattern of action potentials that occurs in the thalamus of patients with central pain. *Brain Res* **496**, 357-360 (1989).
225. Lenz, F.A., *et al.* Single unit analysis of the human ventral thalamic nuclear group: correlation of thalamic "tremor cells" with the 3-6 Hz component of parkinsonian tremor. *J Neurosci* **8**, 754-764 (1988).
226. Jeanmonod, D., Magnin, M. & Morel, A. Low-threshold calcium spike bursts in the human thalamus. Common physiopathology for sensory, motor and limbic positive symptoms. *Brain : a journal of neurology* **119 (Pt 2)**, 363-375 (1996).
227. Zirh, T.A., Lenz, F.A., Reich, S.G. & Dougherty, P.M. Patterns of bursting occurring in thalamic cells during parkinsonian tremor. *Neuroscience* **83**, 107-121 (1998).
228. Ferrarelli, F. & Tononi, G. The thalamic reticular nucleus and schizophrenia. *Schizophr Bull* **37**, 306-315 (2011).
229. Cain, S.M. & Snutch, T.P. T-type calcium channels in burst-firing, network synchrony, and epilepsy. *Biochimica et Biophysica Acta - Biomembranes* **1828**, 1572-1578 (2013).

230. Pratt, J.A. & Morris, B.J. The thalamic reticular nucleus: a functional hub for thalamocortical network dysfunction in schizophrenia and a target for drug discovery. *Journal of psychopharmacology (Oxford, England)* **29**, 127-137 (2015).
231. Andrade, A., *et al.* A rare schizophrenia risk variant of CACNA1I disrupts CaV3.3 channel activity. *Scientific reports* **6**, 34233 (2016).
232. Tehovnik, E.J., Slocum, W.M., Smirnakis, S.M. & Tolias, A.S. Microstimulation of visual cortex to restore vision. in *Progress in Brain Research* (ed. J. Verhaagen, *et al.*) 347-375 (Elsevier, 2009).
233. O'Doherty, J.E., *et al.* Active tactile exploration using a brain-machine-brain interface. *Nature* **479**, 228-231 (2011).
234. Kim, S., *et al.* Behavioral assessment of sensitivity to intracortical microstimulation of primate somatosensory cortex. *Proceedings of the National Academy of Sciences of the United States of America* **112**, 15202-15207 (2015).
235. Bari, B.A., Ollerenshaw, D.R., Millard, D.C., Wang, Q. & Stanley, G.B. Behavioral and Electrophysiological Effects of Cortical Microstimulation Parameters. *PLoS ONE* **8**, e82170 (2013).
236. Rodenkirch, C., Schriver, B. & Wang, Q. Brain-Machine Interfaces: Restoring and Establishing Communication Channels. in *Neural Engineering* (ed. L. Zhang & D. Kaplan) (Springer, 2016).
237. Romo, R., Hernandez, A., Zainos, A. & Salinas, E. Somatosensory discrimination based on cortical microstimulation. *Nature* **392**, 387-390 (1998).
238. Panzeri, S., Safaai, H., De Feo, V. & Vato, A. Implications of the dependence of neuronal activity on neural network states for the design of brain-machine interfaces. *Frontiers in Neuroscience* **10**, 1-8 (2016).
239. Nicolelis, M.A.L. & Fanselow, E.E. Thalamocortical optimization of tactile processing according to behavioral state. *Nature Neuroscience* **5**, 517-523 (2002).
240. Lesica, N.A. & Stanley, G.B. Encoding of Natural Scene Movies by Tonic and Burst Spikes in the Lateral Geniculate Nucleus. *J. Neurosci.* **24**, 10731-10740 (2004).
241. Soto-Sánchez, C., Wang, X., Vaingankar, V., Sommer, F.T. & Hirsch, J.A. Spatial scale of receptive fields in the visual sector of the cat thalamic reticular nucleus. *Nature communications* **8**, 800 (2017).
242. Weyand, T.G., *et al.* Burst and Tonic Response Modes in Thalamic Neurons During Sleep and Wakefulness Burst and Tonic Response Modes in Thalamic Neurons During Sleep and Wakefulness. 1107-1118 (2011).
243. Holdefer, R.N. & Jacobs, B.L. Phasic stimulation of the locus coeruleus: effects on activity in the lateral geniculate nucleus. *Experimental brain research* **79**, 444-452 (1994).
244. Bezdudnaya, T., *et al.* Thalamic burst mode and inattention in the awake LGNd. *Neuron* **49**, 421-432 (2006).

245. Stoelzel, C.R., Bereshpolova, Y. & Swadlow, H.A. Stability of Thalamocortical Synaptic Transmission across Awake Brain States. *Journal of neuroscience* **29**, 6851-6859 (2009).
246. Hirsch, J.A., Wang, X., Sommer, F.T. & Martinez, L.M. How Inhibitory Circuits in the Thalamus Serve Vision. *Annual Review of Neuroscience* **38**, 309-329 (2015).
247. Livingstone, M.S. & Hubel, D.H. Effects of sleep and arousal on the processing of visual information in the cat. *Nature* **291**, 554-561 (1981).
248. Wang, X., Sommer, F.T. & Hirsch, J.a. Inhibitory circuits for visual processing in thalamus. *Current Opinion in Neurobiology* **21**, 726-733 (2011).
249. Escanilla, O., Alperin, S., Youssef, M., Ennis, M. & Linster, C. Noradrenergic but not cholinergic modulation of olfactory bulb during processing of near threshold concentration stimuli. *Behavioral Neuroscience* **126**, 720-728 (2012).
250. Escanilla, O., Arrellanos, A., Karnow, A., Ennis, M. & Linster, C. Noradrenergic modulation of behavioral odor detection and discrimination thresholds in the olfactory bulb. *European Journal of Neuroscience* **32**, 458-468 (2010).
251. Kay, L.M. & Sherman, S.M. An argument for an olfactory thalamus. *Trends in Neurosciences* **30**, 47-53 (2007).
252. Edeline, J.M., Manunta, Y. & Hennevin, E. Induction of selective plasticity in the frequency tuning of auditory cortex and auditory thalamus neurons by locus coeruleus stimulation. *Hearing Research* **274**, 75-84 (2011).
253. Nowak, D.A. & Hermsdorfer, J. Selective deficits of grip force control during object manipulation in patients with reduced sensibility of the grasping digits. *Neuroscience research* **47**, 65-72 (2003).
254. Biesheuvel, J.D., Briaire, J.J., de Jong, M.A.M., Boehringer, S. & Frijns, J.H.M. Channel discrimination along all contacts of the cochlear implant electrode array and its relation to speech perception. *International Journal of Audiology* **58**, 262-268 (2019).